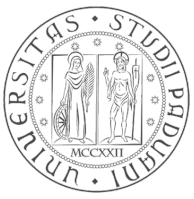

Università degli Studi di Padova

Dipartimento di Ingegneria Industriale

Corso di Laurea Magistrale in Ingegneria Elettrica

Tesi di Laurea Magistrale

Application of Reactive Energy to UK Low Voltage Networks and Embedded Generation Effects on Networks Performance

Relatore
Prof. Roberto Turri
Dipartimento di Ingegneria Industriale

Correlatore
Dr. Huw Griffiths
School of Engineering, Cardiff University

Laureando
Remon Atfy Mosaad

Anno Accademico 2013/2014

A tutti coloro che hanno creduto in me.

Contents

List of Tables

List of Figures

Abstract

The deployment of reactive compensation and DG brings ample technological and environmental benefits to the traditional distribution networks. The appropriate sizing and placement of capacitors banks and DG help to reduce power losses and avoid transmission and distribution system expansion.

The objective of this thesis is to study thoroughly a specific low-voltage network by determining its performance in different scenarios, in order to define voltages and currents in the various nodes with different operating conditions of the network, for a given maximum load provided by historical measures. The operating conditions cited include the reactive compensation using different methods and distributed generation with reactive compensation.

The simulator used in this thesis is OpenDSS and as the name suggests is an open source primarily designed to simulate the low-voltage systems, with the unique ability to analyse the unbalanced three phase systems , especially with the connection of distributed generation. It performs in the frequency domain analysis of the type of power flow, the harmonics, and dynamic analysis, considering not only the conditions of peak load, but also the variation in time of the same, and then simulating both a load curve and PV curves, respectively, in the case of passive users and active ones.

Initially the simulations analysis were carried out with only reactive compensation and then the latter with a high degree of penetration of distributed generation. The lowest total voltage drop is achieved with distributed compensation at 1/3 feeder length, whereas the connection of distributed generation may reduce considerably the voltage drop along the feeder.

Introduction

In this project, a specific low voltage (LV) network was selected for detailed investigation.The study comprised two parts parts; (i) Literature review on load modelling, data analysis and distribution system analysis (ii) to set up detailed computer load flow models of the networks to evaluate their performance under a range of operating conditions including the impact of shunt reactive power compensation and embedded generation.

The network power factor was assumed 0.9, in order to stress the network and study the worst scenarios for a loading peak provided by Western Power Distribution. A new approach to modelling the balanced/unbalanced LV networks was carried out using OpenDSS. Using the network data provided by WPD, load flow models of the five networks were established. Four of the networks were modelled with three-phase cables and assumed balanced three-phase loads. For the largest network, Angus Street, which contains a significant proportion of single phase cable, a detailed unbalance network model was set up. For Angus Street network, the base case study, the effect of load, power factor were examined the effects of embedded generation and reactive power compensation were considered with different approaches. The network simulation results were analysed and presented in terms of voltage and current profiles as a function of feeder route length from the substation. This method of graphical presentation facilitates an overall view of the performance of an entire network performance measured against the relevant limits of current or voltage. The simulation results revealed that, generally, the voltage profiles indicated a falling voltage with distance from the main substation and a significant voltage drop across the 11kV/415 network supply transformer. It was noted that the voltage drop across the supply transformer is more affected by variation in power factor than the voltage drop across the feeders, due to its higher X/R ratio.

The X/R ratios of typical WPD low voltage network cables and lines lie between 0.1 and 0.75, while the X/R ratio of the supply transformers are between 1.5 and 4.3. In the case of Angus St., a significant unbalance in phase voltages was seen and, for the assumed loading conditions, the feeder end voltages appeared close to the lower statutory voltage limit. The current flows were generally within the rated ampacity of network cables, although, ratings were exceeded in some parts of the Angus St. Network for some assumed load conditions.

A study into the effect of reactive compensation applied to LV networks has shown that shunt compensation applied at the main substation may be useful to limit the voltage drop across the transformer. However, downstream compensation is not so effective in reducing feeder voltage drop but may help to reduce network currents and help to operate within cable ampacity. The Angus street network was modelled as an unbalanced network with detailed representation of all 3- phase and single phase cables. The Angus St. simulation results also confirmed that reactive compensation applied at low voltage supply substation can help to improve voltage. In addition, moderate quantities of embedded generation can alleviate voltage drops and current loading along feeders. However, high levels of DG on lighter loaded branches can overload cables. The merits of centralised versus distributed

compensation were investigated and it has been shown that although marginal improvement may be obtained in overall voltage profiles by distributing reactive compensation some distance along feeders (about one-third of the way in the case of Angus St), from a number of practical points of view, centralised compensation provides the only credible solution. A review of commercially available low voltage capacitors from a numbers of leading manufactures indicates that there are adequate size and range of units available for application to voltage control on lv distribution network.

Chapter 1

Load Modelling and Data Analysis Techniques for LV Networks

1.1 Introduction

The load data is needed for defining the requirements of the network's transfer capacity, approximating the losses or estimating the existing network capability to increase loads. Some specifications are required in order to understand the meaning of load classification:

- System location: customer site, low voltage network, transformer, etc.;
- Customer class: industry, urban, rural, etc.;
- Time: year, day of week, weekend, time of day;
- Dimension: KW, A, Power factor;
- Load recording every: 5 min, 10 min, 15 min, 30 min, etc.

Losses along the network and voltage drop are caused basically by load influences. The network voltage U is almost constant, whereas the current and the power factor vary with load. The more active power demanded by load and the more load current is absorbed. As a consequence thermal losses in electrical components increase, as they are proportional to the resistance of a component and square of the load current. An important issue is the thermal ageing of a component such as transformer's coil insulators depending on the load capability. For this reason the load of the transformer should be known. Once loads are classified, in order to get started with load modelling process it is necessary to consider the two categories for different applications as follows:

- Static;
- Dynamic, Time-varying.

Either model considers loads as a voltage magnitude function on the steady state representation of the network in power flow studies. The static application considers only voltage depended characteristic (expresses the active and reactive powers at any instant of time as functions of the bus voltage magnitude and frequency at the same instant. Static load models are used both for essentially static load components, e.g., resistive and lighting load, and as an approximation for dynamic load components, e.g., motor-driven loads. In other words it is not dependent on time, and it describes the relationship of the active and reactive power at all times to the voltage and/or frequency.):

Power Flow (as Harmonic Power Flow) and Voltage Stability, while the Dynamic application (usually represented by differential equations) considers both voltage-depended and frequency depended

characteristics (as Transient and Dynamic stabilities); Dynamic load models can be used to represent the function relation between the active or reactive power of load and the voltage and frequency of load bus at the moment or several times intervals before the moment. Mathematics models have many parameters that are difficult to be identified. Input/output models consider the load as a "system". The input variables are the voltage U and frequency f on load bus; the output variables are all active and reactive power of the load. [IEEE Task Force on Load Representation for Dynamic Performance]

The loads on a distribution system are typically specified by the complex power consumed. The specified load will be the maximum demand derived by a sum of customers demand for each time interval. This demand can be specified as kVA and power factor, kW and power factor, or kW and KVAR.

1.2 Load Models

Loads on a distribution feeder can be modelled as wye-connected or delta-connected. The loads can be three-phase, two-phase, or single-phase with any degree of unbalance, and can be modelled as [7]:

- Constant impedance load (A static load model where the power varies directly with the square of the voltage magnitude);
- Constant current magnitude (A static load model where the power varies directly with the voltage magnitude);
- Constant real and reactive power (constant PQ - Model=1 in OpenDSS): A static load model where the power does not vary with changes in voltage magnitude. It may also be called constant MVA load model. In steady-state power analysis, load is normally modelled as a fixed PQ node, which implies that the load is independent from voltage or frequency;
- Constant P, Fixed Q;
- Constant P, Quadratic Q;
- Any combination of the above.

The general voltage-load current characteristic is plotted in fig 1.1 [19]. The load models developed are to be used in the iterative process of a power flow program where the load voltages are initially assumed. Then, the results of the power-flow analysis replace the assumed voltages with the actual operating load voltages. All models are initially defined by a complex power per phase and an assumed line-to-line voltage (delta load). The units of the complex power can be in volt-amperes and volts, or per-unit volt-amperes and per-unit voltages (Grid only). For all loads the line currents entering the load are required in order to perform the power-flow analysis.

An interesting aspect to investigate in distribution networks is the effect of composite loads, as it is not covered in the literatures that consider DG in distribution networks, and their impact on voltage profile. Common static load models for active and reactive power are expressed in polynomial or exponential forms and can include, if necessary, a frequency dependence term. In this paper, we use the exponential form to represent static load as:

$$P(V) = P_0\left(\frac{V}{V_0}\right)^{\alpha} \tag{1.1}$$

$$Q(V) = Q_0\left(\frac{V}{V_0}\right)^{\beta} \tag{1.2}$$

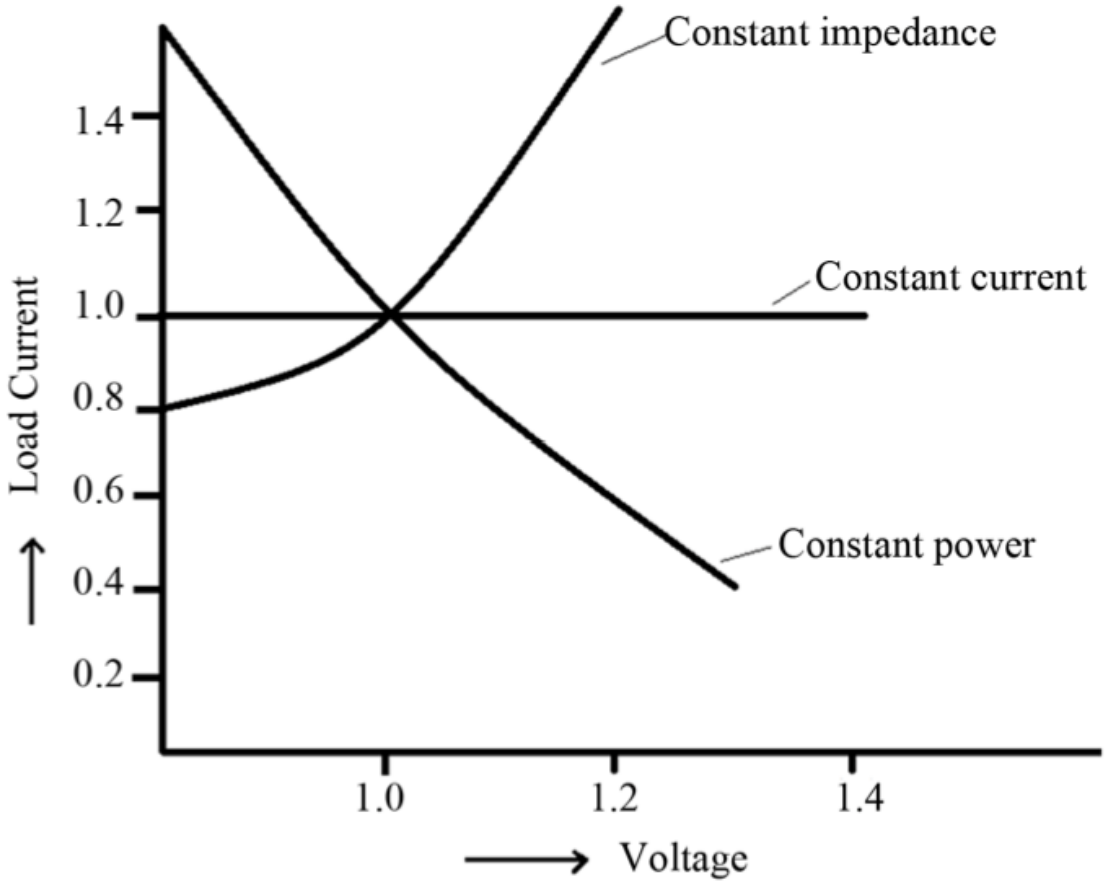

Figure 1.1: V-I characteristics curves for ZIP model

Where P and Q are active and reactive components of load, respectively, when the bus voltage magnitude is V. The subscript 0 identifies the values of the respective variables at the initial operating condition. The parameters of this model are the exponents α and β. With these exponents equal to 0, 1 or 2, the model represents the constant power, constant current or constant impedance characteristics of load components, respectively. [IEEE Task Force on Load Representation for Dynamic Performance] Static models for dynamic load components should be used cautiously. Representation of loads by exponential models with exponent values less than 1.0 (or by equivalent polynomial models) in a dynamic simulation is questionable [Standard Load Models for Power Flow and Dynamic Performance Simulation]

1.2.1 Voltage Dependency

Stability limits tend to increase with the same change of P(v) in the cases where loads are at generating plants and at the sending end of the transmission line. In the studies of cases involving a short circuit fault, the load characteristics during a fault might deserve far more attention than they have customarily commanded. During a short circuit fault, bus-voltages are depressed, power balance is lost, and generators are accelerating as a whole, but likely at all different rates (even at negative rates). Load characteristics can have significant effects on the rates of acceleration or deceleration of individual generators during the fault, and therefore, on eventual stability of the system. Accelerating generators accelerate less during the fault with local constant-power loads than with local constant-impedance load. Voltage dependency of reactive power, Q(v), affects stability in a somewhat more

complicated manner primarily due to its effects on voltages, which in turn affect active power. It is well evidenced that synchronous condensers improve stability and static reactive-power compensators, which tend to stabilize voltages. One noteworthy characteristic of Q(v) is its nonlinearity presumably caused by magnetic saturations in transformers and motors. Magnetic saturation depends on the volts per hertz, and therefore, both the voltage and the frequency dependencies need to be considered together. Typically, the total transformer capacity far exceeds the total generator capacity by a roughly estimated factor of 3 for the total power transformer capacity and by 1.5 for the total distribution transformer capacity. Distribution transformers are often designed to operate closer to saturation, and therefore their effects can be more significant.

1.2.2 Load Representation for Dynamic Performance

In general, the Distribution Network Operator (DNO) has an economic incentive to reduce losses in their networks. Consumers pay the DNO the energy they consume times a standard loss coefficient. Since the installation of DG will have an impact on distribution losses, it will thus have a direct consequence on the DNO profit. If DG decreases actual network losses, the DNO's profit will increase, but if the opposite happens, the DNO's benefits will decrease. The IEEE Task Force on Load Representation for Dynamic Performance defined the voltage dependent load models for residential, industrial, and commercial loads as follows [6],

$$P_L = P_{L0} V^{\alpha} \tag{1.3}$$

$$Q_L = Q_{L0} V^{\beta} \tag{1.4}$$

Where,
α active power exponent
β reactive power exponent
P_{L0} active power operating point
Q_{L0} reactive power operating point

And,
$1.5 < \alpha < 2.0$
$3.0 < \beta < 4.0$
$0.9 < V < 1.1$ p.u.

Typical power component values in various categories and seasons are as follows [Bibliography on load models for power flow and dynamic performance simulation],

TYPICAL LOAD TYPES AND EXPONENT VALUES

Load type		Residential		Commercial		Industrial	
		α	β	α	β	α	β
Summer	Day	0.72	2.96	1.25	3.50	0.18	6.00
	Night	0.92	4.04	0.99	3.95	0.18	6.00
Winter	Day	1.04	4.19	1.50	3.15	0.18	6.00
	Night	1.30	4.38	1.51	3.40	0.18	6.00

Table 1.1: Power component values in various categories for different classes

Transformer saturation

Distribution transformers, which may be considered part of the load, normally operate with significant magnetising induction saturation. Many field tests show large voltage sensitivity of reactive power load following voltage changes. For small changes, reactive power may change as the third to seventh power of voltage. To more correctly represent reactive power demand as seen from the bulk power network, it may be desirable to have compatible transformer saturation models in both stability and power flow programs. Transformer saturation will limit fundamental frequency temporary over-voltages. Accurate evaluation of potentially damaging temporary over-voltages, however, requires evaluation by electromagnetic transients programs.

1.3 Statistical Approaches Used in Load Modelling

Load flow calculations on distribution networks, traditionally are performed by using a deterministic approach referring to a particular pre-established load condition, for example the peak load instant, or by using a statistical simplified method consisting in determining the peak load starting from subscribed power demand. The aim of SLM is to provide an estimate of the load curve of any aggregate of users connected to the network, starting from billing information. SLM considers all the users subdivided into 30 homogeneous groups, called "load classes". Besides, the year has been represented by means of 14 standard days (6 working-days, 4 Saturdays and 4 holidays), each of which represents the homologue days of a period of one or several months. The load curve of each typical day has been subdivided into 96 intervals. For each quarter of an hour 't' of each typical day 'g' and each load class 'c', SLM determines the "mean value" and the "variance" of the active and the reactive power, as well as the "covariance" between active and reactive power by means of the following expressions [22]:

$$\bar{P}_{c,g}(t) = E_c.Kp_{c,g}(t) \tag{1.5}$$

$$\bar{Q}_{c,g}(t) = E_c.Kq_{c,g}(t) \tag{1.6}$$

$$Sp^2_{c,g}(t) = E_c.Hp_{c,g}(t) + E^2_c.\lambda p_{c,g}(t) \tag{1.7}$$

$$Sq^2_{c,g}(t) = E_c.Hq_{c,g}(t) + E^2_c.\lambda q_{c,g}(t) \tag{1.8}$$

$$Spq^2_{c,g}(t) = E_c.Hpq_{c,g}(t) + E^2_c.\lambda pq_{c,g}(t) \tag{1.9}$$

Where,
E_c is the yearly energy of the load class 'c' of the users' aggregate under examination;
$Kp_{c,g}(t), Hp_{c,g}(t), \lambda p_{c,g}(t), Kq_{c,g}(t), Hq_{c,g}(t), \lambda q_{c,g}(t), \lambda pq_{c,g}(t)$ are the parameters that constitute SLM. The values of these last parameters are determined during the SLM construction activity, utilising the load curves of sample users of the 'c' class recorded during survey campaigns. The so structured model ensures additivity property , meaning that it allows a very easy and correct estimate of the mean values and the variances of the power of any aggregate of users belonging to the same class, by simply applying the above expressions to an equivalent user from the point of view of energy consumption. The covariance between the power of two users belonging to the same class, with E_m, and E_n, energy respectively, is:

$$COV[P_{m,g}(t), P_{n,g}(t)] = \lambda p_{c,g}(t).E_m.E_n \tag{1.10}$$

The mean value of the active and the reactive power of a group of users belonging to different classes is provided by the summation of the mean Values of the powers of the individual classes:

$$\bar{P}_g(t) = \sum_c \bar{P}_{c,g}(t) \tag{1.11}$$

$$\bar{Q}_g(t) = \sum_c \bar{Q}_{c,g}(t) \tag{1.12}$$

The variances and the covariances between active and reactive power were calculated as a summation of the variances or covariances of the different classes that constitute the aggregate under examination. This operation implicitly assumes the hypothesis of the statistical independence between the different load classes.

1.3.1 Time and Peak Load Forecasts

The distribution planning is based on annual peak. This needs year-by-year expansion studies during short-term period and plans for selected years in long-term period. It is common to set planning periods of 1 - 7 years ahead for short-term forecast and longer period until 25 years ahead for long-term forecast. The load forecast seeks the annual peak load and in some cases the seasonal peak load, particularly when taking into account the weather conditions. This is because some equipment may be overloaded in the summer due to the high ambient temperature in spite of getting its peak load less than that in the winter. For accurate peak load forecast, the coincidence of service area peaks must be studied. So, forecast of hourly loads of the peak day is usually performed not only for the peak load as a value but also for the peak duration. It is important to study the peak duration because it may allow the system equipment to operate on overload for a short period without failure, that is, no need to replace or add new equipment.

1.3.2 Type of Customer

General shape of the load curves for the traditional customer classes is shown in Figure

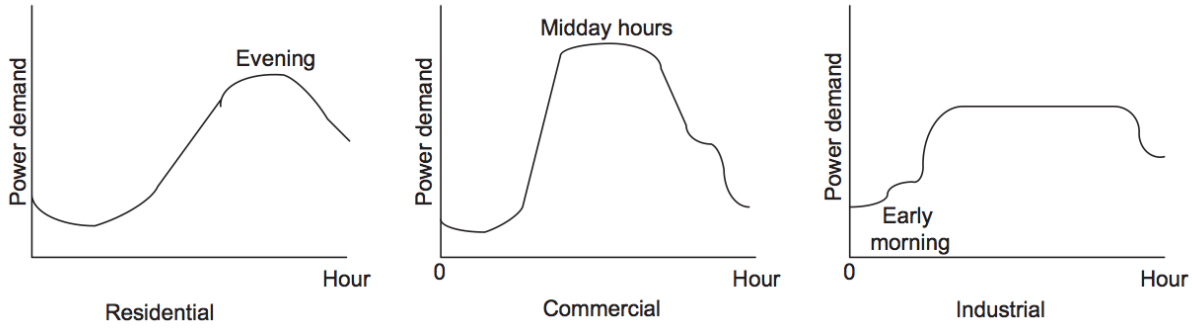

Figure 1.2: Curves for traditional customer classes

For residential class, the peak load is almost in the evening while for commercial class it is at midday hours. The industrial class has low load at early morning, then approximately constant load until shutting down in the afternoon. Distribution systems are planned considering three major points related to each customer in each class:

- The peak load per customer;
- The total energy consumption represented by the area under the curve.

The load curves are recorded and measured over some specific period (1 day, 1 week, 1 month). This period is divided into time intervals where the average power of an interval is calculated by

dividing the area under the curve at this interval by the length of interval. This average power is called "demand" and the time interval is called "demand interval".

Load Factor and Diversity Factor

Load factor (LF) is defined as the ratio of average to peak load. The value of the average load is the total energy consumed during an entire period divided by the number of period hours[18]. Thus,

$$LF = \frac{(KW(average))}{(KW(Maximumdemand))} = \frac{(KWh)}{(KW(Maximumdemand)xHours)} \tag{1.13}$$

To measure and record the daily load curve of two customers, it will not be the algebraic sum of the two customers' individual load curves. This is because the appliances of the two customers do not work in synchronism. It is found that as the number of customers is increased, the load curve gets smoother and the peak value is decreased because of the non-coincidence of individual peaks [10] as shown in figure: The ratio of measured peak load of a number of customers to the summation of

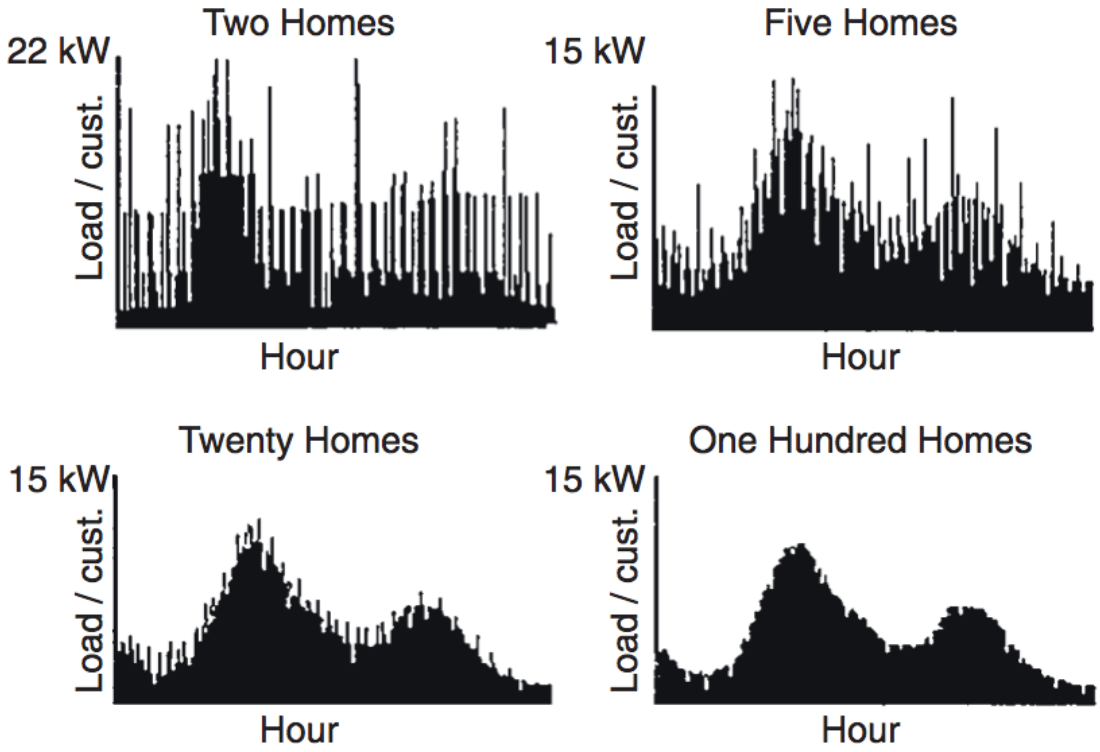

Figure 1.3: Effect of non-coincidence of individual peaks of some customer's groups

individual peaks is defined as the coincidence factor (CF), that is,

$$CF = \frac{(\ Measuredpeakofload)}{\sum(\ Individualpeaks)} \tag{1.14}$$

It is evident that the CF decreases as the number of customers in a group increases.

1.4 Measuring and Recording Load Behaviour

The load behaviour represented by daily, monthly, or annual load curves is an important tool for forecasting. So, the data of these curves must be collected accurately as the load behaviour is based on them. The load curve shape can change depending on the method of measuring and cyclic

recording of these data. The measuring method determines the quantity to be measured. Whether it is the instantaneous load or the energy consumed during a period. This is referred by what is called "sampling method." The data cyclic recording means the number of time intervals per period at which the measured data are recorded, for instance, every 10, 15 or 20 minutes.

There are two sampling methods used:

1. Sampling by Integration: In this method, the measuring instrument measures and records the energy consumed during the sampling interval, that is, integrates the area under the load curve of each interval to be stored and recorded;

2. Discrete Instantaneous Sampling Method: It measures and records the load at the beginning of each sample interval. So, the changes of load during the interval are missed, that is, not measured.

Thus, for the erratic load curve, the sampling by integration is preferred where the error will be large in case of using discrete instantaneous method.

Sampling Rate

The sampling rate, which is the frequency of measuring and recording the load data, depends on the number of customers in a group and the method of sampling. If the number of customers in a group is increased, the peak load of the group is decreased and the peak duration is getting longer. So, the length of sampling period can be longer. In this case, the discrete instantaneous sampling may be used without a risk of big error. Of course, by decreasing the number of customers in a group, the peak load per customer and its duration decrease. The load curve becomes more erratic. So, the sampling rate should be high, that is, small sampling period. The preferred sampling method in this case is sampling by the integration method[10].

1.5 Load Analysis: Statistics, Errors, and Estimates

The distribution of the load for a particular hour of the day can be approximated by a Gaussian distribution curve, which is characterised by its mean value and standard deviation. Load curves can then be used to simulate the load of one customer belonging to a particular customer group by scaling the annual units of that customer to the average of that group. A load of curve for a group of customers can be constructed by summing the individual customer load curves statistically.

Computer simulations such as power-flow studies give exact answers, but in reality we never know the absolutely true state of a physically operating system. Even when great care is taken to ensure accuracy, unavoidable random noise enters into the measurement process to distort more or less the physical results. However, repeated measurements of the same quantity under carefully controlled conditions reveal certain statistical properties from which the true value can be estimated. If the measured values are plotted as a function of their relative frequency of occurrence, a histogram is obtained to which a continuous curve can be fitted as the number of measurements increases (theoretically, to an infinite number). The continuous curve most commonly encountered is the bell-shaped function p(z) shown in figure 1.4. The function p(z), called the Gaussian or normal probability density function, has the formula,

$$p(z) = \frac{1}{(\sigma\sqrt{2}\pi)} \epsilon^{\frac{-1}{2}\left(\frac{z-\mu}{\sigma}\right)^2} \tag{1.15}$$

and the variable representing the values of the measured quantity along the horizontal axis is known as the Gaussian or normal random variable z. Areas under the curve give the probabilities associated

with the corresponding intervals of the horizontal axis. For example, the probability that between the points a and b of figure 1.4 is the area given by

$$Pr(a < z < b) = \int_a^b p(z)dz = \frac{1}{(\sigma\sqrt{2}\pi)} \int_a^b \epsilon^{\frac{-1}{2}\left(\frac{z-\mu}{\sigma}\right)^2} dz \tag{1.16}$$

Where the symbol Pr(.) means the probability of (.) occurring. The total area under the curve p(z) between -∞ and +∞ equals 1 because the value of z is certain (with probability equal to 1 or 100%) to lie between arbitrarily large extreme values. The Gaussian probability density function p(z) is completely determined once the parameters μ and σ are known. Figure 1.4 shows that p(z) has its maximum value when z equals μ, which is the expected value of z denoted by E(z) and defined by

$$\mu = E(z) = \int_{-\infty}^{+\infty} zp(z)dz \tag{1.17}$$

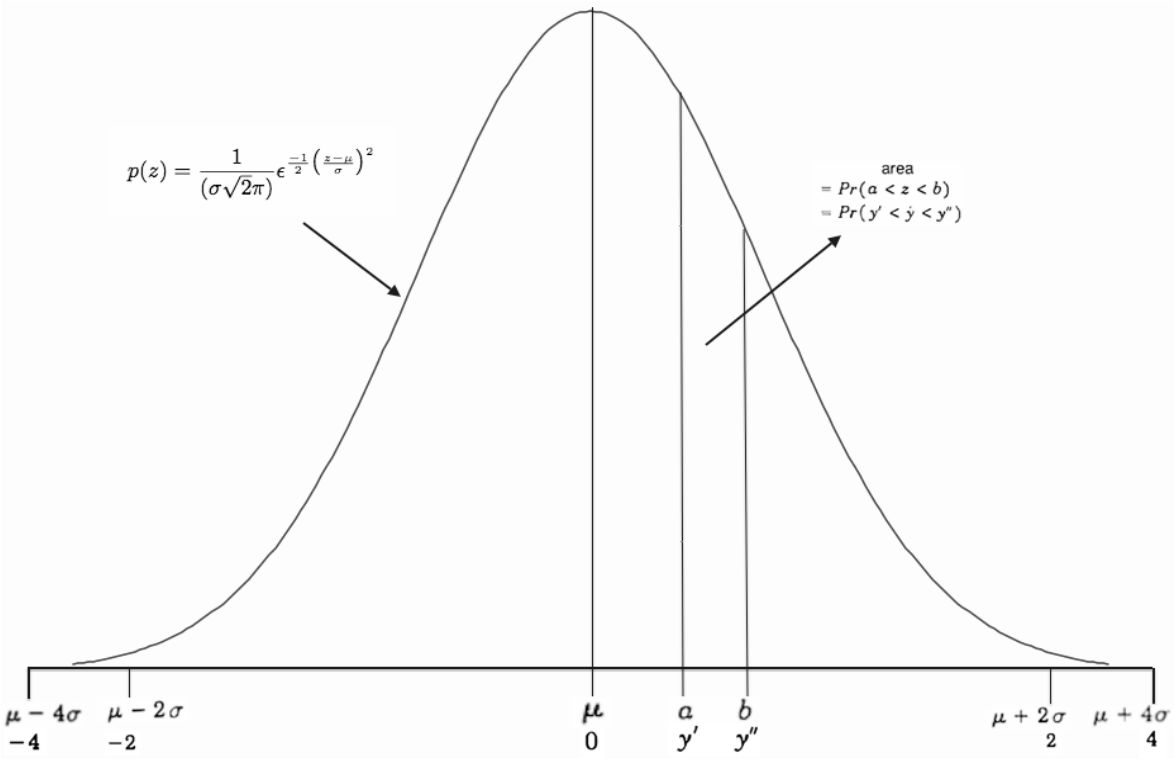

Figure 1.4: The gaussian probability density function p(z) and standard gaussian density function p(y)

The expected value μ is often called the mean since the values of z are symmetrically clustered about μ. The degree to which the curve of p(z) spreads out about μ (that is, the width) depends on the variance σ^2 of z defined by

$$\sigma^2 = E[(z-\mu)^2] = \int_{-\infty}^{+\infty} (z-\mu)^2 p(z)dz \tag{1.18}$$

Thus, the variance of z is the expected value of the square of the deviations of z from its mean; smaller values of σ^2 provide narrower and higher curves with each having unity area centred about μ. The positive square root of the variance is the standard deviation σ of z. The mean and variance are important parameters of many commonly encountered probability density functions. Each such function has a curve with underlying areas, which quantify the probabilities of the associated random variable. The Gaussian distribution plays a very important role in measurement statistics. Because

the density p(z) can not be directly integrated, the areas under the curve, as shown in the figure, have been tabulated for the standard Gaussian density function p(y), which has the parameters μ_y=0 and σ_y=1. Separate tables of the Gaussian distribution for other values of μ and σ are unnecessary since we can rescale the horizontal axis of figure 1.4 , and thereby transform from z to y, using the change-of-variable formula

$$y = \frac{(z-\mu)}{\sigma} \tag{1.19}$$

then,

$$Pr(a) = \frac{1}{\sqrt{2}\pi} \int_0^a \epsilon^{\left(\frac{-1}{2}y^2\right)} dy \tag{1.20}$$

a	Pr(a)	a	Pr(a)	a	Pr(a)
0.05	0.01993879	0.8	0.28837865	1.55	0.45998771
0.1	0.03982781	0.85	0.3026926	1.6	0.47054288
0.15	0.05961765	0.9	0.31646559	1.65	0.48154586
0.2	0.07925967	0.95	0.32970504	1.7	0.49314435
0.25	0.09870633	1	0.34242516	1.75	0.50549841
0.3	0.11791159	1.05	0.35464722	1.8	0.51878079
0.35	0.13683131	1.1	0.3664	1.85	0.53317733
0.4	0.15542354	1.15	0.3777201	1.9	0.54888737
0.45	0.173649	1.2	0.3886524	1.95	0.56612404
0.5	0.19147137	1.25	0.39925033	2	0.58511472
0.55	0.20885771	1.3	0.40957632	2.05	0.60610136
0.6	0.22577882	1.35	0.41970216	2.1	0.62934087
0.65	0.2422096	1.4	0.42970934	2.15	0.6551055
0.7	0.25812945	1.45	0.43968947	2.2	0.6836832
0.75	0.27352264	1.5	0.44974462	2.25	0.71537801

Table 1.2: Standard Gaussian Distribution

It is evident that dz=σdy, and if z takes on values between 'a' and 'b', then y must lie between the corresponding numbers y'=(a-μ)/σ and y"=(b-μ)/σ. Hence, substituting for y in

$$Pr(a < z < b) = \int_a^b p(z)dz = \frac{1}{(\sigma\sqrt{2}\pi)} \int_a^b \epsilon^{\left(\frac{-1(z-\mu)^2}{2 \quad \sigma}\right)} dz \tag{1.21}$$

We obtain

$$Pr(a < z < b) = \frac{1}{(\sigma\sqrt{2}\pi)} \int_{y'}^{y"} \epsilon^{\left(\frac{-1}{2}y^2\right)} \sigma dy = \frac{1}{\sqrt{2}\pi} \int_{y'}^{y"} \epsilon^{\left(\frac{-1}{2}y^2\right)} \sigma dy \tag{1.22}$$
$$= Pr(y' < y < y")$$

Which shows that y is the random variable with the standard Gaussian probability density. Thus, changing scale from z to y allows us to use the tabulated values of y, for any random variable z with normal probability density function as shown in fig.1.5 [17].

In the new scale y tells us how many standard deviations from the mean the corresponding value of z lies. The area under the Gaussian density curve is distributed as follows: 68,27% within the z-limits $\mu \pm \sigma$, 95,45% within the z-limits $\mu \pm 2\sigma$, and 99,73% within the z-limits $\mu \pm 3\sigma$. Accordingly,

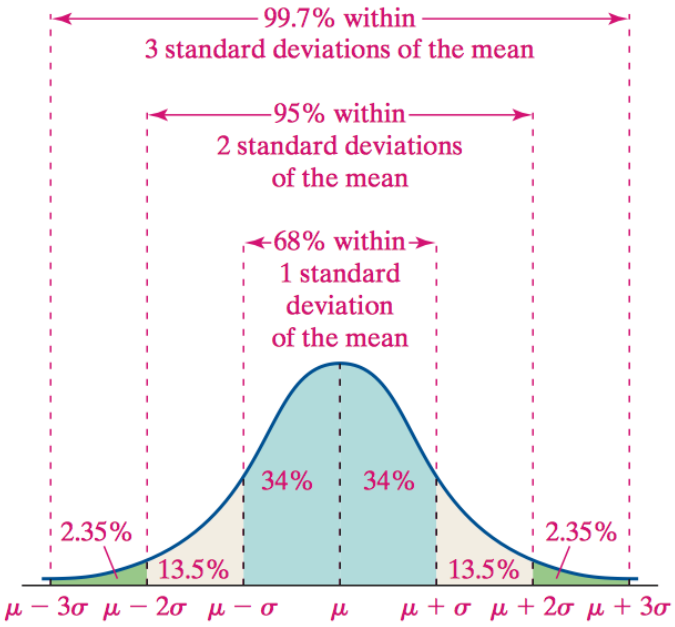

Figure 1.5: Standard Normal Probability Density Function

the probability is 99% that the value of Gaussian random variable z lies within 3σ of its mean μ. Henceforth, we assume that the noise terms e_1, e_2, e_3, and e_4 are independent Gaussian random variables with zero means and the respective σ_1^2, σ_2^2, σ_3^2 and σ_4^2. Two random variables e_i and e_j are independent when E($e_i e_j$)=0 for i ≠ j. The zero-mean assumption implies that the error in each measurement has equal probability of taking on a positive or negative value of a given magnitude. The product of the vector e and its transpose is given by:

$$ee^T = \begin{bmatrix} e_1 \\ e_2 \\ e_3 \\ e_4 \end{bmatrix} [e_1 \quad e_2 \quad e_3 \quad e_4] = \begin{bmatrix} e_1^2 & e_1e_2 & e_1e_3 & e_1e_4 \\ e_2e_1 & e_2^2 & e_2e_3 & e_2e_4 \\ e_3e_1 & e_3e_2 & e_3^2 & e_3e_4 \\ e_4e_1 & e_4e_2 & e_4e_3 & e_4^2 \end{bmatrix}$$

The expected value of ee^T is found calculating the expected value of each entry in the matrix. The expected values of all the off-diagonal elements are zero because the errors are assumed to be independent; the expected values of the diagonal elements are nonzero and correspond to the variance E[e_i^2]= σ_i^2 for i from 1 to 4. The resultant diagonal matrix is usually assigned the symbol R, and the expected value becomes

$$E[ee^T] = \begin{bmatrix} E[e_1^2] & \cdot & \cdot & \cdot \\ \vdots & E[e_2^2] & \cdot & \vdots \\ \cdot & \cdot & E[e_3^2] & \cdot \\ \cdot & \cdot & \cdot & E[e_4^2] \end{bmatrix} = \begin{bmatrix} \sigma_1^2 & \cdot & \cdot & \cdot \\ \cdot & \sigma_2^2 & \cdot & \vdots \\ \vdots & \cdot & \sigma_3^2 & \cdot \\ \cdot & \cdot & \cdot & \sigma_4^2 \end{bmatrix}$$

Furthermore, in order to measure real power, reactive power, voltages, and currents, for instance

in substations, wattmeters, var meters and current meters are used respectively. These quantities are monitored by current and potential transformers installed on the lines and on transformers and buses of substations of the system. The data acquired by the energy control centre always contains inaccuracies since physical measurements cannot be entirely free of errors or noise [15]. These errors can be quantified in a statistical sense. Because of noise, the true values of physical quantities are never known and it is necessary to consider how to calculate the best estimates of the unknown quantities. The best estimates are chosen as those, which minimise the weighted sum of the squares of the measurement error.

Measurements (Z) = True values from system model (hx)+ errors (e).

The measurement Z_1 is the sum of the Gaussian random value e_1 and the constant term hx. The addition of the constant term to e_1 shifts the curve of e1 to the right by the amount of the true value (or to the left if the amount is negative). The shift in no way alters the shape and spread of the probability density function of e1. Hence, Z_1 also has a Gaussian probability density function with a mean value μ_1 equal to the true value and a variance σ_1^2 equal to that of e_1. More accurate measurements are given by choosing the weight wi as the reciprocal of the corresponding variance σ_i^2. Errors of smaller variance thus have greater weight.

$$w_i = R^{-1} = \frac{1}{(\sigma_i^2)} \tag{1.23}$$

Once the variance is known, the corresponding standard deviation is known too and the probability that the ammeter is functioning properly is given by 100% - σ.

1.6 Forecasting Methodology

It is evident that forecasting must be a systematic process dependent on the time period for which it is going to be used. Forecasting methodologies can be classified on the method used. In a more definitive way, they can be categorised as:

- Deterministic;
- Probabilistic;
- A combination of both deterministic and probabilistic methods.
- Artificial intelligence-based techniques, like neural networks, fuzzy logic, expert systems and support vector machines. In load forecasting, optimal algorithms often require the knowledge of underlying densities of measurements and/or noise. As these densities are usually unknown, assumptions are frequently made that compromise the algorithms performance. A common approach to this problem is data density estimation. If a particular density form is assumed or known, then parametric estimation is used. If nothing is assumed about the density shape, non-parametric estimation is the choice [16].

The deterministic approach basically studies the system stability, given a set of network configurations, system loading conditions and disturbances, etc. Since the operation of the power system is stochastic in nature and so are the disturbances, probabilistic approaches have been proposed in order to consider various uncertainties in power systems, such as the loading conditions, fault locations and types, etc [24].

The statistical methods forecast the current load value by using a mathematical combination of the previous loads and/or previous or current values of exogenous factors, typically weather and social variables. Statistical approaches usually require a mathematical model that represents load as

a function of different factors. The two important categories are: additive models and multiplicative models. They differ in whether the forecasted load is the sum (additive) of a number of components or the product (multiplicative) of a number of factors. The additive models are by far more popular. An additive model for predicting the total load Lt may take the form:

$$L_t = L_t^b + L_t^w + L_t^s + \epsilon_t \tag{1.24}$$

Where L_t^b is the base (or normal or weather-normalized) part of the load, which is a set of standardised load shapes for each type of day that has been identified as occurring throughout the year, L_t^w represents the weather sensitive part of the load, L_t^s is a special event component that creates a substantial deviation from the usual load pattern for holidays and other special days, and ϵ_t is the noise. The base load may be further decomposed into the trend (or trend-cycle) component T_t, the seasonal component S_t and the stochastic component Y_t.

Accordingly, the statistical approaches are mathematically based on:

- Extrapolation;
- Correlation;
- A combination of both.

1.6.1 Extrapolation Technique

This is simply a "fitting a trend" approach and the mode of load variation can be obtained from the pattern of historical data and hence the curve fitting function is chosen. Selected well-known functions for the curve fitting are listed below:

- Straight line: Y = a + bx
- Parabola: $Y=a+bx+cx^2$
- Exponential: Y = c.edx

1.6.2 Correlation Technique

This technique is based on the calculation of correlation coefficient, which necessitates the calculation of what is known as variance and covariance as below. Assume two random independent variables x and y, that is, the events x = x_i and y = y_i, are independent events. The product of two random independent variables, xy, is a random variable $x_i y_i$, that is, the expectation of a product is the product of the expectations (only for independent type). That is, E(xy)=E(x)E(y),
Where E represents the "expectation of".
Assume E(x) = μx and E(y) = μy, where μ is defined as the number of events/number of possible outcomes. Therefore, E(xy) =μ_x μ_y.
To measure the deviation from its expected value μ, the quantity σ, defined as standard deviation, is introduced:

$$\sigma = \sqrt{E(X-\mu)^2} \tag{1.25}$$

The variance is defined as

$$\sigma^2 = E(X-\mu)^2 \tag{1.26}$$

The covariance of two independent variables is given by

$$\sigma_{xy}^2 = E(X-\mu_x)E(X-\mu_y) \tag{1.27}$$

Sample variance If x_1, x_2, x_3,..., x_n are n independent observations of a variable x, the sample variance is defined by

$$S_{sv}^2 = (\frac{i}{n})\sum (x_i - \bar{x})^2 \tag{1.28}$$

Where x is the arithmetic mean of the variables, that is,

$$\bar{x} = \frac{(x_1 + x_2 + x_3 + ... + x_n)}{n} = \frac{1}{n}\sum \bar{x} \tag{1.29}$$

For i = 1, 2, 3,..., n. It should be noted that unlike the theoretical σ^2, the sample variance is computed from the observed samples and hence it is actually available. Methods based on correlation technique relate the load to its dependent factors such as weather conditions (humidity, temperature, etc.) and economic and general demographic factors. This could clearly include population data, building permits, and so on.

1.6.3 Method of Least Squares

A curve fit in a polynomial form is represented as below:

$$Y = a_o + a_1 x + a_2 x^2 + ... + A_m x^m \tag{1.30}$$

Start with "simple regression" to fit the straight line $Y = a_1 + a_2 x$ to rectangular points shown in Fig.1.6.

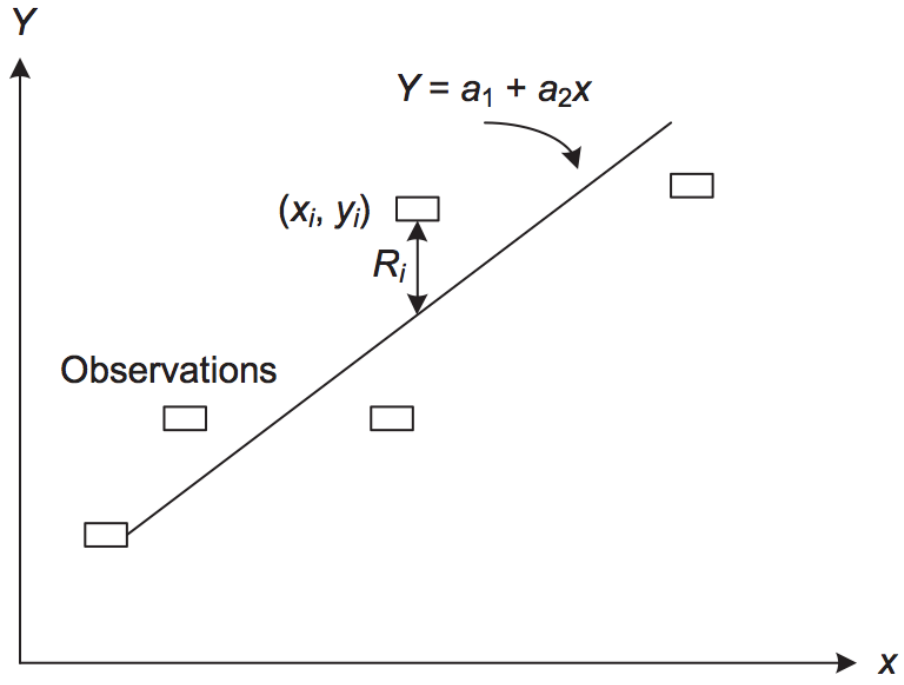

Figure 1.6: Fitting a straight line

The deviation of observation points from the assumed straight line should be minimised. Assuming a set of data (x_i, y_i), i = 1, 2, 3,..., n is represented by some relationship Y = f(x), containing r unknowns $a_1, a_2, a_3, ..., a_r$, the deviations, sometimes called residuals Ri, are formed by

$$R_i = f(x_i) - y_i \tag{1.31}$$

The sum of squares of residuals is

$$S = \sum R_i^2 = sum[f(x_i) - y_i]^2 \tag{1.32}$$

The unknown polynomial coefficients, a's, can be determined so that S is minimum by applying the relations

$$\frac{\partial S_i}{\partial a_i} = 0 \tag{1.33}$$

For i=0,1,...,r This particular form of Equation is known as the "normal equations" and the technique is called the "principle of least squares". The residuals in this case (straight line curve fit) are

$$R_i = (a_1 + a_2 x_i) - y_i \tag{1.34}$$

So that,

$$S = \sum R_i^2 = minimum \tag{1.35}$$

i=1,2,3,...,n.
Thus,

$$S = [(a_1 + a_2 x_1) - y_1]^2 + [(a_1 + a_2 x_2) - y_2]^2 + ... + [(a_1 + a_2 x_n) - y_n]^2 \tag{1.36}$$

Differentiating S partially with respect to a1 and a2, the two relations below are deduced:

$$\frac{\partial S_i}{\partial a_1} = 0 = 2[(a_1 + a_2 x_1) - y_1]^2 + [(a_1 + a_2 x_2) - y_2]^2 + ... + 2[(a_1 + a_2 x_n) - y_n] \tag{1.37}$$

$$\frac{\partial S_i}{\partial a_2} = 0 = 2x_1[(a_1 + a_2 x_1) - y_1] + 2x_2[(a_1 + a_2 x_2) - y_2] + ... + 2x_n[(a_1 + a_2 x_n) - y_n] \tag{1.38}$$

Rearrange the two relations to be written in the form

$$na_1 + (\sum x_i)a_2 = \sum y_i \tag{1.39}$$

$$(\sum x_i)a_1 + (\sum x_i^2)a_2 = \sum x_i y_i \tag{1.40}$$

i=1,2,3,...,n, and in a matrix form

$$\begin{bmatrix} K_{11} & K_{12} \\ K_{21} & K_{22} \end{bmatrix} \begin{bmatrix} a_1 \\ a_2 \end{bmatrix} = \begin{bmatrix} C_1 \\ C_2 \end{bmatrix}$$

where $K_{11} = n, K_{12} = \sum x_i, K_{12} = K_{21}, K_{22} = \sum x_i^2, C_1 = \sum y_i, C_2 = \sum x_i y_i. For i = 1, 2, 3, ..., n.$
The same procedure can be applied when the curve fit is a polynomial of the mth order, where (m + l) linear equations are obtained to be solved for (m + 1) unknowns.

1.6.4 Time-Trend Method

The time-trend method determines the overall trend in historical kWh sales or kW peaks, and develops the forecast based upon that trend known as extrapolation of historical trend [14]. Trending methods forecast future load growth by extrapolating past and present trends into the future. Trending methods are most often categorized according to the mathematical technique used to perform the trend extrapolation. Trending methods work with historical load data, extrapolating past load growth patterns into the future. In this type, the variable to be predicted is expressed purely as a function of time [12]. This function of time is obtained as the function that best explains the available data and is observed to be the most suitable for short-term projections. The most common trending method is polynomial curve fitting, using multiple regressions to fit a polynomial function to historical peak load data and then extrapolating that function into the future to provide the forecast. Polynomial form is the general formula to fit the curves (straight line, parabola, Saturation curve). It depends on the order of the polynomial. Using multiple regressions and deducing the normal equations, it is possible calculate polynomial coefficients. In forecasting a variable that the utilities are concerned with, such as the annual peak load on feeders and substation buses. First, it is necessary to choose or determine a suitable order of the polynomial. The coefficients of this polynomial are then calculated and from that the value of the peak load at any time in the future can be determined. This needs historical data that represent the peak load values at equal spaced time intervals (hourly, weekly, monthly, or annual). The data points must exceed the number of coefficients. Assuming that a cubic polynomial curve fit is used to forecast the peak load of one of the feeders in a distribution system, its form is

$$L_n(t) = a_3t^3 + a_2t^2 + a_1t + a_0 \tag{1.41}$$

$L_n(t)$= annual peak load estimate for feeder n for year t

Where: t represents the year, beginning with t = 1 for the first time period of load history. $a_3, a_2, a_1, anda_o$ are the coefficients of the particular polynomial for feeder n and can be determined by using the multiple regressions method. They may vary from one feeder to another according to the historical data. The same polynomial curve fit could be used for all feeders in the distribution system. On the other hand, different forms of polynomial equations to different feeders could be applied. It depends on the feeder's historical data and the best polynomial to choose. The first step to apply multiple regressions technique is to determine the parameter matrix P. The number of rows of this matrix is equal to the number of years/months of data, while the number of columns is equal to the number of polynomial coefficients. The second step is to determine the load vector L_n whose elements are the peak load readings of the past years/months. The third step is to determine the coefficients a_3, a_2, a_1, and a_o by applying the equation

$$C_n = [P^T P]^{-1} P^T L_n \tag{1.42}$$

Where

$$C_n^T = [a_3 a_2 a_1 a_o] \tag{1.43}$$

Substituting coefficients' values into Equation$L_n(t) = a_3t^3 + a_2t^2 + a_1t + a_0$, the projected value of the peak load for any year following the last historical data point can be calculated.

1.6.5 Regression Methods

Regression is one of the most widely used statistical techniques. The general purpose of multiple regression is to learn more about the relationship between several independent or predictor variables. Multiple regression is based on least squares: the model is fit such that the sum-of-squares of differences

of observed and predicted values is minimised. For electric load forecasting regression methods are usually used to model the relationship of load and other factors such as weather, day type and customer class. The model expresses the load as a linear function of one or more explanatory variables and an error term:

$$L_t = a_0 + a_1 L_t^{(1)} + ... + a_k Lt^{(k)} + \epsilon_t, \tag{1.44}$$

Where L_t is the load, $L_t^{(1)}, \ldots, L_t^{(k)}$ are explanatory variables correlated with the load and, $a_1, ..., a_k$ are the regression coefficients and ϵ_t is the noise. The explanatory variables can be simple, like maximum daily temperature, or complex functions of simple variables, such as squared difference between maximum and minimum daily temperatures. In its classical form, multiple regression assumes that the relationship between variables is linear. Fortunately, multiple regression procedures are not greatly affected by minor deviations from this assumption. However, it is good practice to always look at a scatterplot of the variables of interest. If curvature in the relationships is evident, one may consider either transforming the variables, or explicitly allowing for non-linear components. Despite the large number of alternatives the linear regression models are still among the most popular load-forecasting approaches.

1.6.6 Stochastic Time Series: Autoregressive Model

Time series models are based on the assumption that the data have an internal structure, such as autocorrelation, trend or seasonal variation. The forecasting methods detect and explore such a structure [11]. If the load Lt is assumed to be a linear combination of previous loads, then the Auto-Regressive (AR) model can be used to forecast future load values. A pth-order autoregressive, AR(p), model is defined as:

$$L_t - \sum_{i=1}^{p} \phi_i L_{t-1} = \epsilon_t \tag{1.45}$$

Where ϵ_t is a random load disturbance (or prediction error), and $\phi_1, ..., \phi_p$ are the unknown AR coefficients. The order of the model tells how many lagged past values are included. The simplest AR model is the first-order AR(1). The ϵ_t's are assumed to be Gaussian with zero mean and finite variance σ^2. Intuitively, a process l_t is stationary if its statistical properties do not change over time. More precisely, the probability distributions of the process are time-invariant. It assumes that the mean, variance and autocorrelation structures do not change over time. Strictly speaking, the mean and variance are constant and the auto-covariance is a function of (t - s) only. The auto-regression model can be also viewed as a special case of the multiple regression model, where the independent or predictor variables are the past values of the process itself.

1.6.7 ARIMA model approach for short-term load forecasting

Autoregressive integrated moving average (ARIMA) is a popular procedure among the statistical models for time series analysis and forecasting applications [13]. The ARIMA model originates from the autoregressive (AR) model, moving average (MA) model, and the combination of AR and MA (ARMA) models. Generally, AR, MA, and ARMA time series models are stationary; however, if the series are non-stationary, these series are transformed into a stationary time series using the difference process. Specifically, the autoregressive integrated moving average (ARIMA) model has three types of parameters:

- The autoregressive parameters ($\phi_1, ..., \phi_p$);
- The number of differencing passes at lag 1 (d);

- And the moving average parameters $(\delta_1, ..., \delta_q)$.

In the notation (introduced by Box and Jenkins) a series that needs to be differenced d times at lag 1 and afterwards has orders p and q of the AR and MA components, respectively, is denoted by ARIMA(p,d,q) and can be conveniently written as:

$$\phi_p(B)\nabla^d L_t = \delta_q(B)\epsilon_t \tag{1.46}$$

Where,

$$\nabla x_t \equiv (1 - B)x_t \tag{1.47}$$

is the lag 1 differencing operator, B is the backward shift operator, i.e. $B^h x_t \equiv x_t - h, \phi(B)$ is a shorthand notation for

$$\phi(B) = 1 - \phi_1 B - ... - \phi_p B^p, \tag{1.48}$$

and $\delta(B)$ is a shorthand notation for

$$\delta(B) = 1 + \delta_1 B + ... + \delta_q B^q \tag{1.49}$$

.

1.6.8 ARIMA model procedure

The ARIMA modelling procedure, which was developed by Box and Jenkins (1976), consists of three iterative steps:

1. Model identification;
2. Parameter estimation;
3. Diagnostic checking.

The procedure of the ARIMA model is itemised as follows:

Step 1: Model identification. Determines whether the time series is stationary or non-stationary. If the time series is non-stationary, it is transformed into a stationary time series using a suitable degree of differencing.

Step 2: Parameter estimation. Once the tentative model is formulated, the related model parameters are estimated using the least squares scheme. Parameters are estimated to have zero gradient of forecasting errors to the historical load data. The primary objective of this parameter estimation is to minimise the forecasting error and determine both the model order and its parameters.

Step 3: Diagnostic checking. When the parameters have been well estimated, examining the residuals validates the tentative model accuracy. The residuals should simulate the noise process. These steps are repeated until an adequate model is identified. When the steps in ARIMA modelling are completed, a specific ARIMA model is applied to predict the future load, typically 24 h ahead.

1.7 A State Estimation Framework

A Measurement Based Load Modelling establishes a relationship between certain independent variables such as weather conditions, the day type and the total load. It aims to extract regression coefficients from static past data for possible future forecasting. These models could also incorporate dynamic behaviour such as in ARMAX (Auto Regressive Moving Average and Explanatory variable (X)). The multiple regressions explain the formulation of such modelling as follows [20].

$$S_t = c_t x_t + \epsilon_t \tag{1.50}$$

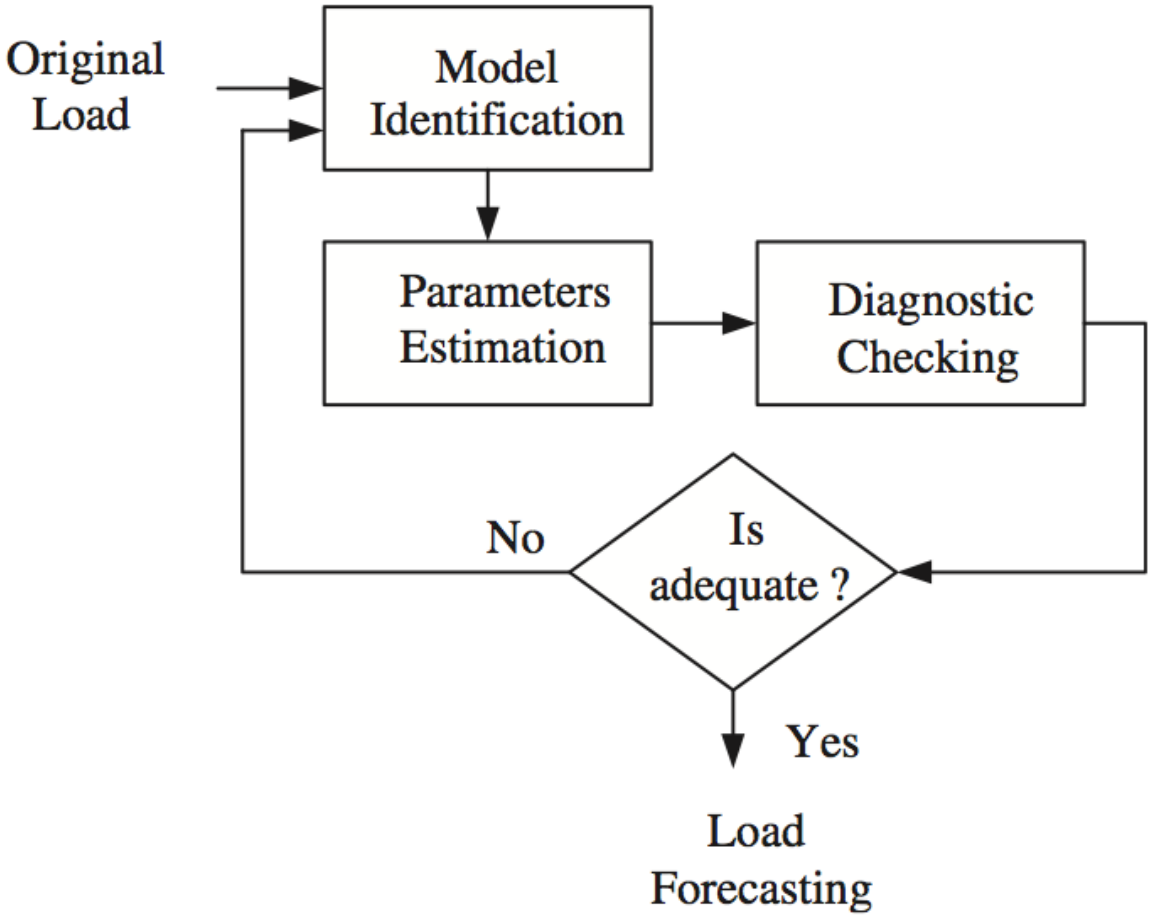

Figure 1.7: ARIMA modelling procedure scheme

Where S_t measured system load data, t sampling time, x_t vector of adapted variables such as time, temperature, light intensity, wind speed, humidity, day type (workday, weekend), etc., c_t regression coefficients, and ϵ_t model error at time t. Households belonging to the direct electric heating group, for instance, will have different regression coefficients to those belonging to the district heating group. The target of this load modelling type is estimating unmeasured load points based on statistical information and other variable measurements, or forecasting future load. A pure time series model with no additional explanatory variables is proposed in [21], as shown by:

$$kWh_{i,today} = \frac{kWh_{i,today-1}}{kWh_{i-1,daybefore}} kWh_{i,daybefore} \tag{1.51}$$

The previous model requires the past hour consumption of customer i. Smart meters, however, collect electricity consumption data at half hour or one hour intervals and this metering data will be sent to the utility the following day. With one day data delay other time series models such as Autoregressive Integrated Moving Average (ARIMA) will also fail to keep up with the dynamism of the load [20]. ARX (Auto Regressive with exogenous input) model could be applied, since it utilises previous day AMR (Automatic Metering Reading) metered consumption data as well as same day explanatory variables such as temperature, day structure, humidity, etc..

The state estimation framework presented in [19] as shown in figure 1.8 consists of three fundamental functions:

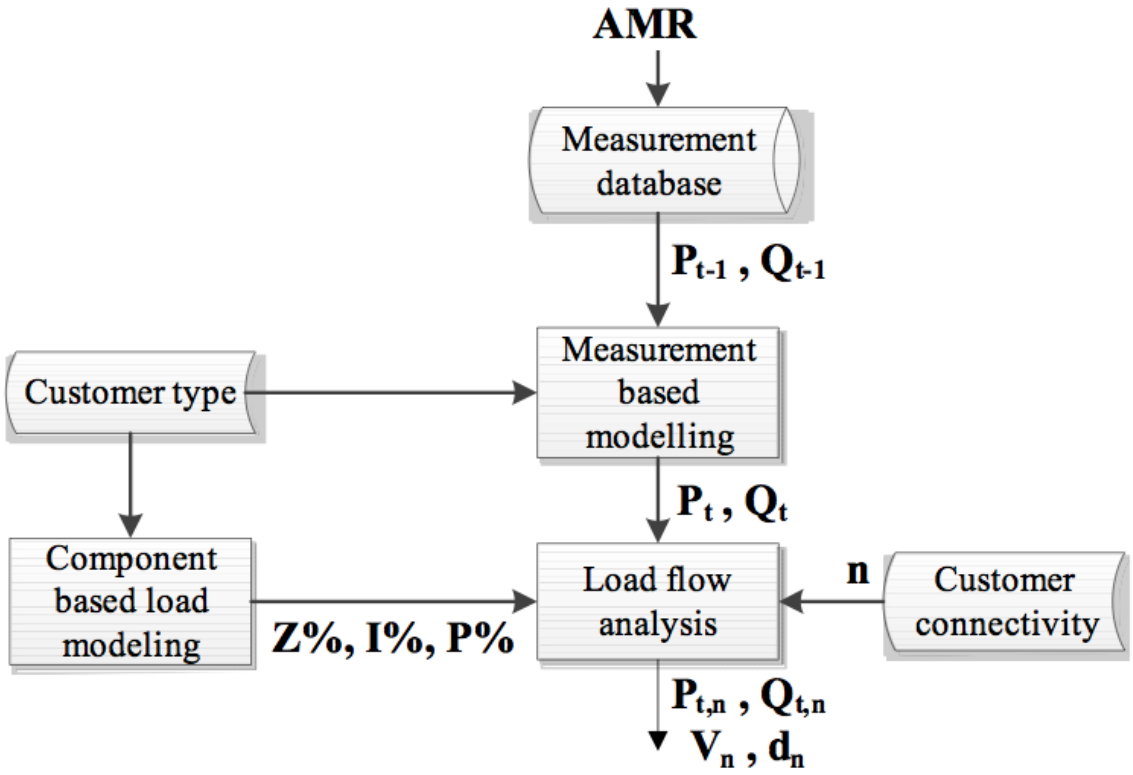

Figure 1.8: A state estimation framework for an active distribution network

1. the measurement based modelling;
2. the component based modelling as illustrated in 1.2;
3. load flow analysis.

The measurement based modelling, explained in previous, provides real time or near future forecasts of the loading situation while the component based modelling in section 1.2 is used to undertake an effective and detailed load flow analysis by translating nodal power demand to voltage magnitude and phase figure 1.8.

1.7.1 Auto-Regressive with exogenous input model

ARX model is an autoregressive model supported by exogenous variables and it is used to perform one day ahead load forecasting. The model has lagging hourly consumption information from the same hour in the previous week and the previous day same hour load, since available measurements are only from the previous day's metering. The effects of the previous two hours' temperatures together with real time temperature are included in the explanatory variable. The day structure effect is included through weekday and weekend dummy variables, as follows:

$$\begin{aligned} Y_t = c + \alpha_1 Y_{t-24} + \alpha_2 Y_{t-168} + \alpha_3 T_t + \alpha_4 T_{t-1} + \\ \alpha_5 T_{t-2} + \alpha_6 DL_d + \alpha_7 WD + \alpha_8 WE + \epsilon_t \end{aligned} \tag{1.52}$$

Where,

Y_t : kWh consumption at hour t
T_t : Temperature at hour t
DL_d : Day length to represent the light amount of day d
WD: Weekday dummy variables (0 or1)
WE : Weekend dummy variables (0 or 1)
c: Constant
ϵ_t : White noise
The parameters $\alpha_1, \alpha_2, \alpha_3, ..., \alpha_8$ could be estimated using an Ordinary Least Squares (OLS) estimator (See subsec:1.6.3) [23].

Chapter 2

Distribution Systems Analysis

2.1 Introduction

For distribution networks load-flow studies are essential to determine the capability of a network under all loading conditions and network configurations. This includes taking account of the loss of one or more circuits including the infeed power sources, whether from DG within the network or from transformer substations where the infeed power is obtained from a higher voltage network. Usually LV networks operate radially and as a consequence analysis of these networks is relatively simple. On the other hand, information about the individual load points is limited with the yearly/monthly unit consumption at low voltage is known. In order to carry out power flow analysis on LV networks it is necessary to apply load shapes. This is because loads do not peak at the same time; otherwise, it will result in too high values of current flows and therefore the overall voltage drop.

2.2 Hosting Capacity of Distribution Networks

Adding new production or consumption in distribution network will affect the power flow. The performance of the network might improve or deteriorate for the majority of connected customers. In [39] the Hosting Capacity is defined as:

The maximum amount of new production or consumption that can be connected without endangering the reliability or quality for other customers.
The amount of Distributed Energy Resources (DER) the network can host depends on a number of parameters such as the characteristics of the generation units, the configuration and operation of the network, the requirements of the loads as well as national and regional requirements. Different distributed generation technologies provide different control capabilities over both the active and reactive power. The impact of distributed generation can be quantified only by using a set of performance indicators. In some cases, the performance of the system will improve after the connection of distributed generation; in other cases, it will deteriorate. It is the latter cases that have received the most attention. A deterioration of the supply is not directly a concern, as long as the resulting quality is within an acceptable range. In other words, for every performance index there exists a limit that should not be exceeded. This is shown schematically in Fig. 2.1.

The hosting capacity is defined as the amount of distributed generation for which the performance becomes unacceptable. The performance index decreases with increasing amount of distributed generation, in this example. For small amounts of distributed generation, the index remains above the limit and the system performance is still acceptable. But for larger amounts of distributed generation,

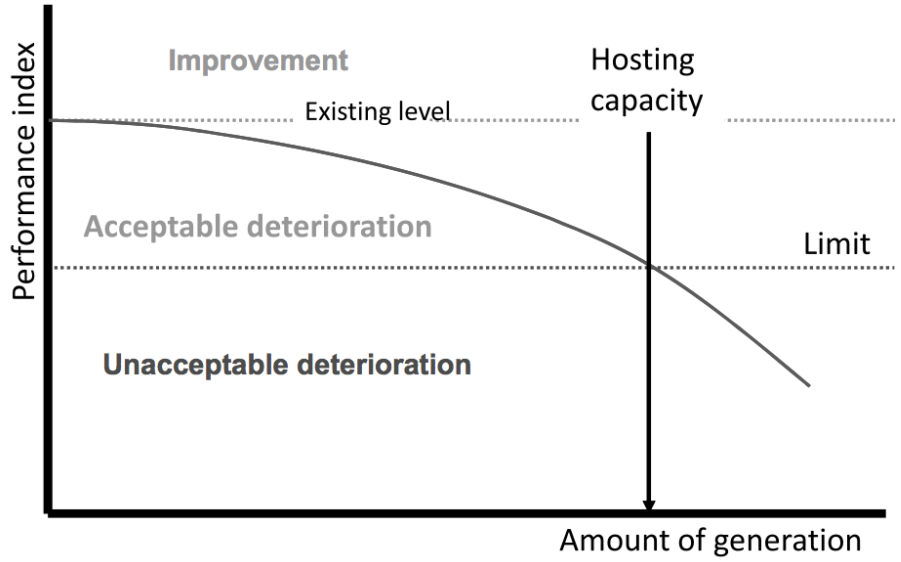

Figure 2.1: High Performance Index for Hosting Capacity

the performance becomes unacceptable.

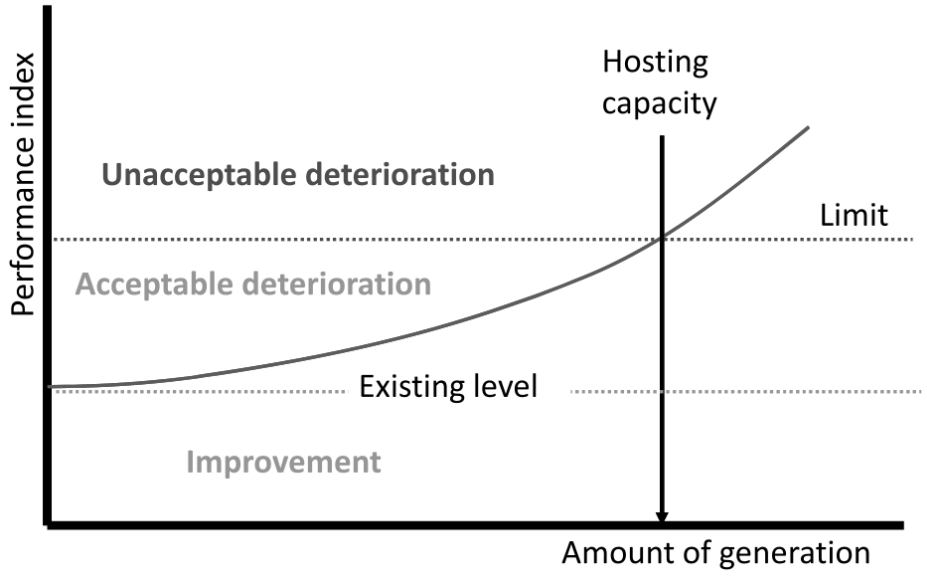

Figure 2.2: Low Performance Index for Hosting Capacity

In Fig 2.1, the performance index was defined such that a higher value corresponds to a better performance. In practice, many performance indices are defined such that a lower value corresponds to a better performance. This is illustrated in Fig 2.2. The deteriorating performance with increasing amount of distributed generation corresponds to the rising level of the performance index. An example is the maximum voltage magnitude experienced by any of the costumers in a distribution network. Adding generation to the feeder will result in an increase for this maximum voltage magnitude. For small amounts of generation the increase will be small, but for larger amounts of generation the voltage could become unacceptably high. In that case, the hosting capacity has been exceeded. An example is the maximum voltage magnitude experienced by any of the costumers in a distribution network as discussed in Section 2.6.1. Adding generation to the feeder will result in an increase for this maximum voltage magnitude. For small amounts of generation the increase will be small, but for larger amounts

of generation the voltage could become unacceptably high. In that case, the hosting capacity has been exceeded [38] . There are also cases in which the introduction of distributed generation will initially result in an increase in performance of the power system. But for large amount of distributed generation, the performance will deteriorate. This is illustrated in Fig 2.3.

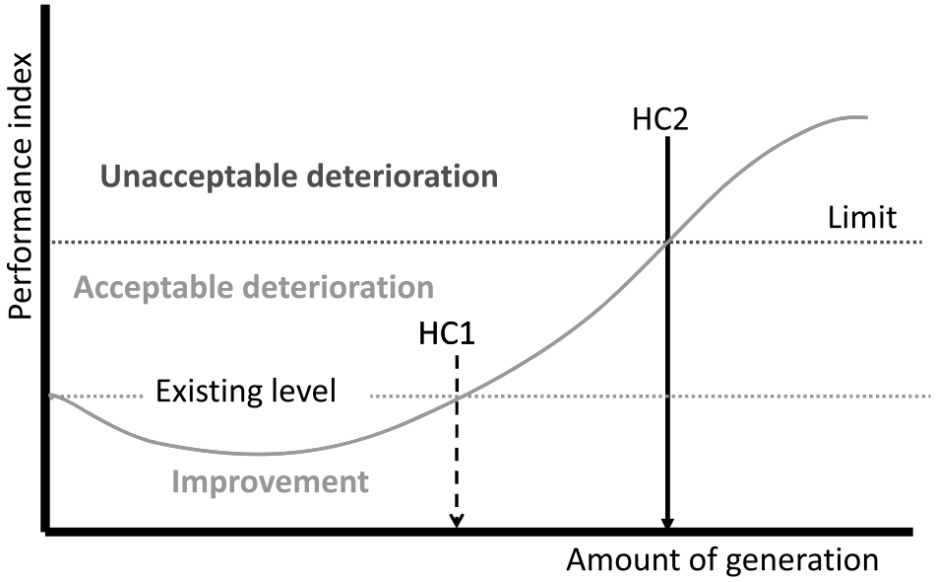

Figure 2.3: initial improvement Performance Index for Hosting Capacity

Two hosting capacities can be distinguished in this case:

- the above hosting capacity which the system performance deteriorates compared to the no generation case;
- the second hosting capacity above which the system performance becomes unacceptable.

Examples of this are the risk of overload and the losses in the grid. Both will initially reduce but will increase when large numbers of distributed generation are connected. To know how much distributed generation can be connected, it is important to define appropriate performance indicators. The hosting capacity is based on this. The choice of index and limit will have a big influence on the amount of distributed generation that can be accepted.

2.3 Impact of load models on power loss calculation in DG planning

The current absorbed by the load shown in figure:

$$I_{Load} = \frac{(P_{Load} + jQ_{Load})}{(\sqrt{3}V_{receiving})} \tag{2.1}$$

Line loss on a distribution feeder without distributed generation is:

$$P_{(Loss-NoDG)} = R.I_{Load}^2 = R.\left(\frac{P_{Load} + jQ_{Load}}{\sqrt{3}V_{receving}}\right)^2 \tag{2.2}$$

Where R includes Ł$_{Load}$ line length. The DG output current injected in the network is given as:

$$I_{DG} = \frac{(P_{DG} - jQ_{DG})}{(\sqrt{3}V_{receiving})} \tag{2.3}$$

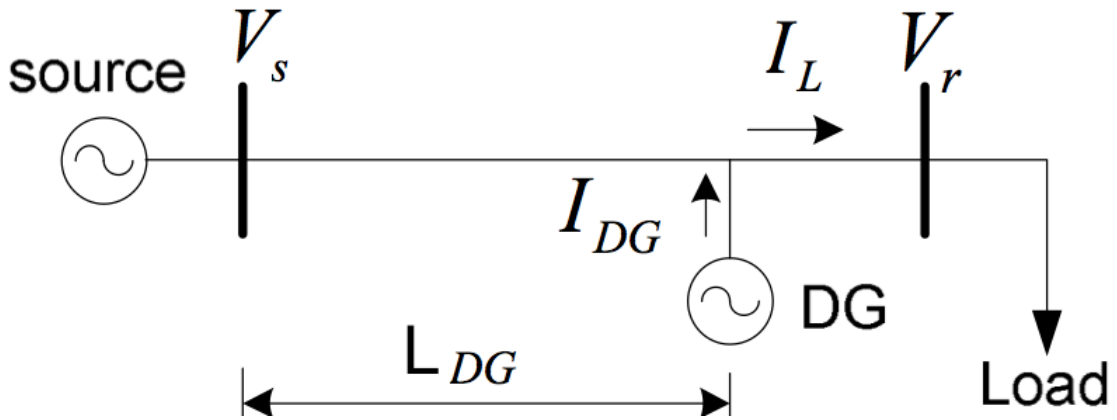

Figure 2.4: Line diagram of a distribution system with DG

Therefore, the total power loss for a fixed PQ load model with P_{Load} and Q_{Load} constant can be expressed as:

$$\begin{aligned} &P_{(Loss-WithDG)} = rL_{Load}.I_{Load}^2 + rL_{DG}.I_{DG}^2 = \\ &\frac{(rL_{Load})}{(\sqrt{3}V_{receiving})^2}.[(P_{Load} + jQ_{Load})^2 + (P_{DG} - jQ_{DG})^2.(\frac{L_{DG}}{L_{Load}})] = \\ &\frac{(rL_{Load})}{(\sqrt{3}V_{receiving})^2}[(P_{Load}^2 + Q_{Load}^2) + (P_{DG}^2 + Q_{DG}^2 - 2P_{Load}P_{DG} - 2Q_{Load}Q_{DG}) \\ &.(\frac{L_{DG}}{L_{Load}})] \end{aligned} \tag{2.4}$$

The power loss equation shows that, in a distribution system including Distributed Generation, a positive sign of power loss indicates that the system loss decreases with the integration of DG. In contrast, the negative sign of power loss implies that DG causes higher system loss. While in terms of voltage dependent load model, the power losses could be obtained as:

$$\begin{aligned} &P_{(Loss-WithDG)} = \frac{(rL_{Load})}{(\sqrt{3}V_{receiving})^2}[(P_{Load}^2 V_{receiving}^{\alpha 2} + Q_{Load}^2 V_{receiving}^{\beta 2}) \\ &+(P_{DG}^2 + Q_{DG}^2 - 2P_{Load}V_{receiving}^{\alpha}P_{DG} - 2Q_{Load}V_{receiving}^{\beta}Q_{DG}).\left(\frac{L_{DG}}{L_{Load}}\right)] \end{aligned} \tag{2.5}$$

It is difficult to find out a mathematical criterion to determine whether the loss is reduced or increased, since $V_{receiving}$, α, β, P_{DG} and Q_{DG} are independent variables.

2.4 DG Power Factor

The load power factor is corrected to unity by capacitors.. However, such device is insufficiently fast and not flexible to compensate for transient events due to the impact of intermittent renewable resources as previously mentioned. DG unit as a fast response device that can deliver both active and reactive power could be installed to correct the system power factor as explained below. Figure 2.5 showa generator convention where the relationship between active and reactive power of DG unit at each bus i can be expressed as

$$Q_{DGi} = a_i P_{DGi} \tag{2.6}$$

where $a_i = \pm tan(cos^{-1}(PF_{DGi}))$

The positive sign for DG reactive power injection, whereas the negative sign is for consumed reactive power. PF_{DGi} correspond to the power factor of DG unit at bus i, while Q_{DGi} and P_{DGi} correspond to the real and reactive power of DG unit at bus i, respectively. Dispatching the power factor is limited by its fixed apparent power capability S_{DGi} and its variable real power generation through the relationship [51]:

$$PF_{DGi} = \frac{P_{DGi}}{S_{DGi}} = \frac{P_{DGi}}{\sqrt{{P_{DGi}}^2 + {Q_{DGi}}^2}} \tag{2.7}$$

It is assumed that S_{DGi} =1p.u., the value PF_{DGi} can be variable in the range from 0 to 1, when the real power output P_{DGi} is varied from 0 to 1 p.u. The power factor depends on the operating conditions and technologies adopted. As illustrated in figure 2.5, DG unit considered in this study can fall in the following types by setting value PF_{DGi} in different ways. The type with a unity power factor is capable of injecting active power only. However depending on the sign as mentioned before, power factor can vary from 0 to 1: in case of positive sign DG units are capable of injecting both real and reactive power, whereas for a negative sign DG units are capable of injecting real power and absorbing reactive power.

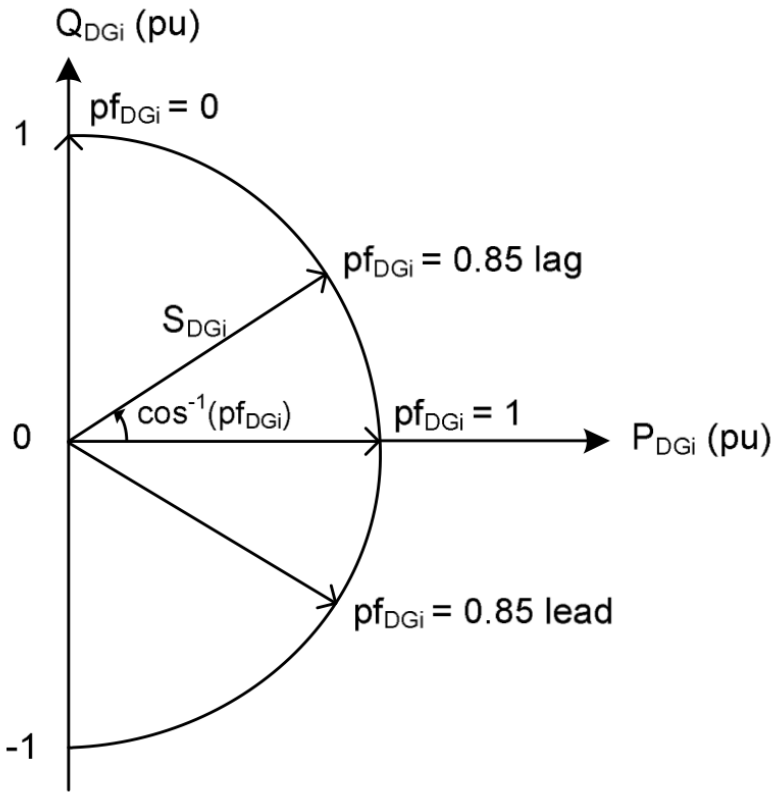

Figure 2.5: Distributed generation capability curve [51]

2.5 Power Flow Analysis

The power-flow analysis of a distribution feeder is similar to that of an interconnected transmission system. Typically, what will be known prior to the analysis will be the three-phase voltages at the substation and the complex power of all of the loads and the load model (constant complex power, constant impedance, constant current, or a combination). Sometimes the input complex power supplied to the feeder from the substation is also known. A power-flow analysis of a feeder can determine the following by phase and total three-phase [6][7]:

- Voltage magnitudes and angles at all nodes of the feeder;
- Line flow in each line section specified in kW and kvar, amps and degrees, or amps and power factor;
- Power loss in each line section;
- Total feeder input kW and KVAR;
- Total feeder power losses;
- Load kW and KVAR based upon the specified model for the load.

2.5.1 Active Power Flow with DG penetration

In Section 2.3, the power loss modelling was discussed considering the DG integration. Referring to the same distribution feeder and neglecting the reactive power flows, the total power flow is given by:

$$P(t) = P_{Loads} - P_{DG} \tag{2.8}$$

We assume that no overloading situation exists before the introduction of distributed generation [40]. As long as the maximum power flow after a DG unit connection is less than that before, and again there will be no overload. The condition to be fulfilled is

$$P_{max} < P_{Loads,max}$$

With large amounts of generation, the maximum power flow occurs for maximum generation and minimum consumption:

$$P_{max} = P_{DG,max} - P_{Loads,min} \tag{2.9}$$

and the condition for guaranteeing no overload is

$$P_{max} < P_{Loads,max}$$

With large amounts of generation, the maximum power flow occurs for maximum generation and minimum consumption:

$$P_{DG,max} < P_{Loads,max} + P_{Loads,min} \tag{2.10}$$

These conditions should be fulfilled for every location on the feeder. This is a sufficient requirement that could be used as a first hosting capacity level. As long as the maximum generation is less than the sum of minimum and maximum consumption, no overloading will occur. When the maximum generation exceeds this first hosting capacity level for any location along a feeder, additional studies are needed to determine a second hosting capacity level. The second hosting capacity is reached when the maximum current becomes equal to the ampacity of the feeder section. The maximum power through the feeder section is again given in Equation 2.9. The maximum power flow must be lower than the maximum permissible power [41] :

$$P_{max} = P_{DG,max} - P_{Loads,min} < P_{max,limit} \tag{2.11}$$

resulting in the following condition:

$$P_{DG,max} < P_{max,limit} + P_{Loads,min} \tag{2.12}$$

This approach requires that minimum and maximum loads are known in order to find the hosting capacity. In reality, information about the minimum load is often not available. This could easily result in an underestimation of the hosting capacity.

2.5.2 Active and Reactive Power Flow with DG penetration

Including the contribution of the reactive power to the current, the expressions become more complicated although the methodology remains the same. The maximum apparent power for a feeder section without generation is equal to

$$S_{max,1} = \sqrt{P_{Loads,max}^2 + Q_{Loads,max}^2} \tag{2.13}$$

Here it is assumed that the time variations in active and reactive power demand are the same, so the maximum reactive power is reached when both active and reactive power consumption are at their maximum. When active and reactive power consumption show significantly different variations with time, this should be included in the study. In this case, a time-domain simulation might be more appropriate. With a substantial amount of generation connected to the feeder, the maximum apparent power is reached for minimum consumption and maximum generation:

$$S_{max,2} = \sqrt{(P_{DG,max} - P_{Loads,min})^2 + Q_{Loads,min}^2} \tag{2.14}$$

where it is assumed that the generation neither produces nor consumes reactive power. The maximum apparent power flow with generation should be less than the maximum apparent power flow without generation.

$$S_{max,2} < S_{max,1} \tag{2.15}$$

$$P_{Loads,max} = \sqrt{S_{max,Ampacity}^2 - Q_{Loads,max}^2} \tag{2.16}$$

This results in the following expression for the first hosting capacity:

$$P_{DG,max} < P_{Loads,min} + P_{Loads,max} \tag{2.17}$$

$$P_{DG,max} < P_{Loads,min} + \sqrt{S_{max,Ampacity}^2 - Q_{Loads,max}^2} \tag{2.18}$$

The second hosting capacity is reached when the current through the feeder section reaches the Ampacity of the feeder. The maximum current, or apparent power, is found from Equation 2.10. This should be less than the maximum permissible apparent power (ampacity times nominal voltage).

After the introduction of distributed generation, the minimum consumption is important, because the Hosting Capacity is directly dependent on the minimum consumption. Every watt reduction in minimum consumption gives 1 W reduction in the hosting capacity. The minimum consumption still needs to be estimated to determine the hosting capacity. In low-voltage networks, the diversity between customers is large because of the low number of customers. The ratio between maximum and

minimum consumption is large at low voltage. The additional hosting capacity due to the minimum consumption is small. Furthermore, the minimum consumption is uncertain, so a low value needs to be chosen to prevent a too high risk of feeder overload. Choosing the minimum consumption equal to zero is an acceptable decision for low-voltage feeders. Obviously, when a more accurate minimum value is available, this one should be used. Accordingly, the load modelling and data analysis techniques play an important role [42].

2.6 Impacts of embedded generation on the distribution system

Distribution networks are designed to operate radially without any generation on the network (Passive mode). Traditionally, electricity was generated by large power plants, delivered to customers through distribution networks. Thus the flow of real and reactive power was from the higher to the lower voltage levels. The connection of distributed generation on the distribution network may have a significant impact on the flow of the power (active and reactive), voltage level and fault currents. DG increases the voltage at its connection point and may reverse the power flow on the feeder [1]. When a large amount of DG power is to be integrated, it should be ensured that the voltage increase along the feeder does not exceed the maximum allowed voltage and the power flow does not exceed conductor ampacity. Nowadays, networks are already complete almost everywhere and the integration of distributed generation into a distribution network changes both the costs and the constraints on distribution network planning. Then restructuring planning is needed to avoid high voltage drop, high costs of network losses, weak electro-thermal conditions, low reliability of power delivery or low short-circuit capability. Load flow calculation can be evaluated and monitored to have precise information about the whole system and to prioritise restructuring targets. In monitoring calculation voltage drops and current faults are calculated on the strength of the network data and load curve models of different customers groups. The objective of the monitoring calculation is to define a state of existing or simulated networks (in a maximum load situation). If the existing network is well dimensioned and allows DG to be connected, then the utilisation is more effective by collecting data from network state and by developing data processing systems. Thus, an over-dimensioning is avoided. [2] In distribution networks over-voltage issues occur when distributed generation output is at maximum and load demand at its minimum. Information on the period of minimum and maximum load should be established. In addition the behaviour of the production must be known. A simple solution to a general network planning including DG is determined by selecting a production level and the calculation of hourly load-flows based on load curves for a period of planning. This analysis is then repeated several times with different production levels.

2.6.1 Voltage profile variation owing to DG penetration on Distribution Networks

Network voltage changes:

Every distribution operator has an obligation to supply its customers a voltage within specified limits. This requirement often determines the design of the distribution circuits. Over the years, techniques have been developed to make the maximum use of distribution circuits to supply customers within the required voltages. The voltage profile of a radial distribution feeder [8] is shown in Figure 2.6. shows that the ratio of the MV/LV transformer has been adjusted using off-circuit taps so that at times of maximum load the most remote customer will receive acceptable voltage. During minimum load the voltage received by all customers is just below the maximum allowed. If an embedded generator is now connected to the end of the circuit then the flows in the circuit will change and hence

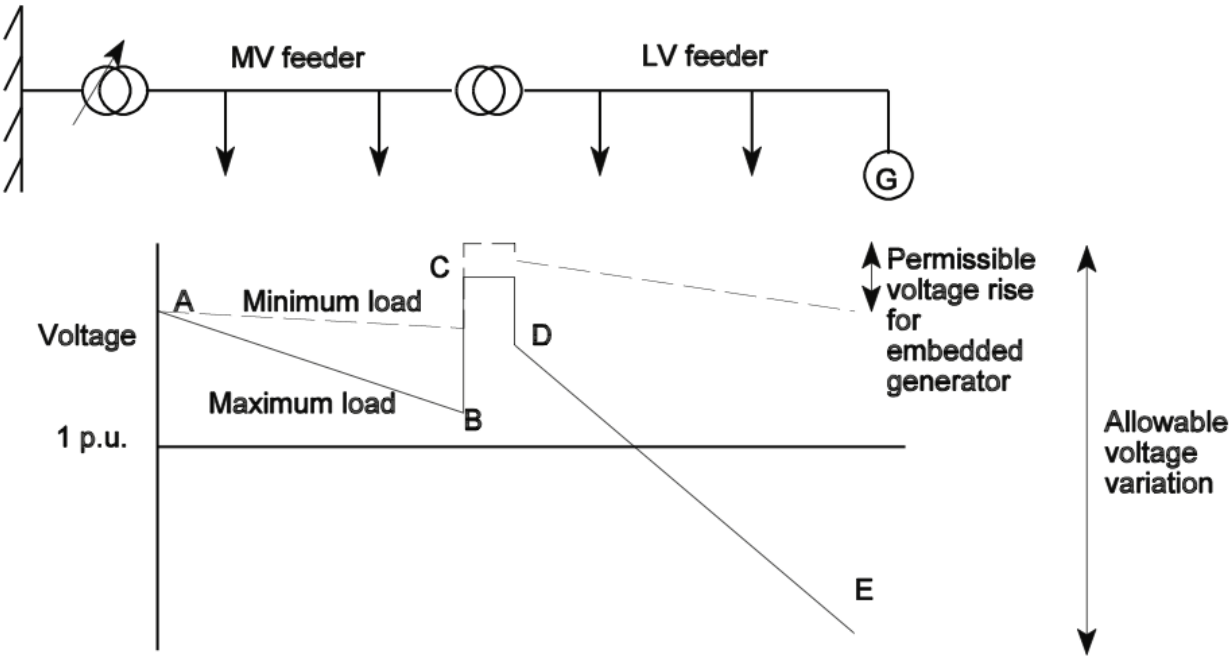

Figure 2.6: DG impact on voltage profile of a radial system [8]

the voltage profile. The most onerous case is likely to be when the customer load on the network is at a minimum and the output of the embedded generator must flow back to the source. For a lightly loaded distribution network the approximate voltage rise (ΔV) due to the generator is given (in per unit) by

$$\Delta V = \frac{PR + XQ}{V} \tag{2.19}$$

In some cases, the voltage rise can be limited by reversing the flow of reactive power (Q) either by using an induction generator or by under-exciting a synchronous machine and operating at leading power factor. This can be effective on MV overhead circuits, which tend to have a higher ratio of X/R. On LV cable distribution circuits the dominant effect is that of the real power (P) and the network resistance (R) and so only very small-embedded generators may generally be connected out on LV networks. For larger generators a point of connection is required either at the LV bus bars of the MV/LV transformer or, for larger plants, directly to an MV or HV circuit. An alternative simple approach to deciding if a generator may be connected is to require that the three-phase short-circuit level (fault level) at the point of connection is a minimum multiple of the embedded generator rating. Some distribution utilities use more sophisticated control of the on-load tap changers of the distribution transformers including the use of a current signal compounded with the voltage measurement. One technique is that of line drop compensation [9] and, as this relies on an assumed power factor of the load, the introduction of embedded generation and the subsequent change in power factor may lead to incorrect operation if the embedded generator is large compared to the customer load.

The connection of a generator to the distribution network will result in a voltage rise at the terminals of the generator and at each point along the feeder wire. The relative voltage rise, in function of the wire's X/R ratio, is approximately equal to:

$$\Delta V = |U - V| = |Z_L I| \tag{2.20}$$

$$\Delta V = |R(1 + \alpha j)\frac{P}{V}(1 + kj)| \tag{2.21}$$

$$\frac{\Delta V}{V} = \frac{PR}{V^2}|1 - \alpha k + (\alpha + k)j| \tag{2.22}$$

Where,
U is the feeder voltage;
V is the wire's receiving end voltage voltage at DG generator terminals;
$Z_L = R + Xj = R(1 + \alpha j)$ is the line impedance;
α is theX/R ratio;
$I = \frac{(P+Qj)}{V} = \frac{P}{V}(1 + kj)$;
k is the Q/P ratio flowing in the line;

In case of no loads connected during the DG generation, the voltage variation depends on the X/R ratio, the P (injected from DG generator to the network, in this case) and the Q/P ratio. And from the latter equation it is evident that the voltage variation at the DG generator terminals may be obtained by setting to zero the X/R ratio:

$$\frac{\Delta V}{V} = \frac{PR}{V^2}|1 - 0k + (0 + k)j| \tag{2.23}$$

Thus,

$$\frac{\Delta V}{V} = \frac{PR}{V^2}|1 + kj| \tag{2.24}$$

Where,
R is the source resistance at the terminals of the generator;
P is the injected active power;
V is the generator's nominal voltage.

The same relative voltage rise is experienced by all customers connected downstream of the generator and holds for all practical cases at distribution level. In Section 2.3 the power loss in a radial system is considered during the injection of power from a DG unit.
The maximum permissible voltage rise, with connection of a distributed generator, is the one that brings the maximum voltage magnitude exactly at the over-voltage limit. The "over-voltage margin" is defined as the difference between the maximum voltage magnitude for a given customer and the over-voltage limit. The "hosting capacity", introduced previously, is the maximum amount of generation that can be connected without resulting in an unacceptable quality or reliability for other customers. From this it follows that when considering over-voltages, the hosting capacity is the amount of generation that gives a voltage rise equal to the over-voltage margin. Each customer has a different over-voltage margin. The connection of a generator to a distribution feeder gives the same relative voltage rise for every location downstream of the generator. The hosting capacity can easily be calculated, considering at the moment active power injection only (k=0) from 2.27 as:

$$P_{max} = \frac{V^2}{R}\delta_{max} \tag{2.25}$$

Where,
$\delta_{max} = \frac{\Delta_{max}}{V}$ the relative over-voltage margin (in percent);
Δ_{max} the absolute voltage margin (in volt).

To understand what impacts the hosting capacity has, it is necessary to look at the relation between the wire's resistance and it's section:

$$R = \rho\frac{l}{A} \tag{2.26}$$

Where "l" is the length and "A" the cross section of the wire. Thus,

$$P_{max} = \frac{V^2}{\rho l} A \delta_{max} \tag{2.27}$$

From the latter equation it is possible to notice that:

- The hosting capacity is proportional to the square of the voltage level and to the relative voltage margin (in percent);
- The hosting capacity is linear with the size of the line;
- The hosting capacity is inversely proportional to the distance between the generator and the transformer. The further away from the transformer, the smaller the hosting capacity.

It should be noted here that, all these parameters are dependent and changing one of those it would have impacts on the others.

2.7 Voltage and Reactive Power Control in Distribution Systems

The voltages in a distribution system and to the consumers must be maintained within a certain plus-minus band around the rated equipment voltage, under varying loading conditions and particularly in case of important DG penetration as seen in Section 2.6 .

2.7.1 Capacitors: Shunt and Series Compensation Reactors

The primary purpose of capacitors is to reduce the reactive power levels. Additional benefits are derived by capacitors location. Locating them as closely as possible to the load derives maximum benefit of capacitors. At this location, the apparent power KVA is confined to the smallest value and the current is decreased as seen on the case study simulation performed with OpenDSS in Section. Thus, power losses are substantially reduced because of proportionality to the square of the current. Capacitors can be connected as well as to feeders and in this case the advantage is that they can be grouped together. When several loads are running not continuously, the capacitors are permitted to be on line all the time, reducing the total reactive power regardless of load. However, static VAR compensators employing thyristor switched capacitors and thyristor controlled reactors to provide or absorb the required reactive power have been developed in [26]. Furthermore, VAR compensation with capacitors could be obtained with two configuration:

- Shunt Capacitors;
- Series Capacitors.

Shunt compensation changes the equivalent impedance of the loads, while series compensation modifies the distribution system parameters [25].

Shunt Capacitors

The principles and theoretical effects of a shunt capacitor in a simple AC system having an inductive load are shown in Fig. 2.7, which comprises two basic cases:

1. whithout compensation;
2. shunt compensator with current source.

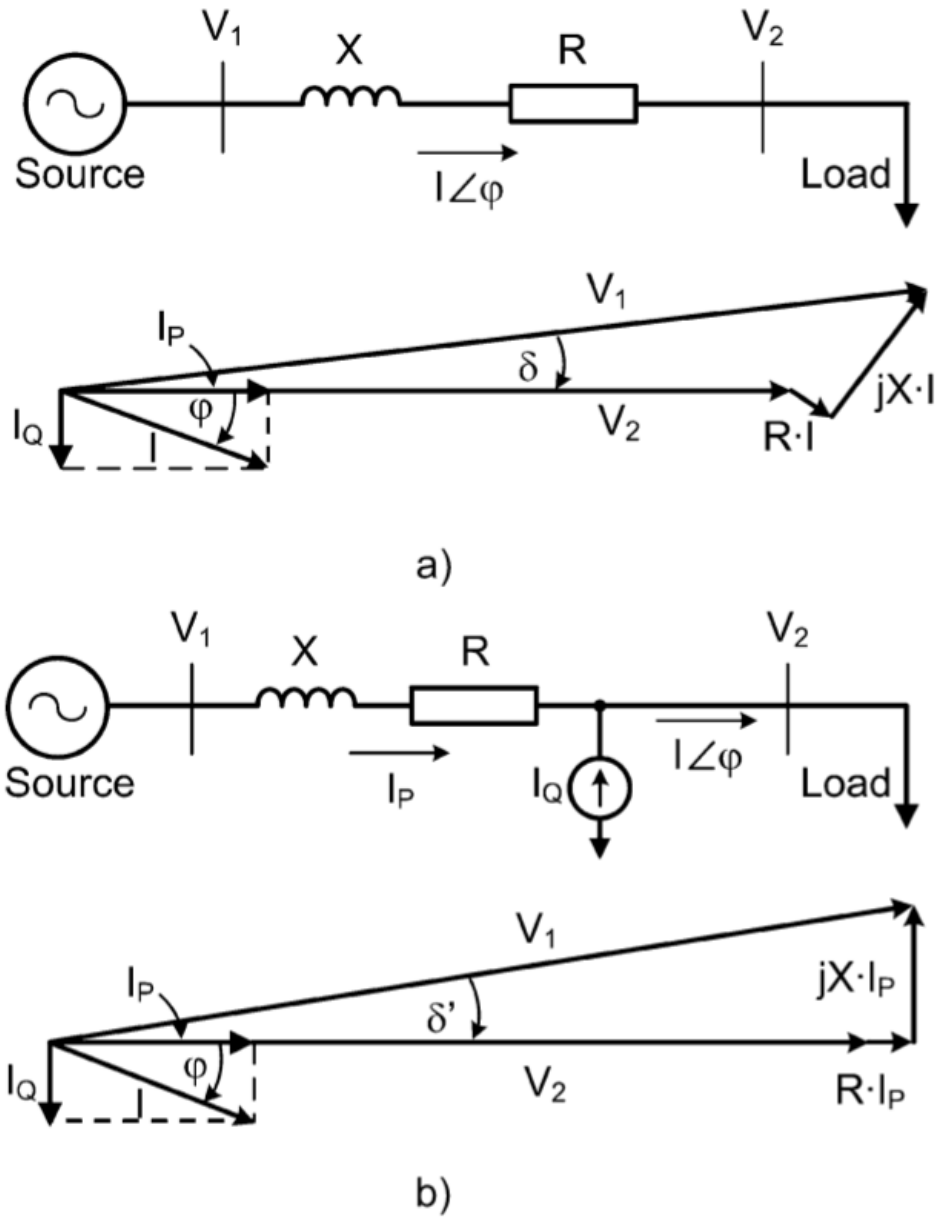

Figure 2.7: Effect of shunt compensation on a simple system: a) Without reactive compensation b) Shunt compensation with a current source.

In the first case the phasor diagram, the phase angle of the current has been related to the load side, which means that the active current I_P is in phase with the load voltage V_2. Since the load is assumed inductive, it requires reactive power for proper operation and hence, the source must supply it, the current increases from the generator through the line to the load. In the second case, a current source device is being used to compensate the reactive component of the load current I_Q. As a result, the system voltage regulation is improved and the reactive current component from the source is reduced or almost eliminated.

Series Capacitors

Typical series compensation systems use capacitors to decrease the equivalent reactance of a line at rated frequency. The connection of a series capacitor generates reactive power that, in a self-regulated manner, balances a fraction of the line's transfer reactance. Figure 5.4 shows the same network of

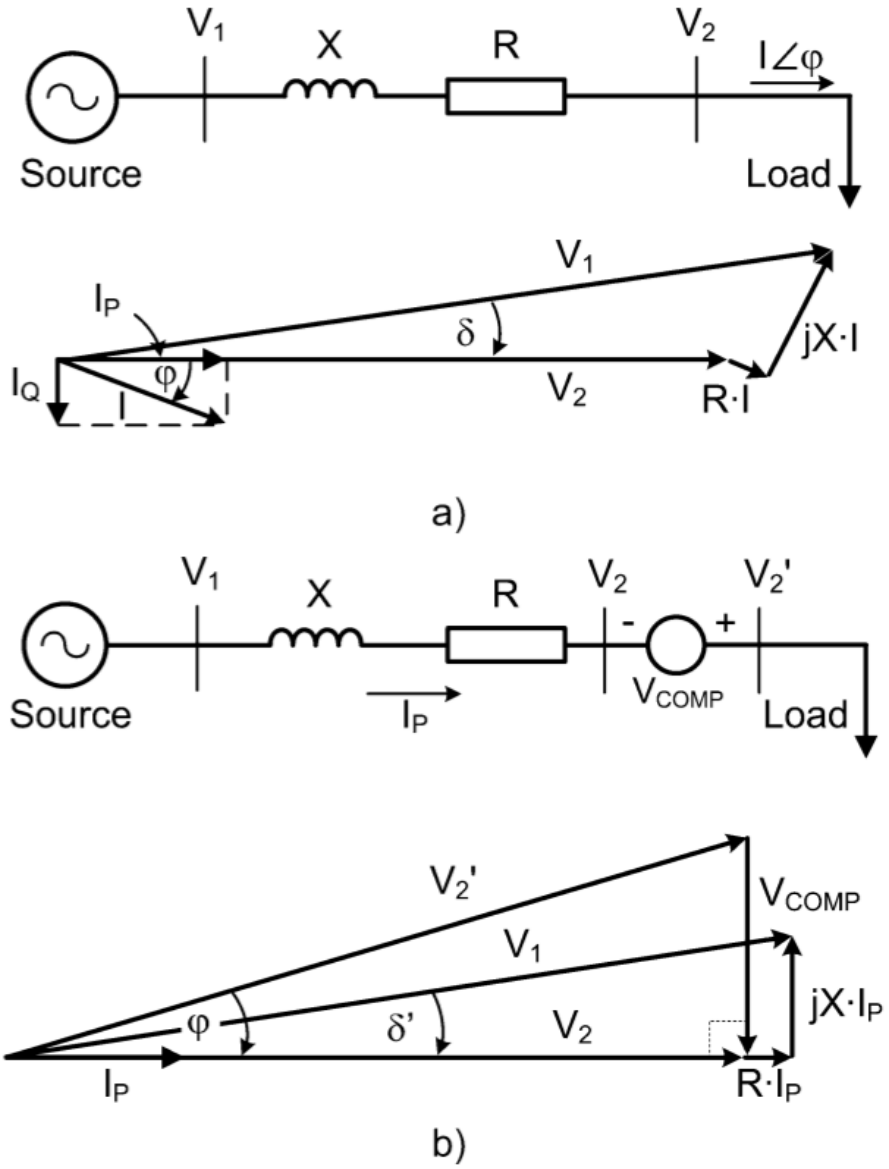

Figure 2.8: Effect of Series compensation on a simple system: a) Without reactive compensation b) Series compensation with a voltage source.

Fig. 2.7, also with the reference angle in V_2, and Fig. 5.4b the results obtained with the series compensation through a voltage source, in order to regulate V_2. However, the compensation strategy is different when compared with shunt compensation. In this case, voltage V_{COMP} has been added between the line and the load to change the angle of V_2', which is now the voltage at the load side. With the appropriate magnitude adjustment of V_{COMP}, unity power factor can again be reached at V_2. As can be seen from the phasor diagram of Fig. 5.4b, V_{COMP} generates a voltage with opposite direction to the voltage drop in the line inductance because it lags the current I_P.

2.7.2 Fixed and Variable Capacitor-Banks

Shunt capacitors could be employed in different configurations:

- Fixed capacitor;
- Mechanically switched capacitor;

- Thyristor switched capacitor and Thyristor-controlled Reactor;
- A combination of a TSC and TCR;

The leading current drawn by the shunt capacitors compensates the lagging current drawn by the load. The selection of shunt capacitors depends on many factors, the most important of which is the amount of lagging reactive power taken by the load. In the case of widely varying load conditions, the reactive power also varies over a wide range. Thus, a fixed capacitor bank may often lead to either over-compensation or under-compensation. Variable VAR compensation is achieved using switched capacitors. Depending on the total VAR requirement, capacitor banks are switched into or switched out of the system. The smoothness of control is solely dependent on the number of capacitors switching units used. The switching is usually accomplished using relays and circuit breakers and because hey generate high inrush currents, and require frequent maintenance, the thyristorized VAR compensators are used. These static VAR compensators (SVC) consist of standard reactive power shunt elements, which are controlled to provide rapid and variable reactive power. Furthermore switched capacitor banks are applied with an automatic switch control, which senses a particular condition. If the condition is within a preset level, the control's output level will initiate a trip or close signal to the switches that will either connect or disconnect the capacitor bank from the power system.

Thyristor-Switched Capacitors

Figure 2.9 shows the basic scheme of a static compensator of the thyristor-switched capacitor (TSC) type. The TSCs are cheaper devices that achieve appropriate results in the reactive power

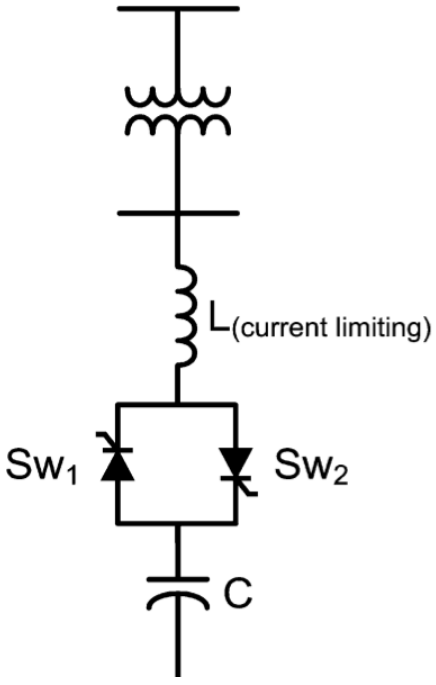

Figure 2.9: Basic thyristor-switched capacitor configuration Scheme

compensation, and they have important advantages like stepwise control, an average delay of one half a cycle and a limited generation of harmonics. As it is shown in Fig. 2.9 a TSC consists of two thyristors in anti-parallel connected to the capacitor to be switched. In addition, a series inductance is considered and it is used to limit inrush current through the thyristors and to prevent resonance with the network (normally 6% with respect to X_C). The capacitor may be switched with a minimum of transients if the thyristor is turned on at the instant when the capacitor voltage and the network

voltage have the same value. The current that flows through the capacitor at a given time is defined by the following expression:

$$i(t) = \frac{V_m}{(X_C - X_L)}\cos(\omega t + \alpha) - \frac{V_m}{X_C - X_L}\cos(\alpha)\cos(\omega_r t) + \left[\frac{X_C V_m}{\omega_r L(X_C - X_L)} - \frac{V_{co}}{\omega_r L}\right]\sin(\omega_r t) \tag{2.28}$$

where X_c and X_L are the compensator capacitive and inductive reactance,
V_m the source maximum instantaneous voltage,
α the voltage phase-shift angle at which the capacitor is connected,
ω_r the system resonant frequency $\omega_r = \frac{1}{\sqrt{LC}}$
V_{co} capacitor voltage at $t = 0^-$.
This expression has been obtained assuming that the system equivalent resistance is negligible as compared with the system reactance. If the capacitor is connected at the moment that the source voltage is maximum and is equal to the source voltage peak value $V_m(\alpha = \pm\frac{\pi}{2})$ the current transient component is zero[27].
The shunt capacitor bank is split up into appropriately small steps, which are individually switched in and out using bidirectional thyristor switches as Fig. 2.9 shows. It is obvious that each capacitor bank requires a separate thyristor switch and while the steady state voltage across the nonconducting thyristor switch is twice the peak supply voltage, a protection is needed. A possible solution is to replace one of the thyristor switches by a diode. In this case, inrush currents are eliminated when thyristors are fired at the right time, and a more continuous reactive power control can be achieved if the rated power of each capacitor bank is selected following a binary combination, as described in [28]. To connect each branch, a firing pulse is applied at the thyristor gate, but only when the voltage supply reaches its maximum negative value. In this way, a soft connection is obtained. The current will increase starting from zero without distortion, following a sinusoidal waveform, and after the cycle is completed, the capacitor voltage will have the voltage $-V_m$, and the thyristor automatically will block

Thyristor-controlled Reactor

In this arrangement, a fixed capacitor bank is connected to a TCR (thyristor controlled reactor) through a busbar Fig. 2.10. The rating of the reactor is chosen larger than the rating of the capacitor by an amount to provide the maximum lagging vars that have to be absorbed from the system[38].
By changing the firing angle of the thyristor controlling the reactor from $90°C$ to $180°C$, the reactive power can be varied over the entire range from maximum lagging vars to leading vars that can be absorbed from the system by this compensator.
When phase-angle control is used, a continuous range of reactive power consumption is obtained. It results, however, in the generation of odd harmonic current components during the control process. Full conduction is achieved with a gating angle of $90°C$. Partial conduction is obtained with gating angles between $90°C$ and $180°C$, as shown in Fig. 2.11. By increasing the thyristor gating angle, the fundamental component of the current reactor is reduced. This is equivalent to increase the inductance, reducing the reactive power absorbed by the reactor. However, it should be pointed out that the change in the reactor current may only take place at discrete points of time, which means that adjustments cannot be made more frequently than once per half-cycle. Static compensators of the TCR type are characterised by the ability to perform continuous control, maximum delay of one half-cycle, and practically no transients. The principal disadvantages of this configuration are the generation of low-frequency harmonic current components, and higher losses when working in the inductive region (i.e., absorbing reactive power) [29].

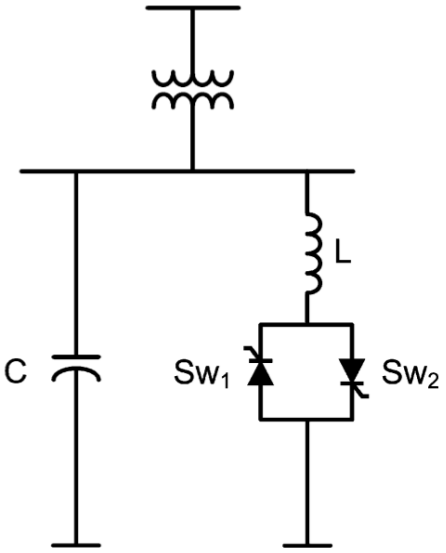

Figure 2.10: Basic thyristor-controlled Reactor configuration Scheme

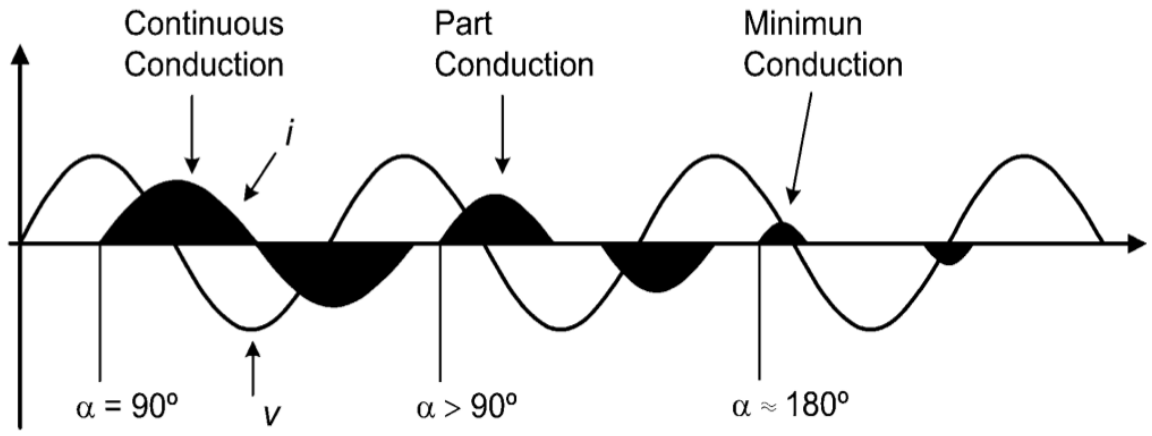

Figure 2.11: voltage and current waveforms in a TCR for different thyristor phase-shift angles, α

Combined TSC and TCR

This compensator overcomes two major shortcomings of the earlier compensators by reducing losses under operating conditions and better performance under large system disturbances.
Figure 2.12 shows the arrangement of this SVC with a TCR in parallel with several TSC banks (say, n). In view of the smaller rating of each capacitor bank, the rating of the reactor bank will be $\frac{1}{n}$ times the maximum output of the SVC, thus reducing the harmonics generated by the reactor. In those situations where harmonics have to be reduced further, a small amount of fixed compensators tuned as filters may be connected in parallel with the TCR.

2.7.3 Fixed versus Switched Capacitors

Most LV systems have some variability in loading throughout the day. Typically, commercial and light industrial loads peak during the day and are substantially lower overnight like the urban LV network simulated in the next chapter and because of this variability in loading, switched capacitors are often required to regulate voltage, and to minimise the system loading chapter 5, section 5.3.2. Switched capacitors give added flexibility to control system voltage, power factor, and losses. Switched

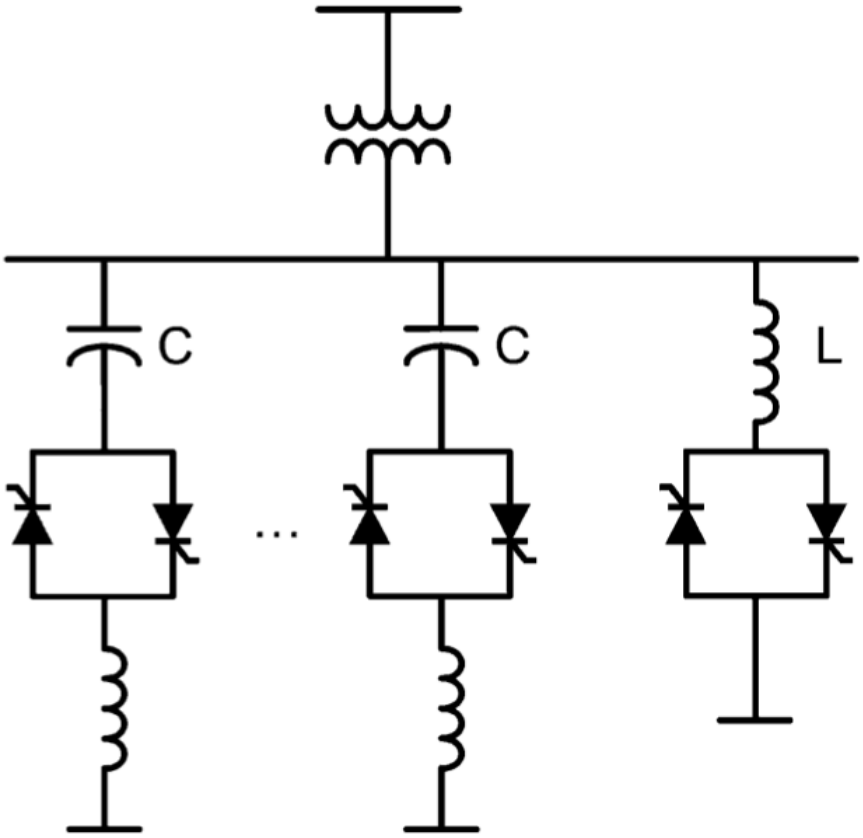

Figure 2.12: Combined TSC and TCR configuration

capacitors are usually applied with some type of automatic switch control. The control senses a particular condition. If the condition is within a preset level, the control's output level will initiate a close or trip signal to the switches that will either connect or disconnect the capacitor bank from the distribution line. Switched capacitor banks have an electronic controller that measures system voltage within the capacitor bank and system current via an external CT or CTs and regulates the number of steps that are activated. The controller is programmed to raise the system power factor to a "target" power factor.

Fixed capacitor banks are usually left energised on a continuing basis. However, in areas with significant seasonal demand changes, select banks may be manually switched on a seasonal basis.

2.7.4 Distribution-Transformers TAP Settings

In MV/LV substations the distribution transformer can be provided with tapped MV windings which permit off-load adjustment of the transformer MV/LV ratio. The actual tapping used is determined by the need to maintain the voltage supplied to low-voltage customers within the required tolerances. Typically, the range of tappings is ± 5% in 2.5% or 5% steps either side of the nominal ratio. The tapping selected depends on the voltage drop along the MV feeder, the voltage drop through the distribution transformer, which is a function of the transformer loading, the maximum low-voltage-distributor voltage drop, and the automatic voltage control and line-drop compensation arrangements on the source HV/MV transformers. Generally there are zones in a distribution network within which standard distribution transformers can all operate on the same tapping. Calculations to optimise the voltage conditions across the MV and LV networks are generally aimed at identifying and defining the boundaries of these zones. In some boundary areas of the network there may be an

overlap of zones with a subsequent choice of tapping. If the loading on a particular distribution transformer does not bear the same relationship to transformer rating as the other transformers in a 'tap zone', or its associated low-voltage-network voltage drop varies considerably from the average value within the zone, it may be necessary to utilise a different tap from that one used for the particular tap zone. Usually one tap higher or lower is adequate. There is evidence that, where voltage compounding is in use on MV bus bar of the associated infeed HV/MV transformer substation, most MV and LV networks operate satisfactorily with a range of 5% being used for the distribution-transformer tappings. The major difficult in resolving a distribution-network voltage problem is the coordination of the various voltage-control facilities, given that much of the information required is not readily available or is of unknown accuracy. In distribution systems medium-voltage drops are relatively low, and the voltage elasticity on the LV networks is also small, then there may be little benefit in using MV/LV transformers with taps instead of those HV/MV ones. Thus by suitable values of source bus bar voltage, voltage compounding on the HV/MV transformer(s) supplying the MV networks, and adjusting distribution-transformer tappings, acceptable voltage levels can be maintained for the LV customers across the range of system loading.

Chapter 3

Centralised versus Distributed Compensation Benefits on LV Networks

3.1 Introduction

Centralized reactive power compensation involves flow of larger quantities of reactive power than the distributed compensation. Almost all loads absorb reactive power. As a consequence, the phasor of the current circulating through the distribution lines (I) will have two components: a real component (active current) and an imaginary component (reactive current). The transmission and distribution of the reactive power Q cause several problems to the electric utility. First, it limits the active power (P) generation capacity: in the power plants, the generators have a limited apparent power (S) generation capacity. Indeed, the maximum apparent power of a three-phase generator ($S = \sqrt{3}UI$) is limited by the maximum line voltage (V) and current (I) that the generator can withstand; the first is determined by the generator insulations, while the second is determined by the cross-sectional areas of its conductors. In other words, the higher reactive power is generated and the lower active power can be produced:

$$S = \sqrt{(P^2 + Q^2)} \tag{3.1}$$

Second, networks such as distribution systems have long radial feeders which occur active and reactive power losses. In existing distribution systems, reactive power losses might be a problem, particularly when demand is at the peak, as wire are planned to carry less current. One possible solution to this issue is to use local compensation. Either methods of compensation have different impacts on both LV and MV networks.

3.2 Case Study 1: Generic study

A hypothetical radial LV network with a realistic parameters has been simulated by OpenDSS and its graphical interface DSSim in order to investigate how the way of compensation affects the voltage profiles of the LV network. In figure 3.3 are shown the results of a power flow run with the graphical interface. A line diagram of the MV/LV network is shown in figure 3.1, where an 11 kV/0.415 KV transformer is connected to the main bus. Three feeders are joined to the substation bus (Bus B, Bus C and Bus D). In addition, meters are used to monitor the power flow over each line and the voltage at different feeders is balanced as shown. A 0.9 power factor was considered with 45 kW load

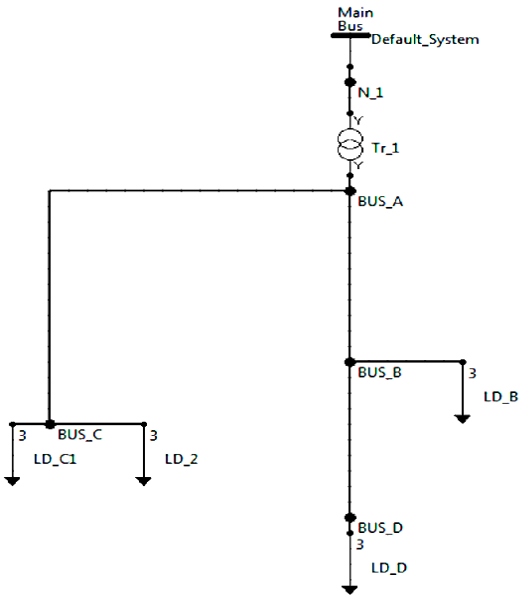

Figure 3.1: Line diagram of a radial network performed with DSSim

distributed among the three buses. The transformer has 250 kVA capacity of full load and thus there is no concern about thermal limits. Two simulations were carried out as follows, figure 3.2:

- A shunt-bank capacitor connected to the LV substation bus (Centralized Compensation);
- A shunt-bank capacitor situated on each of the three feeders Bus B, Bus C and Bus D (Individual compensation).

As the initial $\cos\phi$ is known, the power factor correction could be assessed with the following expression choosing the final desired $\cos\phi$ of the entire network:

$$Q_c = P.[\tan\phi - \tan\phi'] \tag{3.2}$$

Where,
Q_c is the corrected reactive power rating of the capacitor bank;
ϕ is the angle of the average power factor of the network before compensation;
ϕ' is the angle of the average final power factor desired for the network.
In order to compensate to unity, according to equation 3.3 a 22 kVAr capacitor bank was needed. The same procedure was was used at each bus in order to estimate the reactive energy in the local compensation case.

3.2.1 Simulation results: Voltage profiles for base case and compensation cases

In figures 3.4, 3.5 and 3.6 are depicted the voltage profiles of the base case, centralised and distributed compensation respectively. As the graphs show, the voltage drop over the transformer is almost zero in the centralised compensation case, whereas it is about 0.2 (V) in the second case. Furthermore, the voltage drop along the feeders is slightly higher with the application of the centralised compensation case.

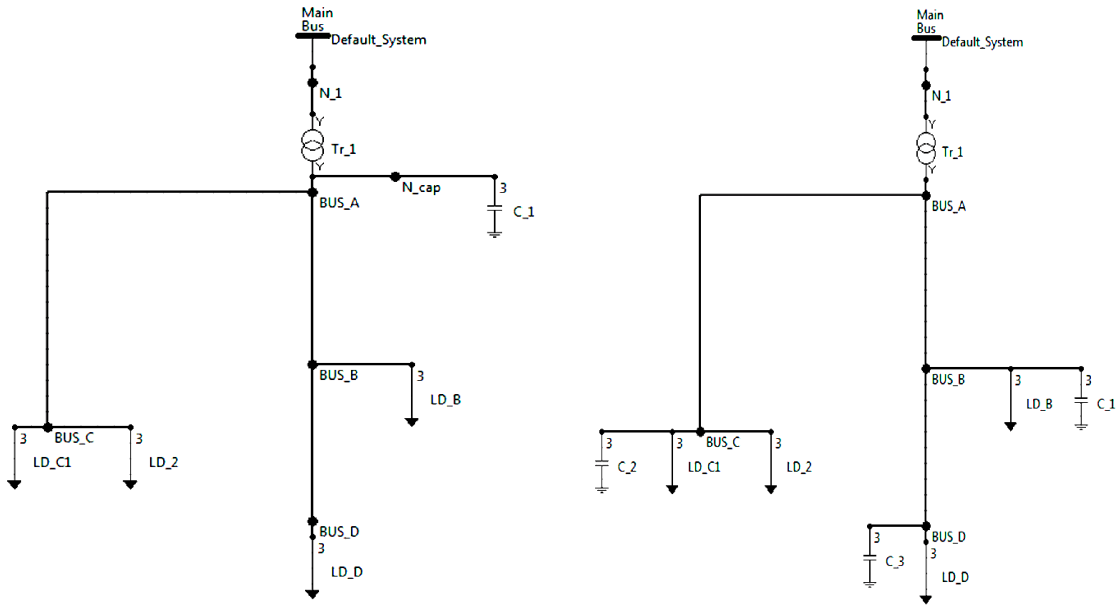

Figure 3.2: Line diagram performed in DSSim including Centralised and distributed composition configurations

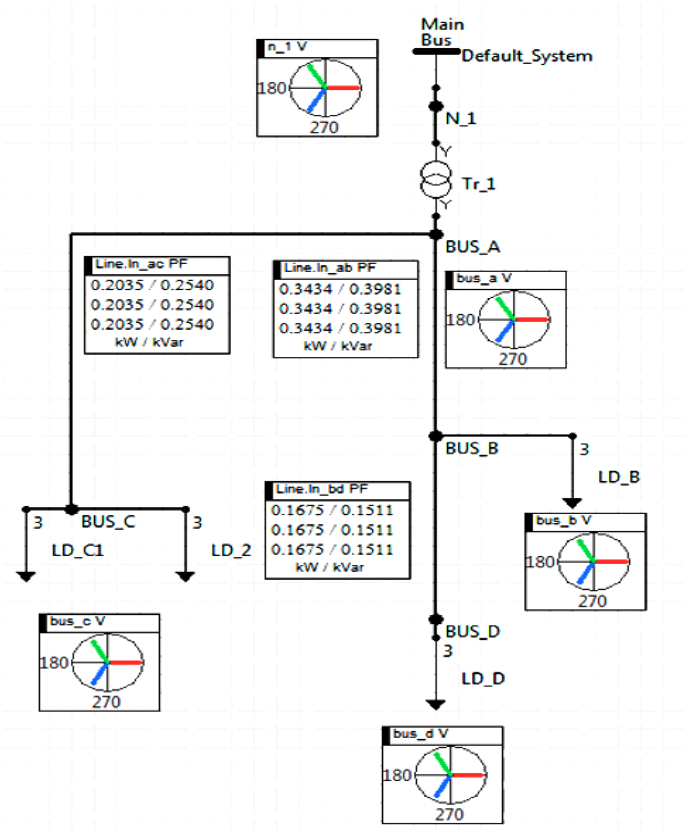

Figure 3.3: Power flow results showed with graphical interface DSSim

Figure 3.4: Base case voltage profile

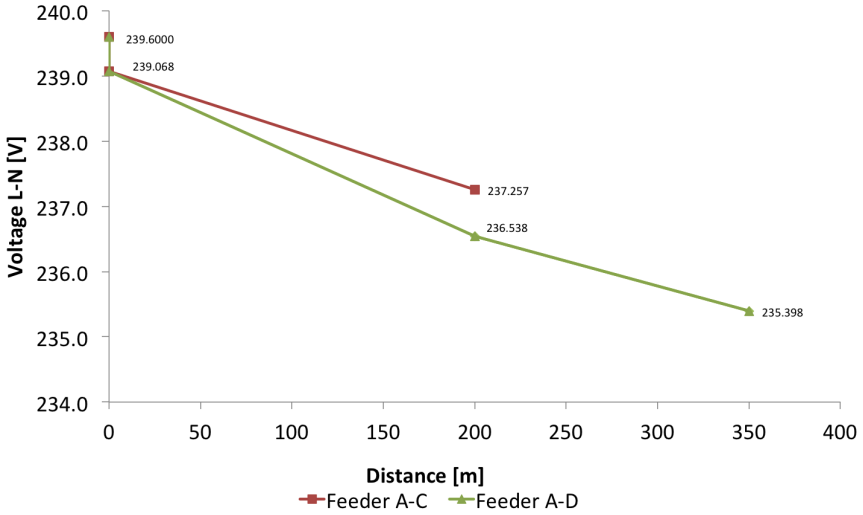

Figure 3.5: Centralised compensation voltage profile

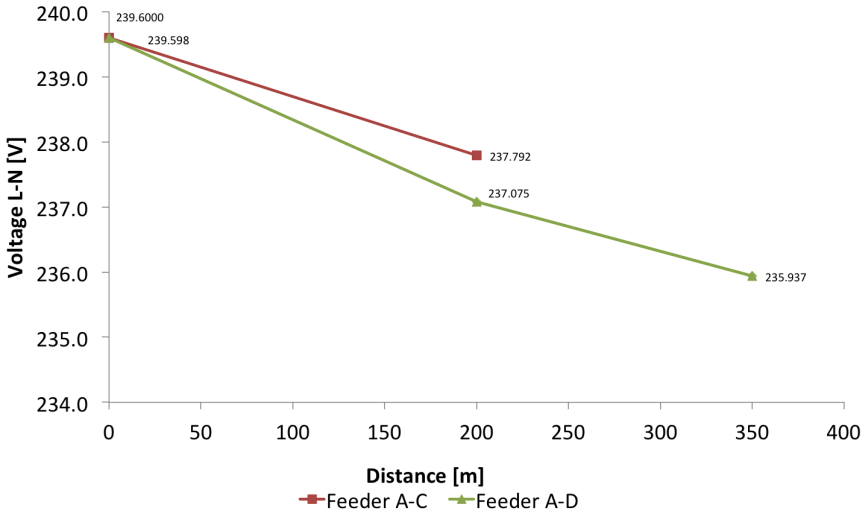

Figure 3.6: Distributed compensation voltage profile

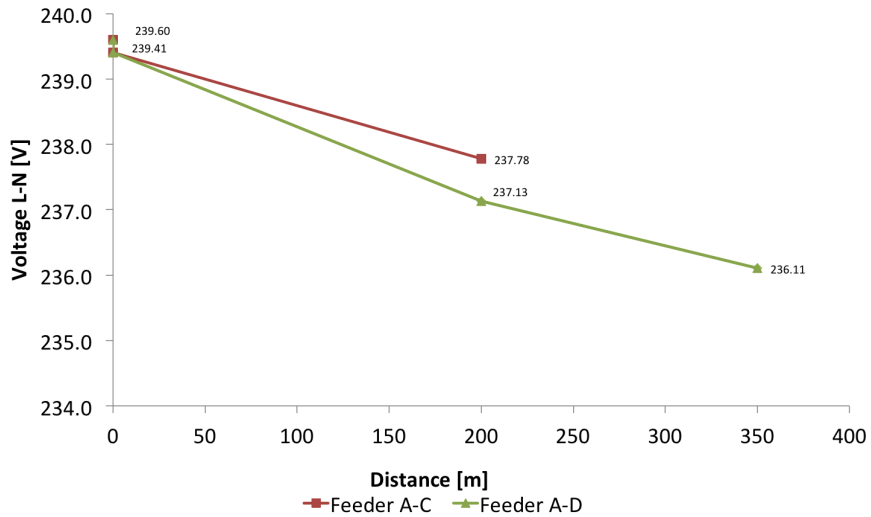

3.3 Case study 2: Angus Street network

The Angus Street network is an urban fully unbalanced network modelled in OpenDSS and in order to investigate the impact of centralised and local compensation different number of simulations with different strategies will be carried out with Fixed three-phase capacitors and Controlled three-phase capacitors. The first case is performed in consideration of the thermal margins and the voltage's variation in function of each compensation strategy.

3.3.1 Network description

A line diagram is shown in figure 3.7, the network consists of 5 main feeders, 100 buses and a 52 loads which are a mixture of three-phase and single-phase figure 3.8. Furthermore, for the simulations, load was distributed among 39 key nodes over the 5 feeders identified by WPD. According to the statistical analysis for load measures during a six-month period the power factor recorded is 0.982.

3.3.2 Base case simulation results

In the first place, a power flow was solved and results are reported in table 3.1 and 3.2:

Max p.u. voltage	***Min p.u. voltage***	***kW losses***	***kVAr losses***
1	0.9	36	40

Table 3.1: Overview of simulation results - voltage and losses

	P1 (kW)	***P2 (kW)***	***P3 (kW)***	***Q1 (kVAr)***	***Q2 (kVAr)***	***Q3 (kVAr)***
Sub-Bus	203	188	227	98	93	110
Feeder 10	10	9.5	12	5	5	6
Feeder 20	12	2	28	6	1	14
Feeder 30	40	39	30	22	22	18
Feeder 40	64	37	54	29	16	23
Feeder 50	77	100	102	37	49	50

Table 3.2: Angus Street network power flow

Figure 3.9 shows the voltage profiles (L-N) of network branches at Angus Street under the nominal maximum load case of 620kW and with a power factor 0.9 (lagging) - Base case. The most affected branches by voltage drop are shown in graphs. There is a small voltage drop across the 11kV/415V transformer at the main busbar (Sub-Bus) of 2.1% (average value of the three phases). The results in figure 3.9 shows clearly the significant difference between phase voltages. There is also a quite significant voltage drop along particular feeders, e.g. along SUBFDR50 branch, where there is a voltage drop of 7.9% on Phase 3.

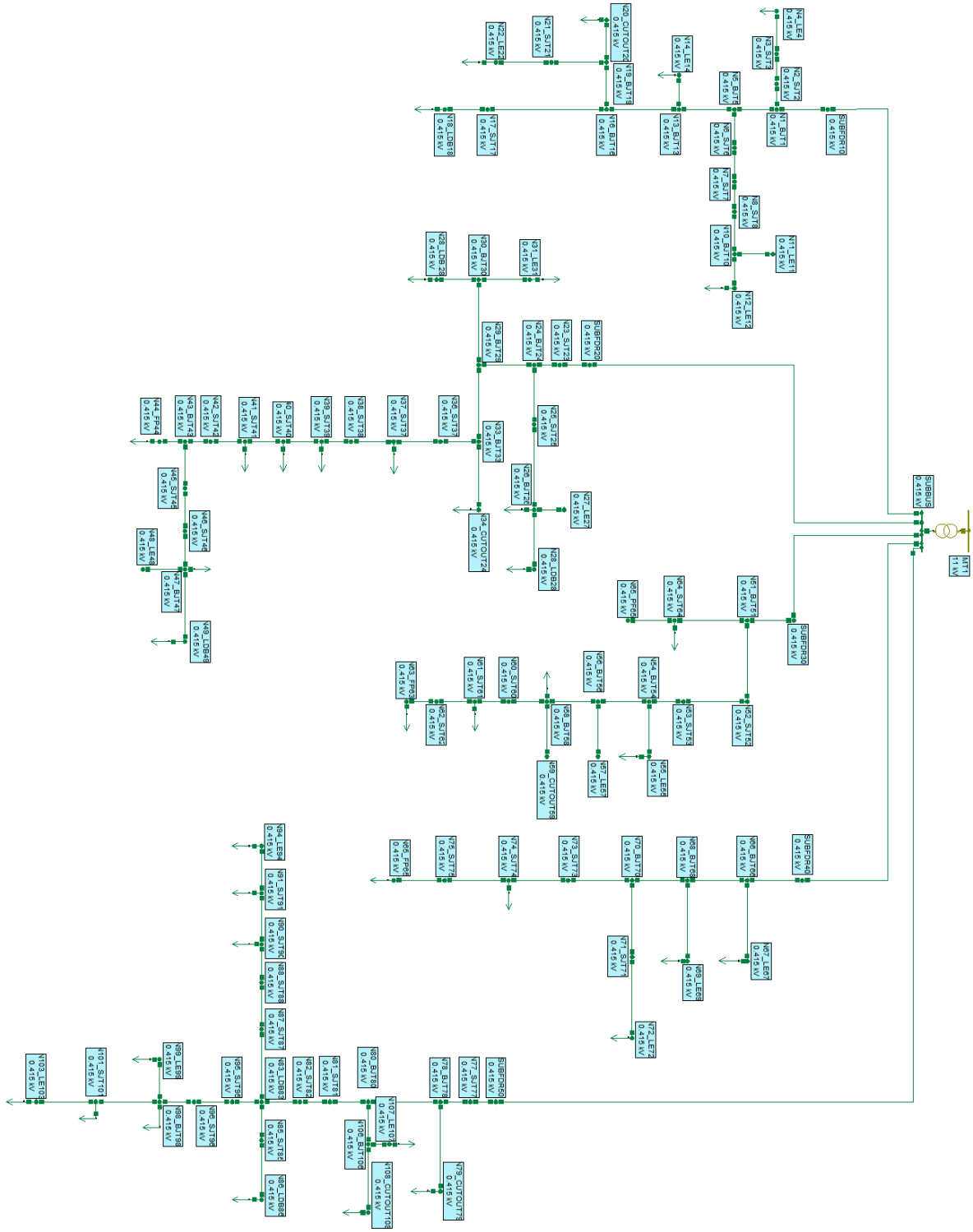

Figure 3.7: Line diagram of Angus street network

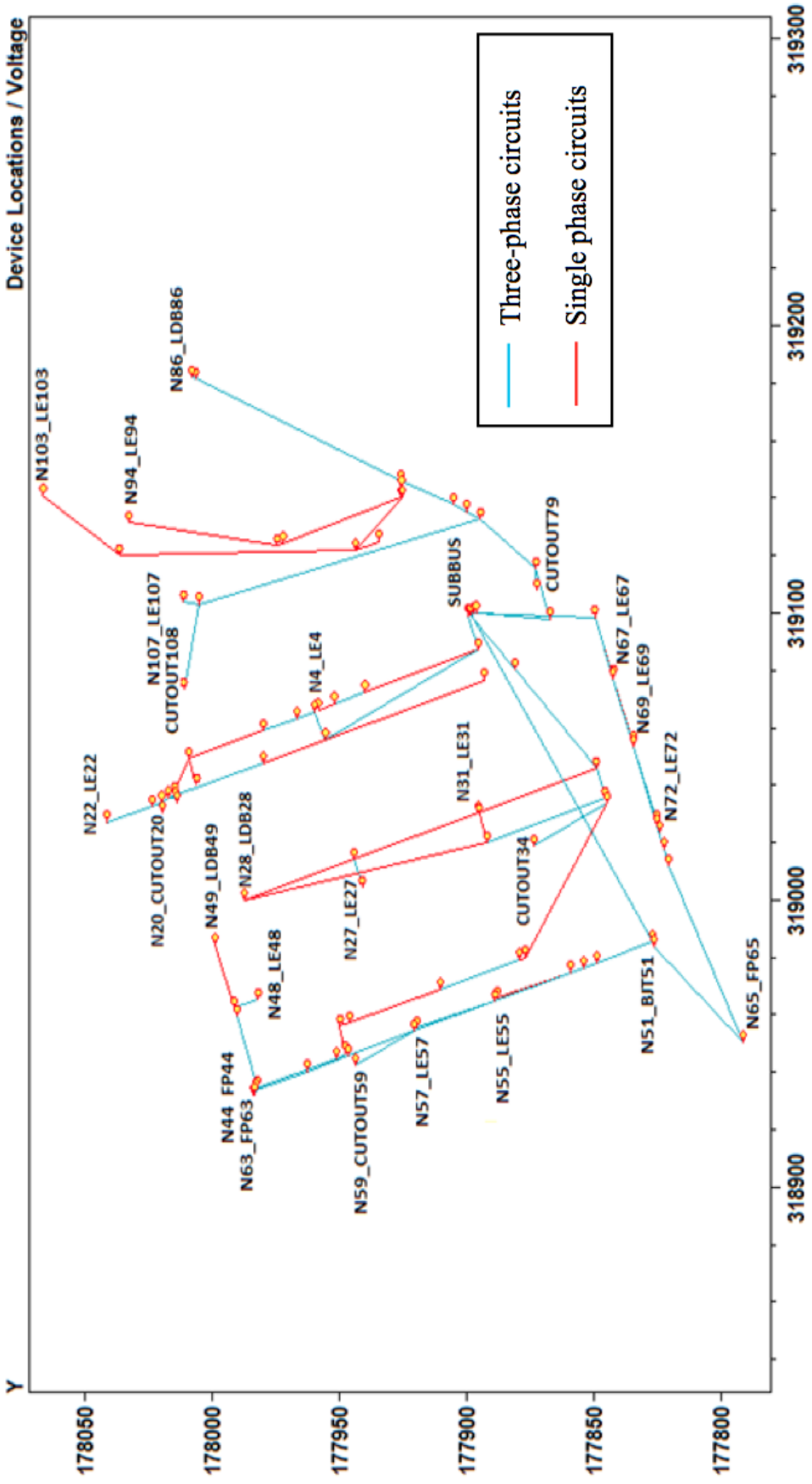

Figure 3.8: OpenDSS generated Quasi-Geographic diagram

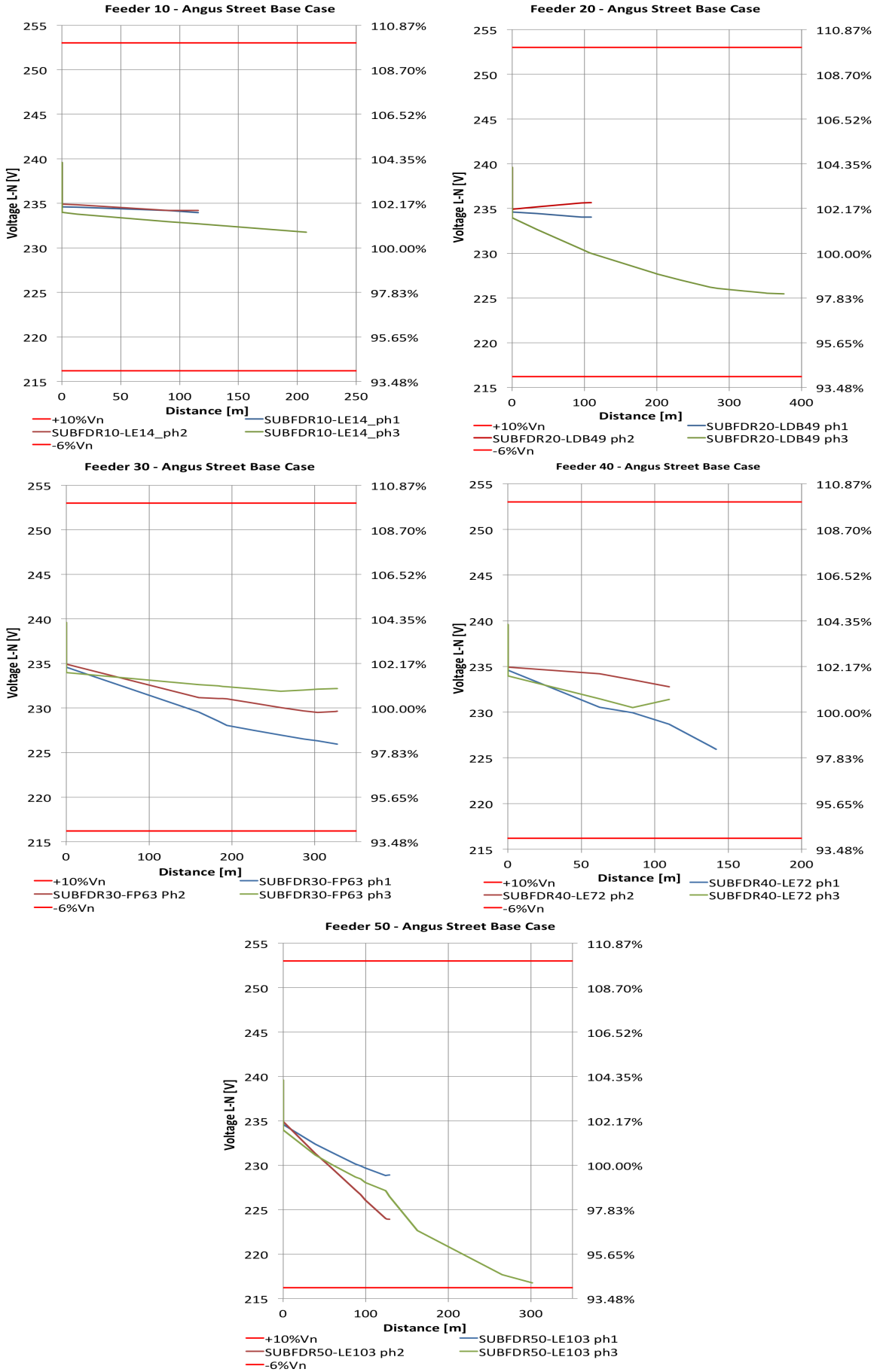

Figure 3.9: Angus street Base Case voltage profiles - 5 Sub-Feeders

3.3.3 Simulation cases for reactive power correction

Firstly, base case with fixed three-phase capacitors is investigated with an assumed overall power factor $\cos\phi$=0.9 of the entire network and for the simulations, 620 kW load was distributed among 39 key nodes over the 5 feeders identified by WPD. Initially, a simulation with no compensation has been carried out to determine the A, kW and kVAr peaks at Sub-Bus and Sub-Feedsrs. Since the network is fully unbalanced, the maximum current has been detected through the third phase, which was crossed by I_3=1078 (A) with real power equals to 227 kW. While the maximum reactive power has been registered through the third phase at the Sub-Bus and it was about 110 kVAr. As the initial $\cos\phi$ is known, the power factor correction could be assessed with the following expression choosing the final desired $\cos\phi$ of the entire network:

$$Q_c = P.[\tan\phi - \tan\phi'] \tag{3.3}$$

Where,
Q_c is the corrected reactive power rating of the capacitor bank;
ϕ is the angle of the average power factor of the network before compensation;
ϕ' is the angle of the average final power factor desired for the network.

Having assumed a 0.9 power factor, according to equation 3.3 for a unity correction, the capacitor bank amount for a central compensation is Q_c = 300 kVAr and it is placed on the main Sub-Bus. Same procedure was used to determine the correcting reactive power amount for the distributed compensation as reported in table 3.4.

	Compensation strategy	***Capacitor Bank(s)***
1	Centralised	300 kVAr
2	Distributed at 1/3 feeder lengths	300 kVAr
3	Distributed at the lowest voltage	300 kVAr

Table 3.3: Compensation to unity cases - Angus Street network: Load Magnitude = 620 kW and Load PF=0.9

	kW phase 1	***kW phase 2***	***kW phase 3***	***3-ph kVAr***
Sub-Feeder 10	10	9.5	12	15
Sub-Feeder 20	12	2	28	20
Sub-Feeder 30	40	39	30	50
Sub-Feeder 40	64	37	54	75
Sub-Feeder 50	77	100	102	140

Table 3.4: Reactive power sizing for distributed compensation to unity - Angus Street network: Total distributed reactive power Q = 300 kVAr

The same capacitive power amount is used in either centralised and distributed compensation as shown in table 3.3. The sizing of correcting reactive power amount per Sub-Feeder in consideration of distributed compensation is obtained by summing up the three real powers (unbalanced network) and then multiplying by $tan\phi$. Furthermore, two cases for the distributed compensation were carried out, where the capacitor banks were positioned at 1/3 of the feeder lengths from each Sub-feeder and then at the end of the three-phase connection of feeders as shown in figure 3.10.

3.3.4 Reactive compensation on Angus St. Network: Results

The reactive power injected into the network improves the voltage profiles and mitigates the active and reactive losses. In table 6.3 are shown the results of the different strategies of compensation: The maximum and minimum p.u. voltage, the kW and kVAr losses.

	Max voltage	***Min voltage***	***kW***	***kVAr***
Base case	1	0.904	36	40
Central compensation	1	0.917	35	35
Distributed 1/3 feeder length	1	0.922	34	34
Distributed at lowest voltage	1	0.922	39	37

Table 3.5: Reactive compensation strategies - p.u. voltage and losses

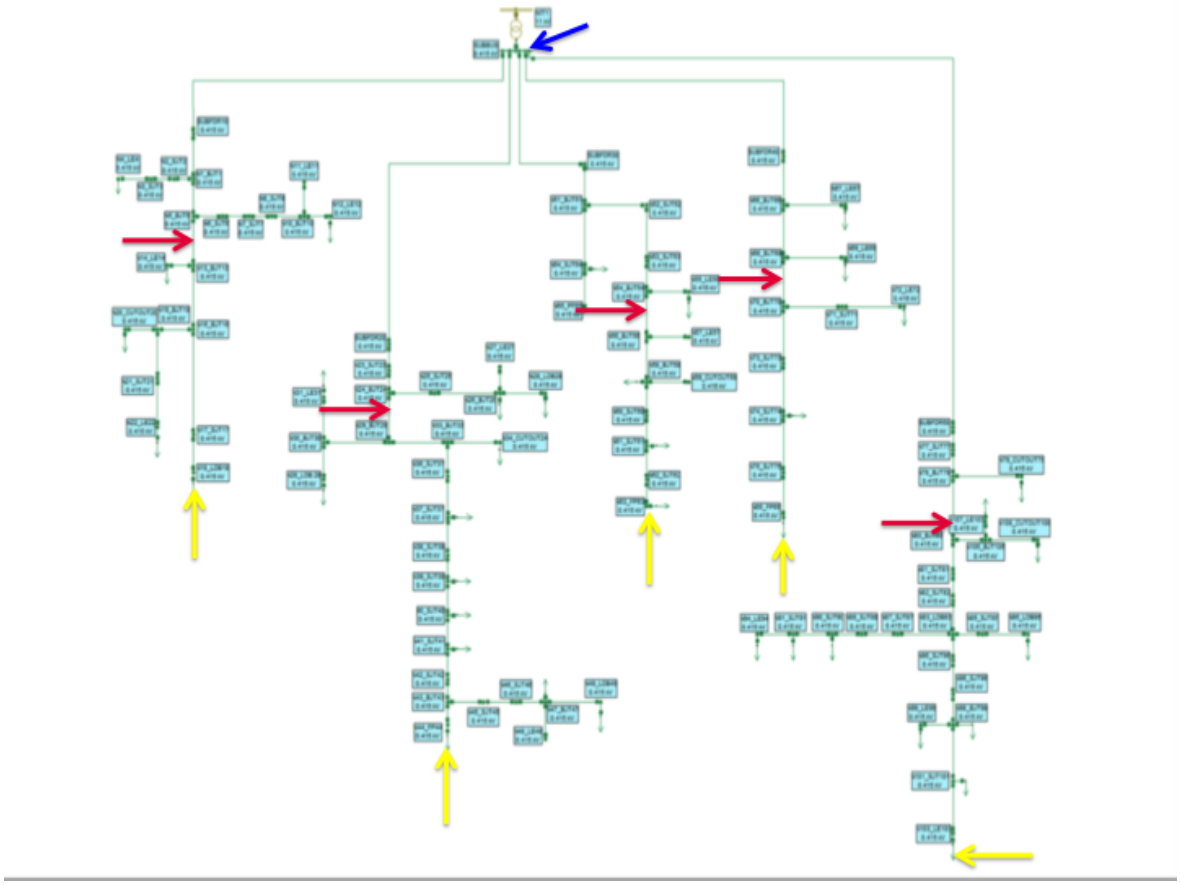

Figure 3.10: Location options used in simulations

3.3.5 Centralised compensation voltage profiles

Figure 3.11 shows the voltage profiles (L-N) of network branches with central capacitor bank placed at the main Sub-Bus on Angus Street network. The improvement in voltage of the most affected branches by voltage drop are shown in graphs. The voltage drop across the 11kV/415V transformer at the main busbar is 0.95%. The voltage drop along SUBFDR50 branch, is 7.9% on Phase 3.

3.3.6 Distributed compensation voltage profiles: 1/3 feeder lengths

Figure 3.12 shows the voltage profiles (L-N) of network branches with capacitor banks placed at one-third feeder lengths from each sub-feeder on Angus Street network. The improvement in voltage of the most affected branches by voltage drop are shown in graphs. The voltage drop across the 11kV/415V transformer at the main busbar is 1%. The voltage drop along SUBFDR50 branch, is 7.2% on Phase 3.

3.3.7 Distributed compensation voltage profiles: feeder ends (lowest voltages)

Figure 3.13 shows the voltage profiles (L-N) of network branches with capacitor banks placed at each feeder end (at the lowest voltage of each feeder) on Angus Street network. The improvement in voltage of the most affected branches by voltage drop are shown in graphs. The voltage drop across the 11kV/415V transformer at the main busbar is 1%. The voltage drop along SUBFDR50 branch, is 7.6% on Phase 3.

3.3.8 Reactive compensation approaches: voltage drop summary

In tables 3.6 and 3.7 is shown a comparison between the voltage drop of the different compensation types in both percentage and absolute values, respectively. The results show that the lowest voltage drop across the transformer is obtained with the centralised compensation which is 0.95% compared to 1% voltage drop achieved with distributed compensation cases. Furthermore, the lowest total voltage drop is achieved with the distributed compensation at one-third feeder length which is 8.2 % compared to the other two cases. It is important to notice how the losses are considerably reduced along the feeder with a distributed compensation approach rather than a centralised one where the losses are very slightly decreased over the feeder.

	Total $\Delta V\%$	***Transformer*** $\Delta V\%$	***Feeder*** $\Delta V\%$
Base case	10	2.1	7.9
Central compensation	8.85	0.95	7.9
Distributed 1/3 feeder length	8.2	1	7.2
Distributed at lowest voltage	8.6	1	7.6

Table 3.6: Voltage drop percentage for reactive compensation approaches

3.3.9 Reactive compensation approaches: maximum transformer LV current summary

The X/R ratio for MV lines, cables and 11kV/0.415kV transformers is usually greater than one, while the ratio is lower than one for LV wires. Therefore, in order to release more capacity to the

	Total ΔV	***Transformer*** ΔV	***Feeder*** ΔV
Base case	22.8	5.1	17.7
Central compensation	19.8	2.3	17.5
Distributed 1/3 feeder length	18.4	2.4	16
Distributed at lowest voltage	19.3	2.4	16.9

Table 3.7: Absolute voltage drop for reactive compensation approaches

transformer [1391 (A) of a full load transformer on Angus street network], the compensation type should reduce as long as possible the current at the LV side. In table 3.8 are shown the maximum transformer LV side current for each compensation approach. As can be seen, there is a significant unbalance between phases and the third phase is the most loaded.

	I1 (A)	***I2 (A)***	***I3 (A)***	***Reduction*** %
Base case	960	891	1078	-
Central compensation	865	800	976	10.5
Distributed 1/3 feeder length	867	802	980	10.1
Distributed at lowest voltage	875	811	989	9.1

Table 3.8: Transformer LV side current for the different reactive compensation approaches with a transformer Ampacity of 1391 (A)

As the transformer on Angus street network has 1000 kVA of full load capacity which is not fully loaded with an experienced peak load demand of 689 kVA and therefore, a capacity of 313 (A) is left. In addition the simulation results show that a centralised compensation to unity releases 102 (A) capacity to the transformer on the third phase. Furthermore, a A reduction in current up to 10.5% is achieved with the centralised compensation and the transformer LV side current has been increased with the first and second case of distributed compensation. In other words, the further capacitor banks are placed along the sub-feeders, the less effective is current reduction at the transformer.

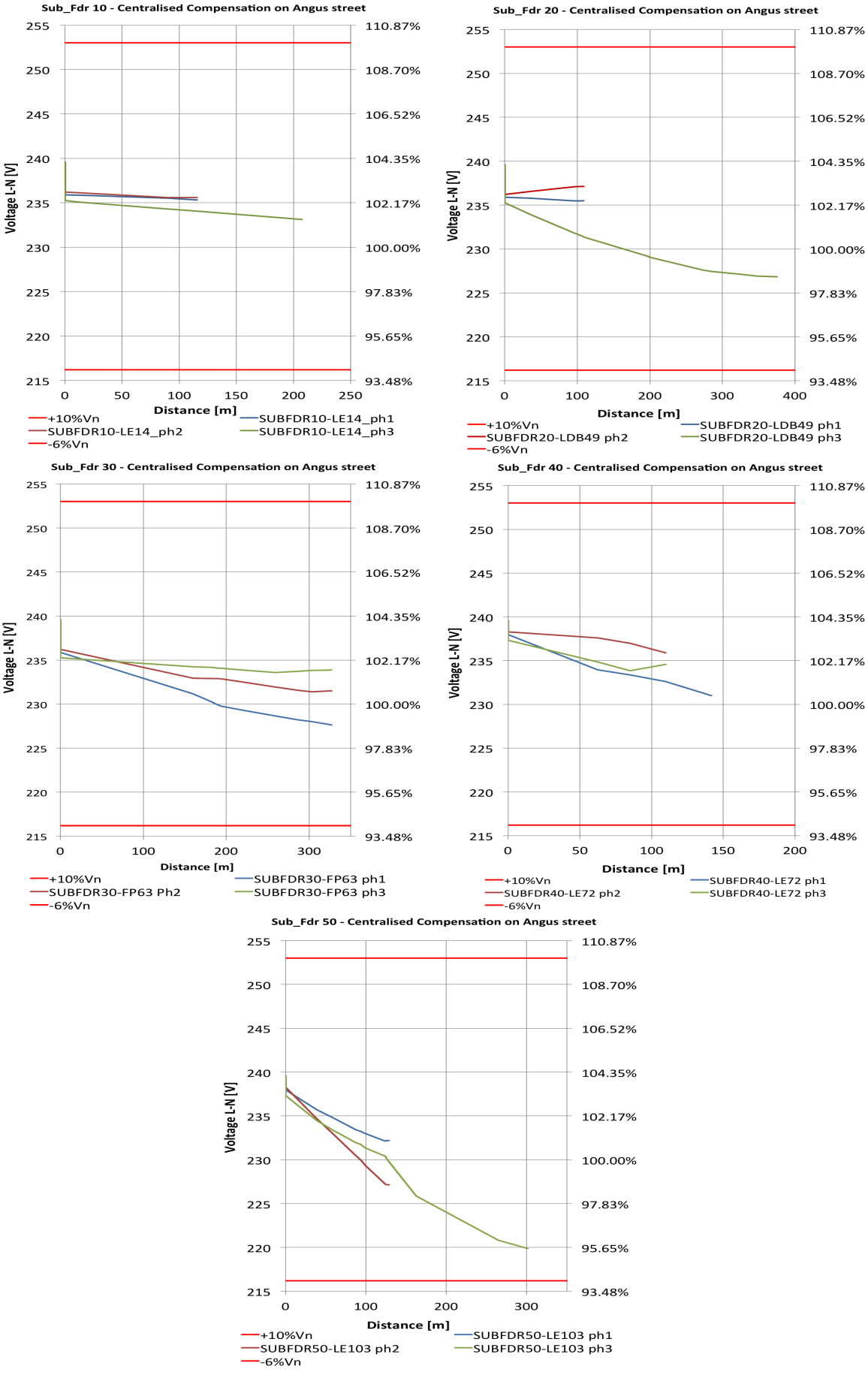

Figure 3.11: Centralised compensation - Angus street voltage profiles - 5 Sub-Feeders

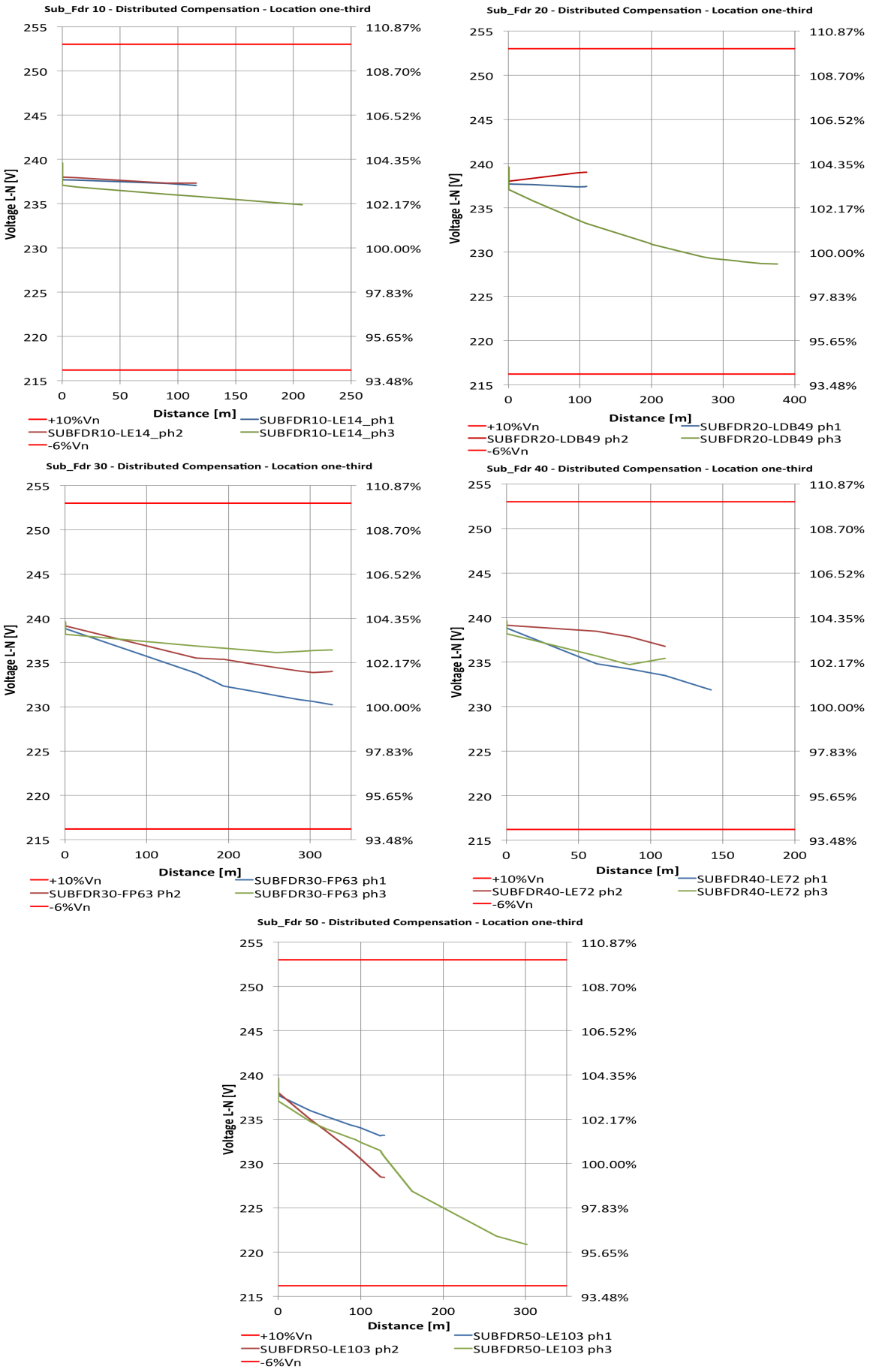

Figure 3.12: Distributed compensation 1/3 feeder lengths - Angus street voltage profiles - 5 Sub-Feeders

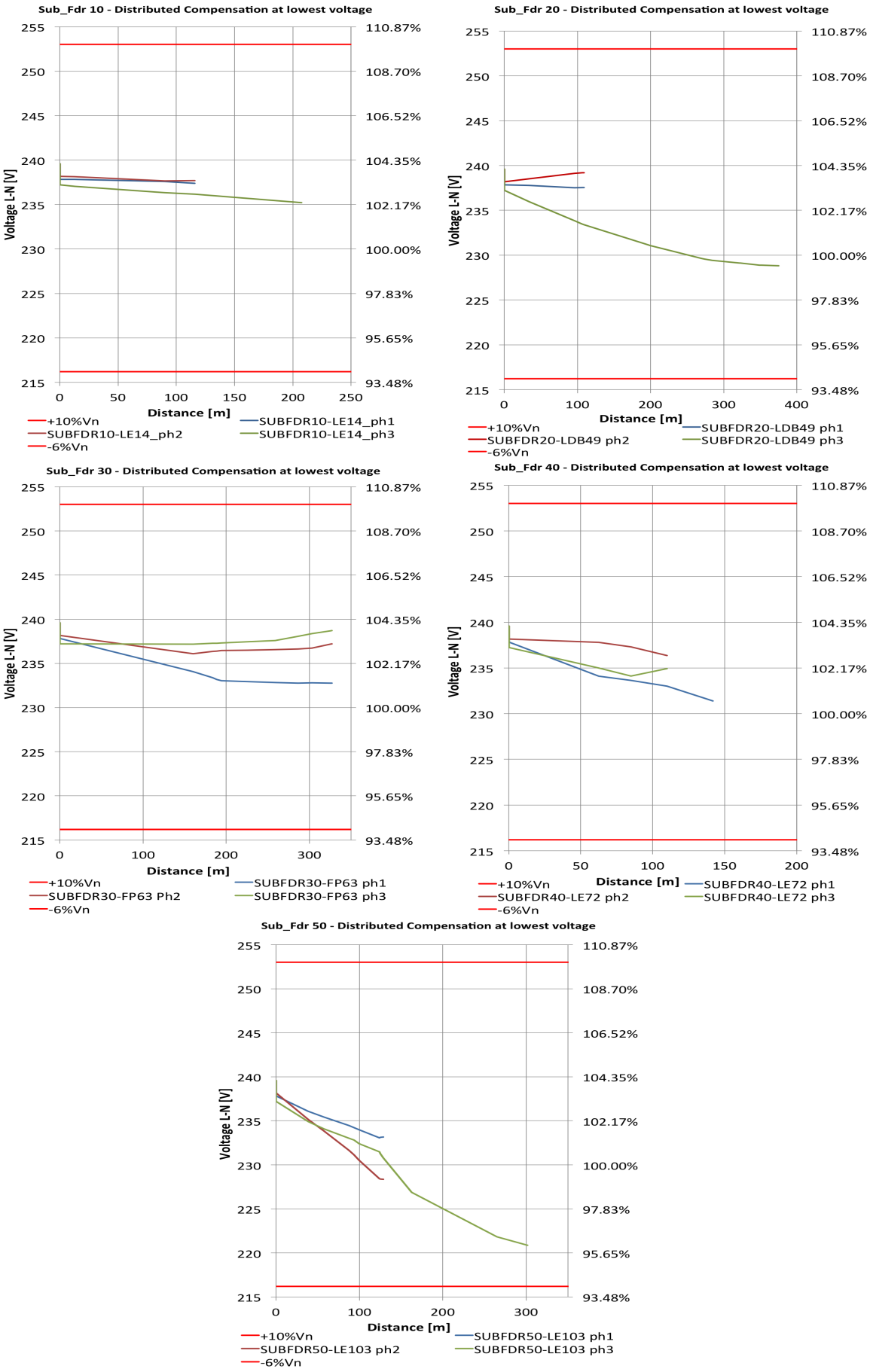

Figure 3.13: Distributed compensation at lowest voltage - Angus street voltage profiles - 5 Sub-Feeders

Chapter 4

Reactive Compensation Manufactured Units

In this chapter are reported briefly practical aspects and specifications of LV capacitors. Devices currently available for VAr support and power factor correction are[30]:

→ Fixed capacitor banks (FCB)	- where load and power factor are relatively constant
→Automatic capacitor banks (ACB)	- Supplies variable quantities of Q in response to changing load conditions (magnitude and power factor) - for systems with relatively low THD and TDD (Clean network)
→De-tuned capacitor banks (DACB)	- for controlled power factor correction with harmonic suppression (polluted network) - (i) Reduce flow of harmonic currents in capacitors - (ii) Damp in-rush current
→ Transient free compensation systems	- Electronic switching of capacitor stages to avoid transients generation

Four mainly manufacturers' of LV capacitor banks were identified:

1. ABB
2. Eaton capacitors
3. Schneider
4. Gentec

4.1 Products specifications

Specifications of the latter devices are shown in the tables below [31], [32], [33] and [34]. The prices included in the tables have been provided by correspondence with various UK suppliers. In appendix F is included Schneider-Electric's quotation for standard and detuned power factor correction.

4.1.1 Standard IP Ratings

Each device has the relative ingress Protection rating (IP) and it is used to specify the environmental protection - electrical enclosure - of electrical equipment [35]. However, manufacturers could change IP ratings as requested by customers.

The IP rating normally has two numbers:

1. Protection from solid objects or materials;
2. Protection from liquids (water).

IP10:(Schneider)

Protected against solid objects 50mm;

No protection against liquid object.

IP20:(Schneider)

Protected against solid objects 12.5mm;

No protection against liquid object.

IP21:(ABB)

Protected against fingers or similar objects

Protection against vertically falling drops of water.

IP31:(Eaton capacitors - Schneider)

Protected against solid objects over 2.5 mm (tools and wires);

Protection against vertically falling drops of water.

IP42 :

Protected against solid objects over 1 mm;

Protection against direct sprays of water up to 15o from the vertical.

Product	Series	Voltage	Steps	kVAr	Max kVAr	Weight	Dimensions	Costs £
ABB	100	400/415	3	15	45	90 lb	24 x 20 x 10	n/a
	300	400/415	3	50	150	200 lb	36 x 30 x 16	2892
	500	400/415	5	50	250	300 lb	60 x 36 x 16	4380
	700	400/415	5	100	500	500 lb	72 x 42 x 20	n/a
	300R	400/415	3	50	150	450 lb	60 x 36 x 16	n/a
	500R	400/415	5	50	250	600 lb	72 x 42 x 20	n/a
	CLM3 – Automatic capacitor bank	400/415	4	100	400	Depend on bank configuration	90 x 38 x 20	n/a
	CLMR – Detuned capacitor bank (with reactors)	400/415	3	100	300	Depend on bank configuration	90 x 38 x 20	n/a
Schneider	Varplus M	400/415	2	15	30			n/a
		400/415	3	15 + 12.5 + 12.5	40			n/a
		400/415	2	60 + 15	75			n/a
		400/415	3	50 + 15 + 15	80			n/a
		400/415	4	60 + 15 +12.5 + 12.5	100			n/a
	Varpact	400	1	-	15	9 kg		n/a
		400	1	-	20	10 kg		n/a
		400	1	-	25	10 kg		n/a
		400	1	-	30	10 kg		n/a
		400	1	-	35	12 kg		n/a
		400	1	-	45	12 kg		n/a
		400	1	-	60	13 kg		n/a
		400	1	-	70	14.5 kg		n/a
		400	1	-	90	15 kg		n/a
		400	2	15 + 15	30	10 kg		n/a
		400	2	15 +30	45	12.7 kg		

		400	2	15 + 45	60	13.7 kg		n/a
		400	2	30 + 30	60	14.5 kg		n/a
		400	2	30 + 60	90	16.5 kg		n/a
		400	2	45 + 45	90	16.5 kg		n/a
	ACB	400	5	25	125	/		2769
	DACB	400	5	25	125	/		3750
Eaton	AUTOVAR 300 Automatic Power Factor Correction	480	5	10	50	90.8 kg	36 x 36 x 13	n/a
		480	5	15	75	95.3 kg		n/a
		480	5	20	100	95.3 kg		n/a
		480	5	25	125	109 kg		n/a
		480	5	30	150	109 kg		n/a
		480	5	35	175	118 kg		n/a
		480	5	40	200	122.6 kg		n/a
		480	5	45	225	131.7 kg		n/a
		480	5	50	250	132.6 kg		n/a
		480	5	60	300	140.7 kg		n/a
	AUTOVAR 600 Automatic Power Factor Correction	480	3	50	150	287 kg	80 x 39 x 25	n/a
		480	4	50	200	306.9 kg		n/a
		480	5	50	250	326.9 kg		n/a
		480	6	50	300	346.9 kg		n/a
	Transient-Free Reactive Power	480	≈5	31	156		31.5 x 23.6 x 82.7	n/a
		480	≈5	37.5	187			n/a
		480	≈7	31	219			n/a
		480	≈5	50	250			n/a
		480	≈7	37.5	262			n/a
		480	≈5	62.5	312			n/a
	Eaton capacitors 300 standard	415	5	25	125	210 kg	2100 x 600 x 600 (mm)	n/a
		415	3	50	150	235 kg		n/a
		415	4	3 x 50 + 1 x 25	175	24		n/a

		415	4	50	200	260 kg		n/a
		415	5	4 x 50 + 1 x 25	225	270 kg		n/a
		415	5	50	250	280 kg		n/a
		415	6	5 x 50 + 1 x 25	275	290 kg		n/a
		415	6	50	300	300 kg		n/a
	Eaton capacitors 300 detuned	415	2	50	100	230 kg	2400 x 600 x 600 (mm)	n/a
		415	3	2 x 50 + 1x 25	125	240 kg		n/a
		415	3	50	150	260 kg		n/a
		415	4	3 x 50 + 1 x 25	175	400 kg		n/a
		415	4	50	200	420 kg		n/a
		415	5	4 x 50 + 1 x 25	225	430 kg		n/a
		415	5	50	250	440 kg		n/a
		415	6	5 x 50 + 1 x 25	275	450 kg		n/a
		415	6	50	300	470 kg		n/a
	Eaton capacitors 100 auto	415	1	25	25	20/21 kg	905 x 400 x 200 (mm)	n/a
		415	2	25	50	25/26 kg		n/a
		415	3	25	75	31/33 kg		n/a
		415	4	25	100	35/37 kg		n/a
Gentec	C100 series Automatic Low Voltage Power Factor Correction	480	5	10	50	122 kg	1220 x 710 x 406 (mm)	n/a
		480	5	15	75	122 kg		n/a
		480	5	20	100	126 kg		n/a
		480	5	25	125	172 kg		n/a
		480	3	50	150	185 kg		n/a
		480	7	25	175	193 kg		n/a
		480	4	50	200	198 kg		n/a
		480	9	25	225	295 kg		n/a
		480	5	50	250	300 kg		n/a
		480	11	25	275	316 kg		n/a
		480	6	50	300	359 kg		n/a

4.2 Principle of automatic compensation

Switched capacitor banks are applied with an automatic switch control, which senses a particular condition. If the condition is within a preset level, the control's output level will initiate a trip or close signal to the switches that will either connect or disconnect the capacitor bank from the power system. Capacitor controllers can be chosen to switch capacitors in and out of the system depending upon the desired control quantity, which are [36]:

- Voltage: The capacitor switches on and off, based on voltage. The user provides the threshold minimum and maximum voltages as well as time delays and bandwidths to prevent excessive operations. Voltage control is most appropriate when the primary role of a capacitor is voltage support and regulation.
- Current: The capacitor switches on and off based on the line current. Current control engages the capacitor during heavy loads, which usually corresponds to the highest needs for vars.
- Time switch: The simplest scheme: the controller switches capacitors on and off based on the time of day. The on time and the off time are programmable. Modern controllers allow settings for weekends and holidays. This control is the cheapest but also the most susceptible to energising the capacitor at the wrong time (due to loads being different from those expected, to holidays or other unexpected light periods, and especially to mistakenly set or inaccurate clocks).
- Vars: The capacitor uses var measurements to determine switching. This is the most accurate method of ensuring that the capacitor is on at the appropriate times for maximum reduction of losses.
- Temperature: The controller switches the capacitor bank on or off depending on temperature. Normally these might be set to turn the capacitors on in the range of 85 and 90°F and turn them off at temperatures somewhere between 75 and 80°F.

Many controllers offer many or all of these possibilities. Many are usable in combination; turn capacitors on for low voltage or for high temperature. Var, power factor, voltage, or current controllers require voltage or current sensing or both. Capacitor bank switching is not based on power factor because both the voltage and current would have to be monitored and a microprocessor is required to calculate the power factor. Furthermore, voltage control provides extra safety to prevent capacitors from causing over-voltages. Some controllers offer types of voltage override control; the primary control may be current, vars, temperature, or time of day, but the controller trips the bank if it detects excessive voltage. A controller may also restrain from switching in if the extra voltage rise from the bank would push the voltage above a given limit. In order to minimise the cost and complexity, controllers often switch all three phases using sensors on just one phase. To coordinate more than one capacitor with switched var controls, set the most-distant unit to have the shortest time delay. Increase the time delay on successive units progressing back to the substation. This leaves the unit closest to the substation with the longest time delay. The most distant unit switches first. Upstream units see the change and do not need to respond. For var-controlled banks, locate the current sensor on the source (substation) side of the bank. Then, the controller can detect the reactive power change when the capacitor switches. To properly calculate vars, the wiring for the CT and PT must provide correct polarities to the controller.

In figure 4.1 is shown a wiring diagram of an automatic capacitor bank manufactured by Schneider. The absorbed reactive energy is detected by a varmeter relay which automatically controls closing and opening of the sections in relation to the load and the required power factor. A similar wiring diagram of an automatic capacitor bank manufactured by ABB is shown in figure 4.2. The figure shows also the

protection needed for the device installation. Both wiring diagrams show the position of the current transformer CT that must be upstream the capacitor bank and where it matches the total current.

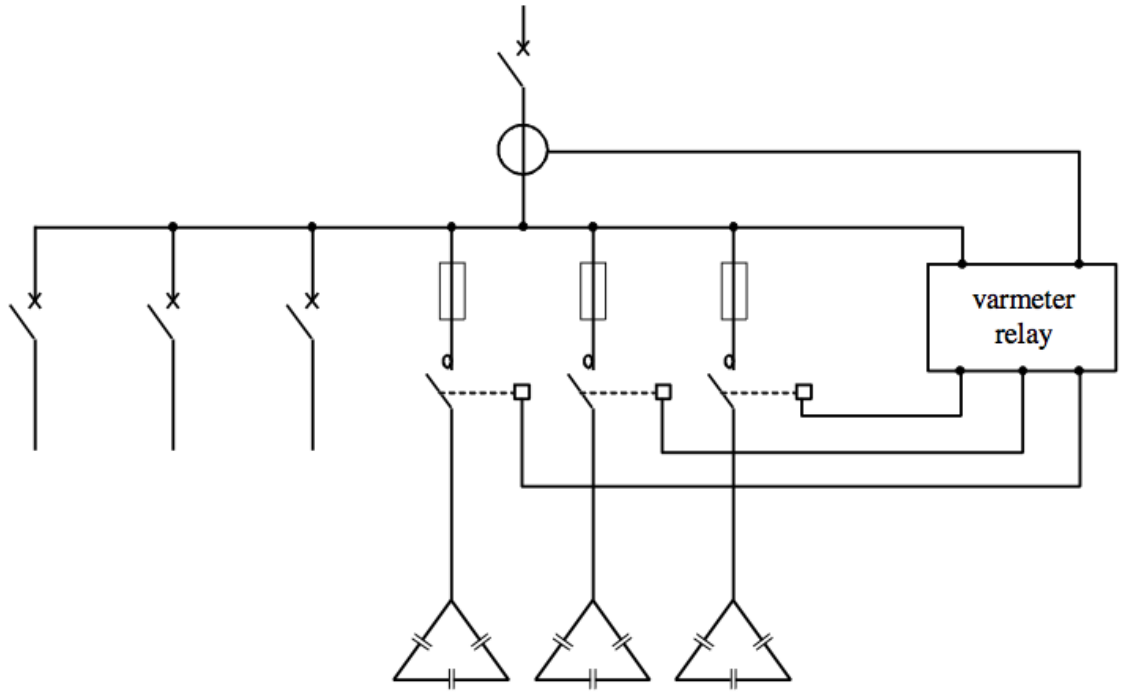

Figure 4.1: Schneider wiring diagram: principle of automatic compensation of an installation [36]

The reactive compensation units consist of capacitor(s), contactor(s), fuses and a reactive power controller as shown in ABB wiring diagram. The reactive power controller needs two factors for correct control:

- the voltage taken internally from the compensation unit
- the value of the apparent current taken from the feed-in or metering point in using a current transformer with a defined transforming ratio.

Manufacturers' first goal is to produce compensation banks as economically as possible. This is why small units consist of capacitors of different sizes, for example 10, 20 and 40 kvar (ratio 1:2:4) to achieve total 70 kvar switching in seven steps. Bigger compensation banks (greater than 200 kvar) are assembled with capacitors of equal size, for example 50 kvar. The market offers basic and extension modules. The reactive power controller senses the reactive power steadily at the point where the current transformer has been located. In some installations often one central-type compensation is quite sufficient. The power factor requested by the electricity supplier is to be kept on average within one billing period. Brief deviations from the power factor target must not be controlled quickly. Thus switching time delays per step of 30 to 40 s are quite sufficient. It must be taken into consideration that shorter delays increase the number of switching operations, which often are counted up by modern power factor relays. An important criterion for choosing compensation banks is the type of consumer: if there are only a few consumers with high rated power, a capacitor bank with rough stepping control is applicable. Installations with many middle- or small-sized consumers require compensation with fine-stepping control. For this purpose more expensive compensation units with up to 12 or even 14 steps could be custom built and designed to specific load requirements. Older power factor relays control with a fixed switching program, the so-called 'geometrical switching sequence' as shown in figure 4.3.

- C1...C12 capacitor steps
- FMAIN main fuses or protective devices (not provided)
- FAUX auxiliary fuses
- F1...F12 capacitor step fuses
- K1...K12 contactors
- RVC Power Factor controller
- T1 power transformer
- TAUX auxiliary transformer (optional)
- CT current transformer (not provided)
- V fan(s)
- R1...R12 reactors (APCR03 only)
- AUX auxiliary power supply

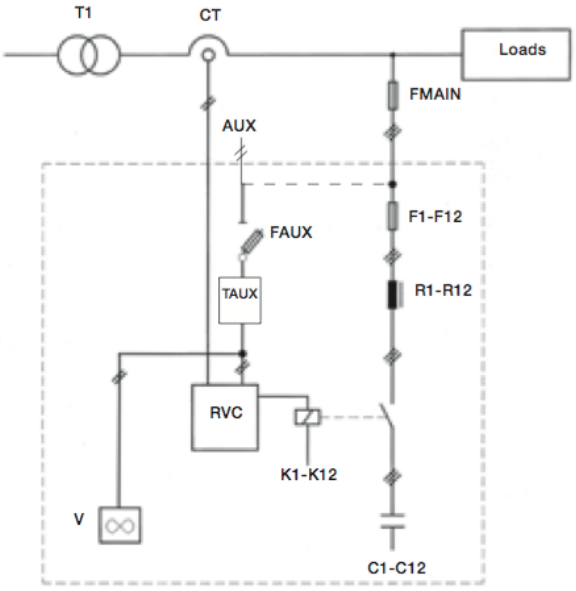

Figure 4.2: ABB wiring diagram: principle of automatic compensation of an installation [37]

4.2.1 Lifetime of Capacitors

The data sheets of manufacturers often indicate a guaranteed lifetime of capacitor units up to 100,000 hours. This information should be regarded as a statistical value - premature failures are possible. The guaranteed lifetime is defined at nominal operation conditions, that is at rated voltage and an average ambient temperature of 35 °C, unless otherwise specified. According to EN 60831 and EN 60871, operation of capacitors with higher voltages and higher currents than the nominal values is allowed depending on the duration [48]. Current loading and over-voltage stress reduce the lifetime of the capacitors. Furthermore, increased operating temperature causes a reduction of the lifetime of capacitors as shown in [48] for a rated life of 100,000 hours of operation and the lifetime is reduced by 50% for a temperature increase of 7 °C.

4.2.2 Preset Switching Time Delay per Capacitor Step

Manufacturers deliver the compensation banks with preset switching time delays usually in the range of 20 to 30 s. It is up to the customer to change it according to the expected fluctuations of lagging reactive power demand of the consumers. If few fluctuations are expected, switching time delays between 40 and 60s are quite sufficient. More frequent changes in reactive power require switching time delays between 20 and 40 s. The main goal of reactive power compensation is to follow the desired power factor, for example 0.95 on average within one billing period. Therefore it is recommended to check the first two or three energy invoices of the electricity distribution company. A

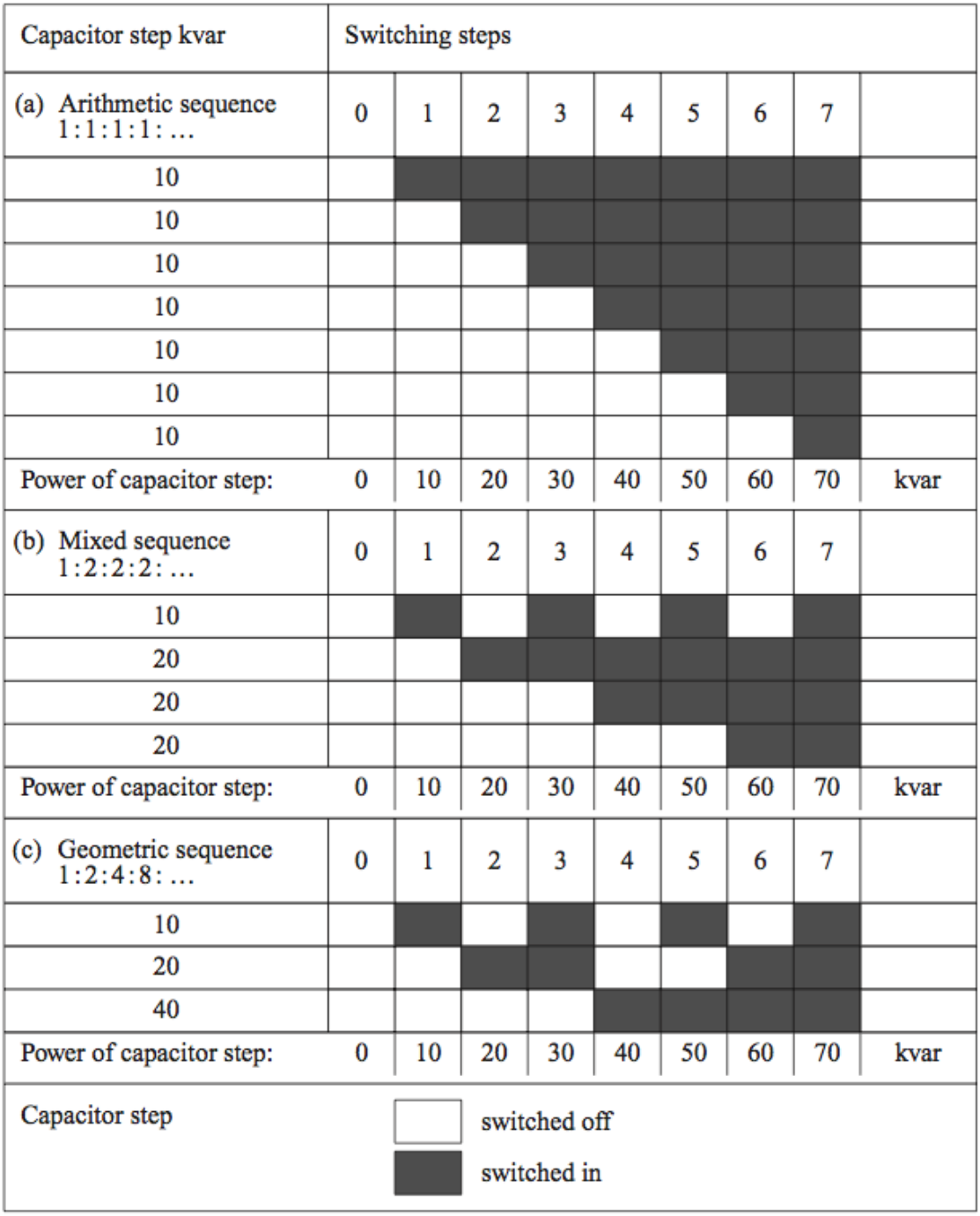

Figure 4.3: Fixed switching programs for equal- or unequal-sized capacitors [48]

correction may become necessary at any time in changing either the switching time delay or the preset power factor target. Preset switching time delays shorter than 20 s are not recommended. Note that shorter switching time delays increase the switching frequency; longer switching time delays spare both the switching devices like air contactors and the capacitors with regard to lifetime. Furthermore, this ensures that any capacitor step ready for re-energising will be unloaded since the last operating period. It must be underlined that the recommended switching time delays refer exclusively to LV compensation banks.

4.3 Capacitor Ratings

Capacitors must be built to tolerate voltages and currents in excess of their ratings according to standards. The applicable standard for power capacitors is IEEE Std 18-2002, IEEE Standard for Shunt Power Capacitors. Additional information is given in IEEE Std 1036-1992, IEEE Guide for Application of Shunt Power Capacitors. IEEE Std 18-2002 gives the following continuous overload limits. These are "intended for contingencies and not intended to be used for a nominal design basis." [46]:

- 110% of rated rms voltage
- 120% of rated peak voltage
- 135% of rated rms current (nominal current based on rated kvar and voltage)
- 135% of rated reactive power

Short time overload voltages were specified in IEEE Std 18- 1992 (on older version of the standard) and IEEE Std 1036- 1992 and are listed below. These standards state that a capacitor may be expected to see a combination of 300 such over-voltages in its service life. Note that these over-voltages are "without superimposed transients or harmonic content."

- 2.20 per unit rms voltage for 0.1 seconds (6 cycles of rms fundamental frequency)
- 2.00 per unit rms voltage for 0.25 seconds (15 cycles of rms fundamental frequency)
- 1.70 per unit rms voltage for 1 second
- 1.40 per unit rms voltage for 15 seconds
- 1.30 per unit rms voltage for 1 minute
- 1.25 per unit rms voltage for 30 minutes

4.4 Maintenance

Before any operation, disconnect the capacitor or the bank, wait 5 minutes, short-circuit and earth the terminals. Do not touch any capacitor terminals if not short circuited and earthed in advance. Periodical checks and inspections are required to ensure reliable operations: disregarding the following basic maintenance rules may result in severe operation, bursting and fire [47].

Two weeks after installation: check the tightness of the connection and terminals. This operation is always required before the start up.

Once a month:

- clean the bushings and terminal boards to avoid short circuit due to dust or contaminants.
- check the tightness of the connection and terminals;
- perform a visual inspection in order to check mechanical deformation
- check ambient temperature of the cabinet where the capacitors are installed. An increase of temperature could be an indication of reduced efficiency of the cooling systems due to dust and other contaminants.

Once a 6 months:

- check the surface temperature of energised capacitors. In case of excessive temperature is recommended to replace the capacitor. This could be due to an increase of loss angle which is an indication of reached end of life.
- Perform a current measurement, by means of a true effective rms meter or an harmonic analyser, and compare with nominal current. In case of current above nominal value check your application-systems for modification.
- In case of an increase of harmonics due to an increased use of non linear load, the installation of detuning reactors must be considered.
- Check the functionality of discharge resistors: switching off the capacitors and measuring the voltage between terminals. Within 3 min the voltage must be less than 75V.

A more thorough maintenance schedule has to be established according to the specific operating conditions. For instance, in a polluted environment cleaning may be more frequently necessary.

Chapter 5

Control of Centrally Located Reactive Compensation in LV Networks

To enhance the voltage level at both transformer LV side and the furthest node, capacitors could be used as a regulating devices. When a shunt capacitor is connected in parallel to the main substation, the voltage increases by reducing the inductive VARs. On the other hand, another important aspect is that a distribution transformer would be very inductive and have a very low power factor, particularly in a completely unloaded transformer (high X/R ratio), and as a consequence its power factor varies considerably as a function of the load since the power factor depends on the real/apparent power ratio. Table 5.1 outlines some values of the reactive power demand of three-phase transformers from Siemens AG. The reactive power at rated load is up to four times the reactive power at no load due to the leakage reactance.

		Reactive power losses	
Rated apparent power (kVA)	Impedance voltage (%)	No load (kvar)	Full load (kvar)
100	4	3.5	7.5
160	4	5.0	11.4
250	4	7.0	17.0
400	4	10.0	26.0
500	4	12.0	32.0
630	4	14.5	40.0
800	6	17.0	49.0
1000	6	20.0	80.0
1250	6	24.0	99.0
1600	6	28.0	124.0

Table 5.1: Reactive power demand of LV transformers (mean values)

5.1 Generic study: Effect of variation in centralised reactive compensation on transformer LV side voltage

For the voltage regulation utilising centralised capacitors devices, the case study 1 in section 3.2 was considered including variation of the power factor allover the network. Three cases were investigated with 0.7, 0.8 and 0.9 power factors. According to section 3.2, each case requires different amount of reactive power in order to compensate to unity. In table 5.2 are reported the reactive power amounts for the three cases. The transformer utilised in the simulations is a typical MV/LV transformer of 250kVA and $V_{Sc} = 4\%$. In figure 5.1 are showed the trends of the three cases for the voltage variation at transformer LV side. As can be seen the voltage trend is linear for each case and varying the power factor the voltage trend is still linear. As the simulations results show, the voltage level is lower for a poor power factor, for instance 0.7 pf, and it increases with the percentage of compensation till it reaches the same voltage level for all cases at 100% of compensation. It must be noticed that in a network with a poor power factor an over-compensation must be avoided as a higher over-voltage level is obtained compared to networks with pf close to unity: see figure 5.1 at 125% of compensation.

Power factor	***Reactive power amount kVAr***
0.7	46
0.8	34
0.9	22

Table 5.2: Reactive energy needed for a central unity compensation - figure 5.1

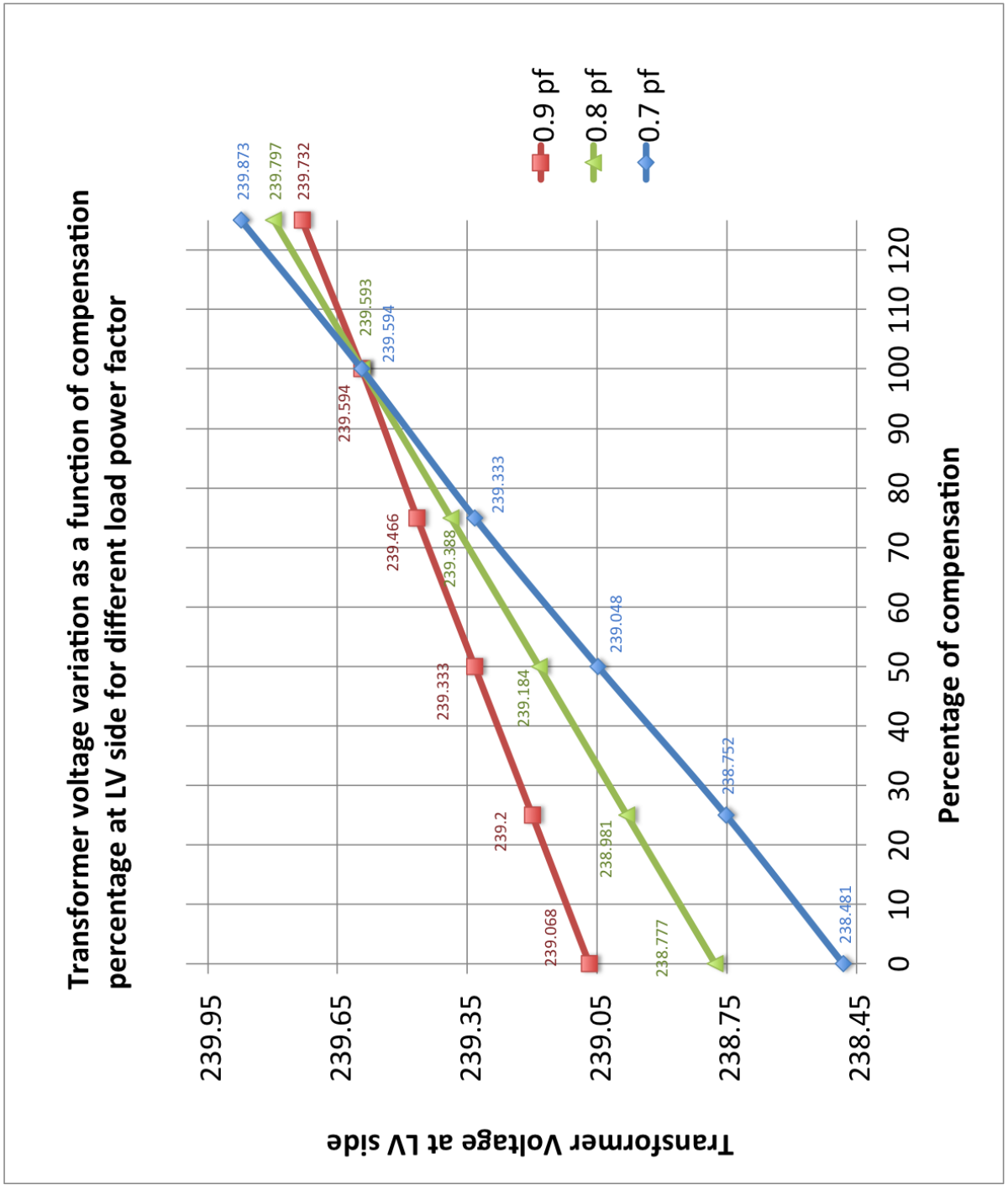

Figure 5.1: Voltage regulation at transformer LV side (with a central capacitor bank connected) including power factor variation

5.2 Western Power Distribution low voltage networks

5.2.1 Angus street network: Effect of variation in centralised reactive compensation on transformer LV side and feeder end voltage

Considering Angus street network simulated in the previous chapter in section 3.3.5, figures 5.2 and 5.3 show the voltage profiles improvement at transformer LV side and feeder end as a function of the percentage of compensation, respectively. The graphs show the results of some simulations data carried out by OpenDSS with different amounts of correcting capacitive power, in order to display the voltage trends which increase linearly with the percentage of compensation. The voltage at the transformer LV side has been enhanced on the third phase (the most loaded) from 233.97 (V) to 237.3 (V) at 100% of compensation (300 kVARs injected). The lowest voltage at feeder ends has increased linearly as a function of compensation percentage same as the voltage improvement at the main substation, and for instance at the end of feeder 50 as can be seen from the graph, there is a voltage enhance of about three volts.

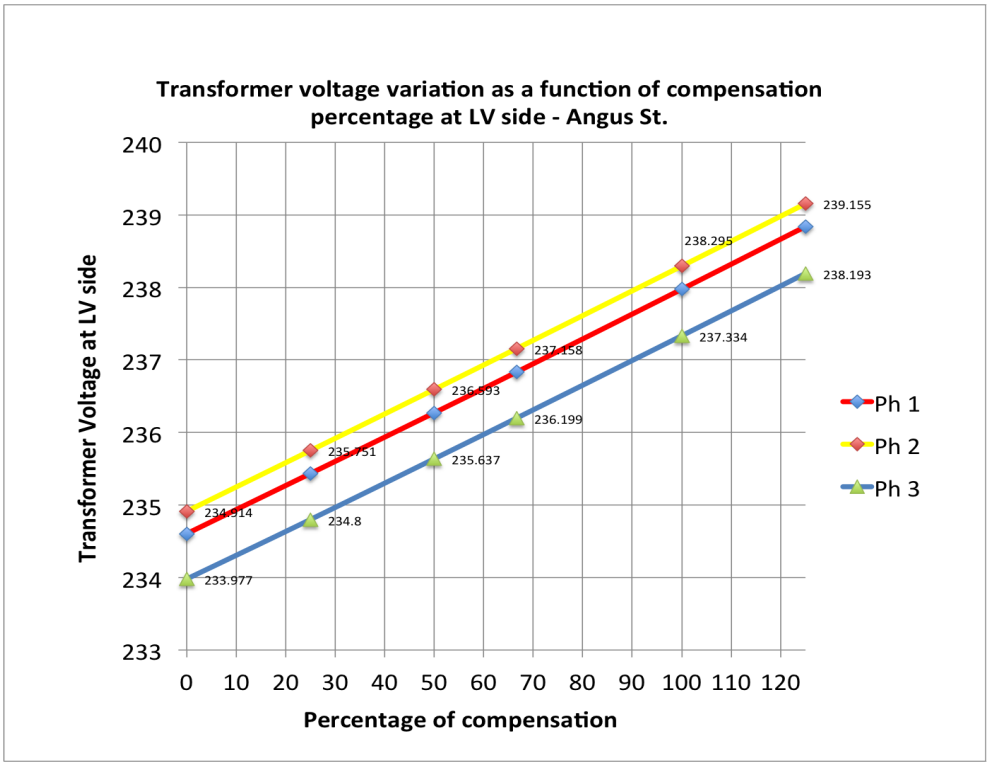

Figure 5.2: Voltage regulation at transformer LV side with a central capacitor bank connected

The same procedure was applied to another three LV networks run by Western Power Distribution, as listed:

1. Stuttgarter Strasse (urban), Cardiff
2. Nettlefold Road (urban), Cardiff
3. Rhos Wenallt, Abernant (rural), Aberdare

In figures 5.4, 5.5 and 5.6 are shown the graphs of the latter networks at the transformer LV sides, respectively.

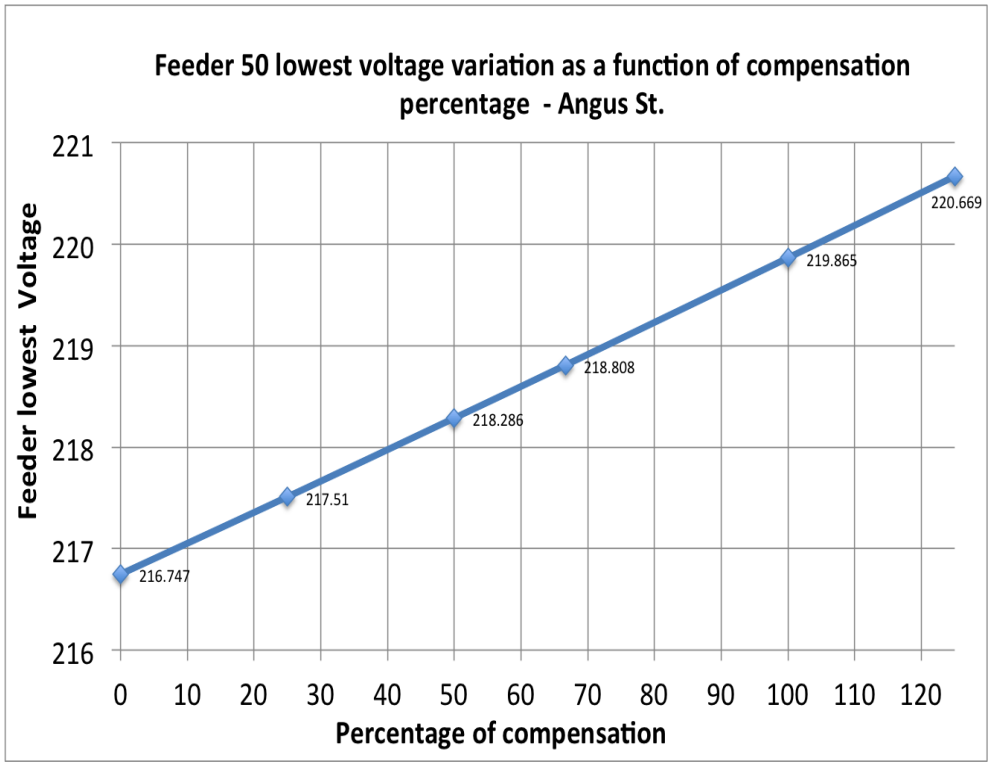

Figure 5.3: Voltage regulation at feeder ends with a central capacitor bank connected

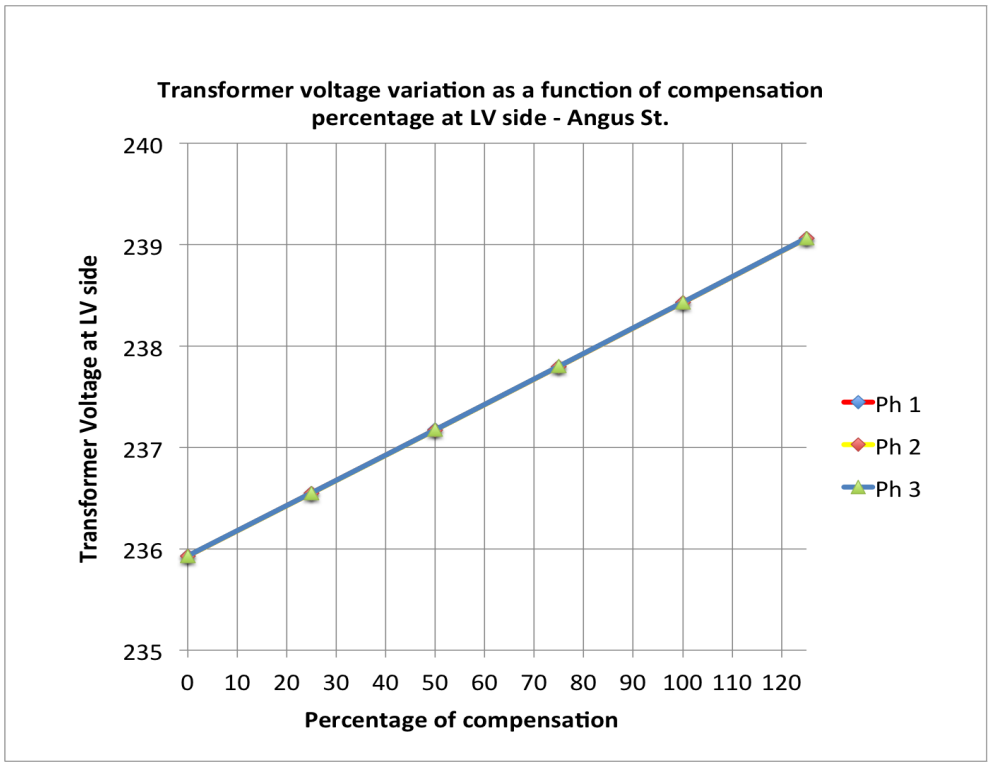

Figure 5.4: Stuttgarter Strasse network: Voltage regulation at transformer LV side with a central capacitor bank connected including power factor variation

5.2.2 Angus street network: Effect of variation in centralised reactive compensation on transformer LV current

In figure 5.7 are shown the current trends of the three-phase system at the main substation.

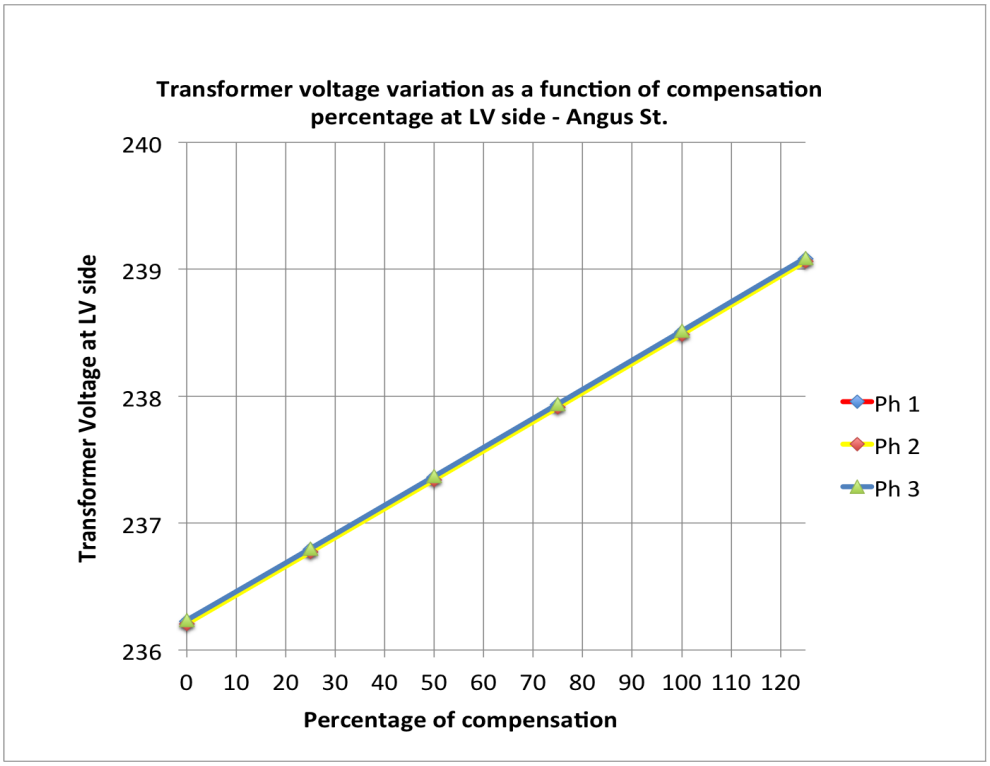

Figure 5.5: Nettlefold Road network: Voltage regulation at transformer LV side with a central capacitor bank connected including power factor variation

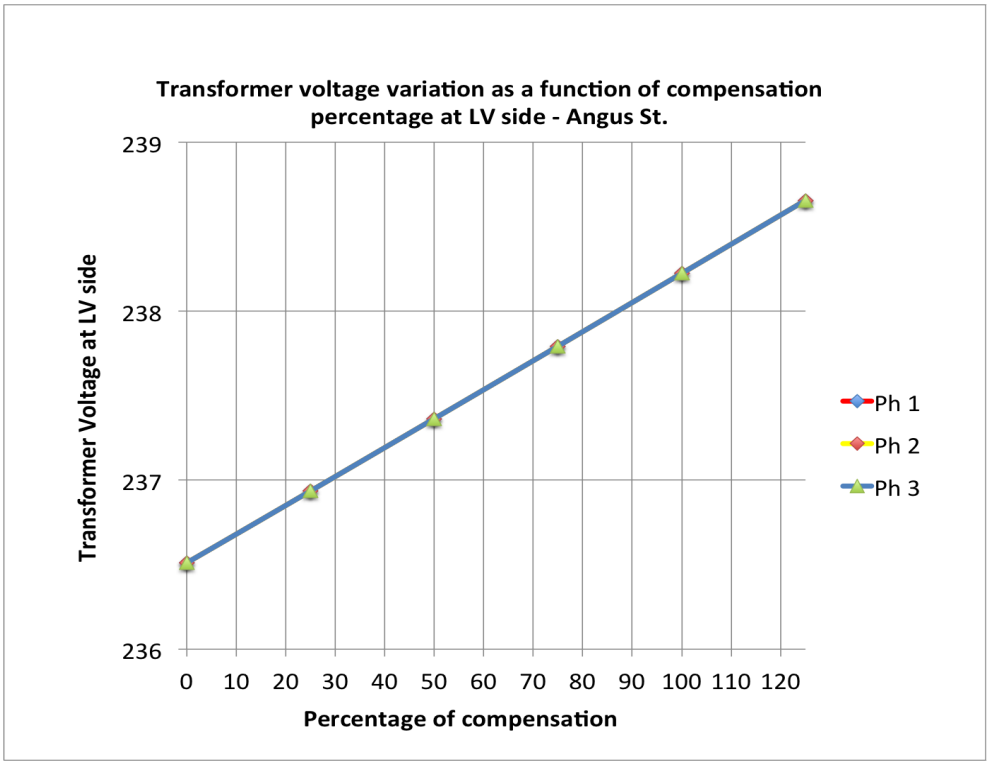

Figure 5.6: Rhos Wenallt, Abernant network: Voltage regulation at transformer LV side with a central capacitor bank connected including power factor variation

The transformer LV side currents decrease significantly initially as the compensation is applied with a non-linear trends and as expected, currents reach the minimum at 100% of compensation.

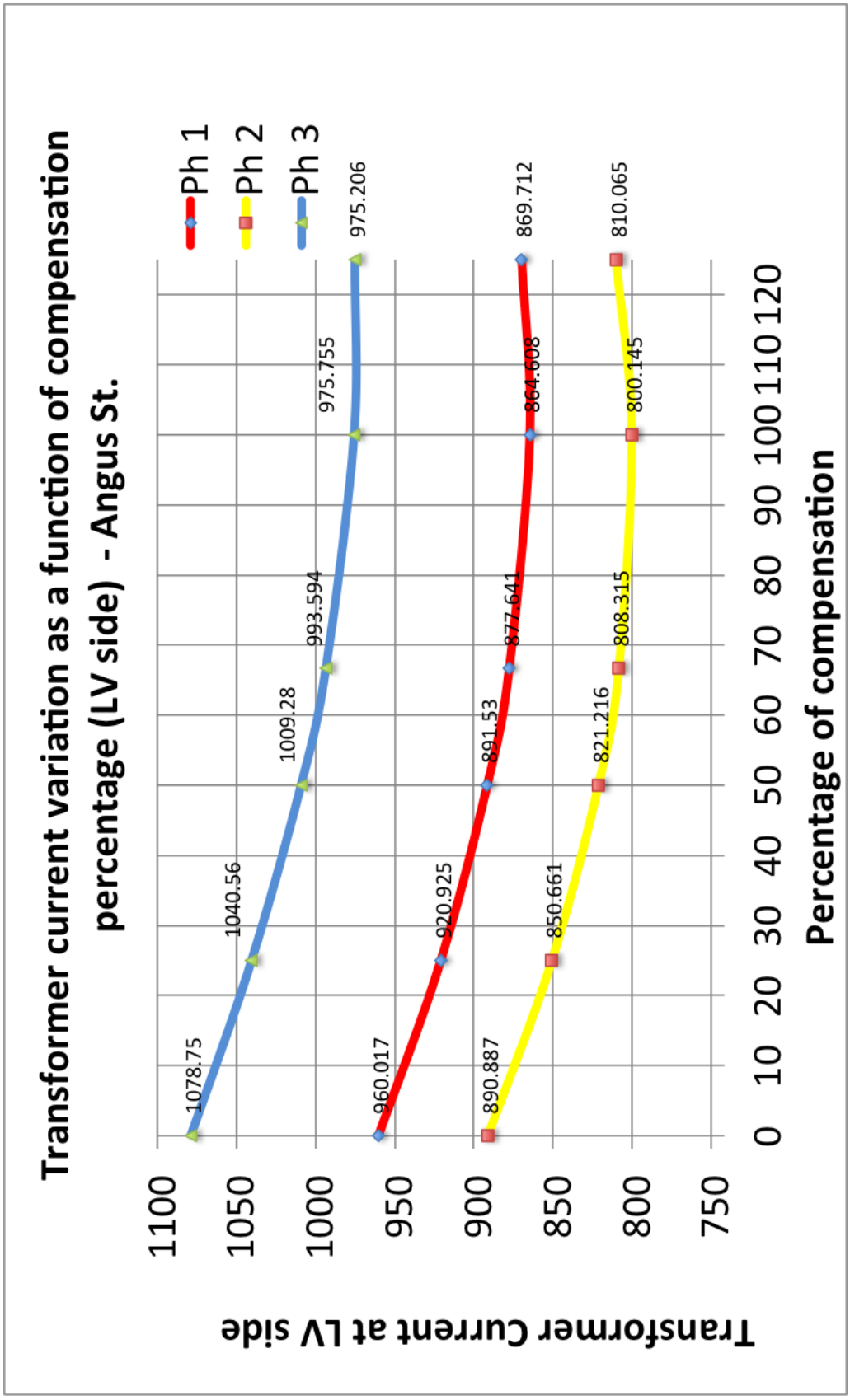

Figure 5.7: Current trends at transformer LV side with a central capacitor bank connected

5.3 Voltage and Var support through the deployment of automatic capacitor bank

Automatic capacitor banks are the most suitable solution for a centralised compensation in low voltage networks. These equipments could be supplied completely assembled and ready for use or custom built and designed to specific load requirements. Automatic capacitor banks are provided by controllers which enable reduction in energy demand increasing the distribution grid efficiency by improving power factor and releasing capacity. Furthermore, they supply variable quantities of Q in response to changing load conditions (magnitude and power factor) by incrementing or decrementing the active step. Generally, this capacitor bank type is used for systems with relatively low THD and TDD "Clean network", whereas for polluted network are used the de-tuned ones with the aim of harmonic suppression and dumping in-rush currents. In chapter 4 are showed some selected LV switched capacitors of four mainly manufactures to use on the analysed network: ABB, Schneider, Eaton capacitors and Gentec. Depending on the size of a compensation unit, it is assembled with capacitors of equal size or of different size. A unit with a total reactive power of 300 kvar consists of six power capacitors, of 50 kvar each. Thus the number of capacitors is identical to the number of steps: six capacitors controlled by six steps. However, compensation banks with unequal steps, for example 30 kvar and 20 kvar enable compensation in fine-stepping mode.

5.3.1 Daily load shape used in the network simulation

In the first part of the project [43] , a daily variation of measured phase values of real and reactive power of Angus Street network were illustrated for the 25th April 2012, which has been chosen as the date of peak load demand of the provided recorded data after a seasonal load analyses and it is shown in figure 5.8.

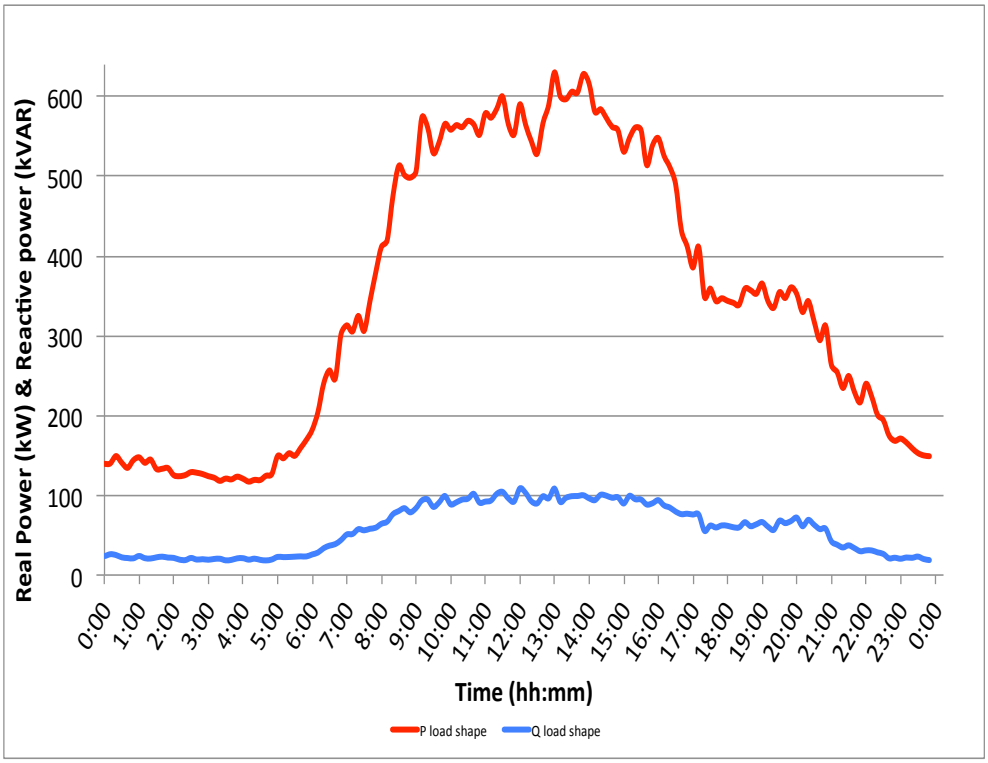

Figure 5.8: Angus street daily load shape on the 25th April 2012

The simulations were carried out using the latter real and reactive power trends with a 0.9 power

factor in order to analyse an extreme case by stressing the whole network.

5.3.2 Central Volt/VAr regulation at the main sub-station of a daily voltage variation

In this section, the voltage regulation is performed in OpenDSS using automatic central capacitor banks at the transformer LV side with different number of steps. Firstly, the voltage variation of the base case is shown in figure 5.10 and as can be seen from the voltage (L-N) result simulations of the three phases at the feeding point, before the reactive power compensation, there are voltage fluctuations over the day which are more evident from 06:00 a.m. until 09:00 p.m., but all of the phases follow almost the same trends even if it is unbalanced network. The voltages remain within the range 234.5 : 238.5 (V) and this is within statutory limits (-6%/+10% of 230V) [44] . Furthermore, a centralised compensation executed with a fixed central capacitor bank would not be suitable and would cause an over-compensation during the light load demand as shown in figure 5.11 [45], where the voltage trend over the day is basically shifted up with no regulation and there would still be a fluctuation of 4.75 (V) between the maximum and minimum voltage over the day. To avoid that voltage fluctuation, two simulations with a central automatic capacitor bank are carried out as follows:

1. Six-steps capacitor bank
2. Ten-steps capacitor bank

The reactive power amount is referred to a unity compensation and it is a 300 kVAr as discussed in chapter 3, section 3.3.3.

5.3.3 Control Scheme of Reactive Power and Simulations Results

The regulation of Volt/VAr in this study is carried out by measuring the reactive power every ten minutes as follows:

If Q $> Q_n$

Then $Q_n = +50$ (Six-steps) or $Q_n = +30$ (Ten-Steps)

Where,
Q is the measured reactive power
Q_n is the reactive power per each step activated with n=1, 2, .., 6 (Six-Steps case) or n=1, 2, ..., 10 (Ten-Steps case)

As a consequence, in the first case 300 kVAr are dived by six and each step is ratched up by the capacitor controller and a plus 50 kVAr is injected to the network until it reaches the maximum as follows: Q_n=[50, 100, 150, 200, 250, 300] kVar. In the second case, there is more regulation due to the higher number of stages compared to the previous case, where 30 kVar are injected into the network per each step activated until it reaches the maximum reactive power as follows: Q_n=[30, 60, 90, 120, 150, 180, 210, 240, 270, 300] kVAr. In both cases the only first step kVAr was not used for this particular day even with the slightest load demand.

As a result of voltage regulation with automatic capacitor banks, the voltage fluctuations are reduced to 2.43 and 2.25 (V) in the first and second case on the third phase, respectively. In the two different regulation cases the voltage trend is the same when the network is heavily loaded which occurs between 10:00 a.m. and 03:30 p.m. and on the remain part over the day are different and more

regulated in the second case with more steps where there is less fluctuation, for instance, from 20:00 to 21:00 as it can be seen in figures 5.12 and 5.13. Particularly, when the load varies greatly, switched capacitors with steps larger than required for correcting the power factor may lead to overcompensation and excessive leading power factor. The most substantial issues resulting from leading power factor are system over-voltage and generator regulation issues. Simply stated, generators prefer a lagging power factor load. A generator can find it difficult to properly regulate its output voltage when serving a leading load.

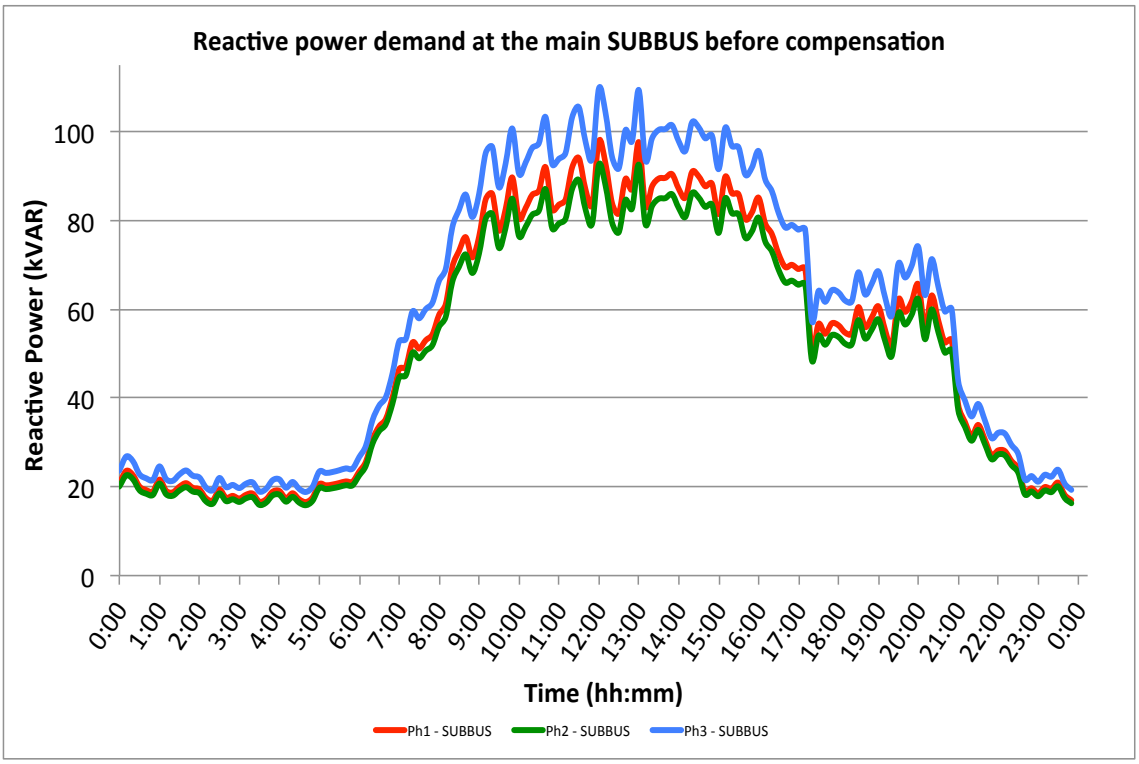

Figure 5.9: Reactive power demand at the main SUBBUS before compensation

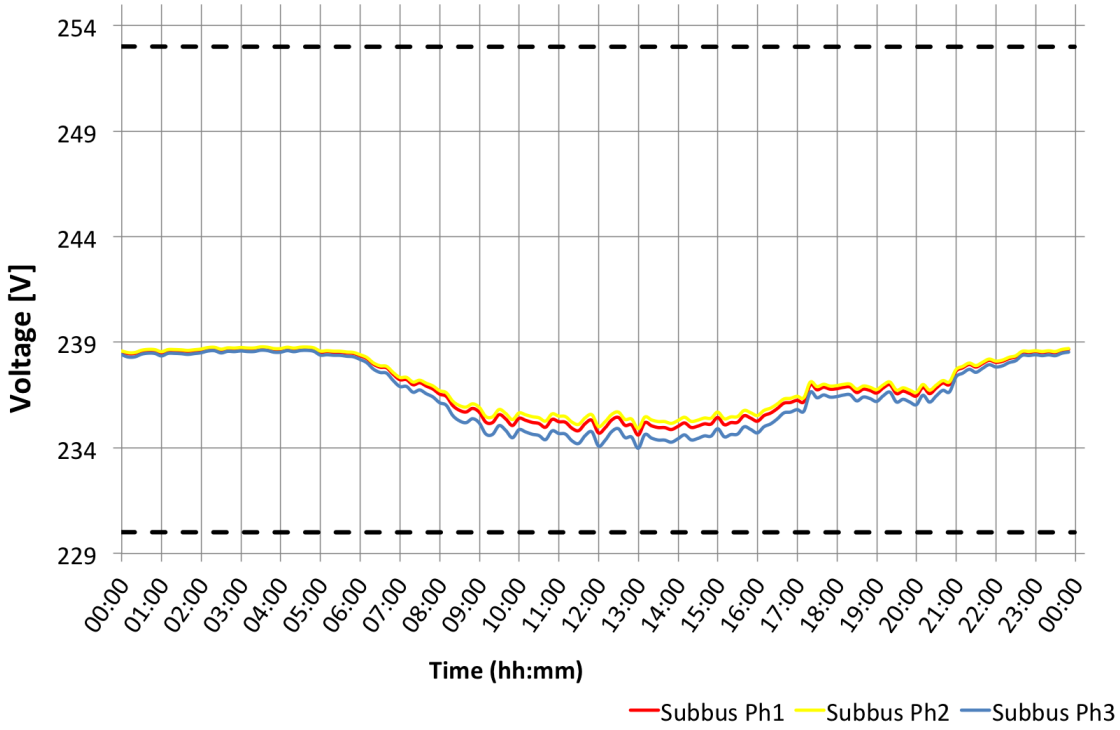

Figure 5.10: Base case voltage variation at the main sub-station

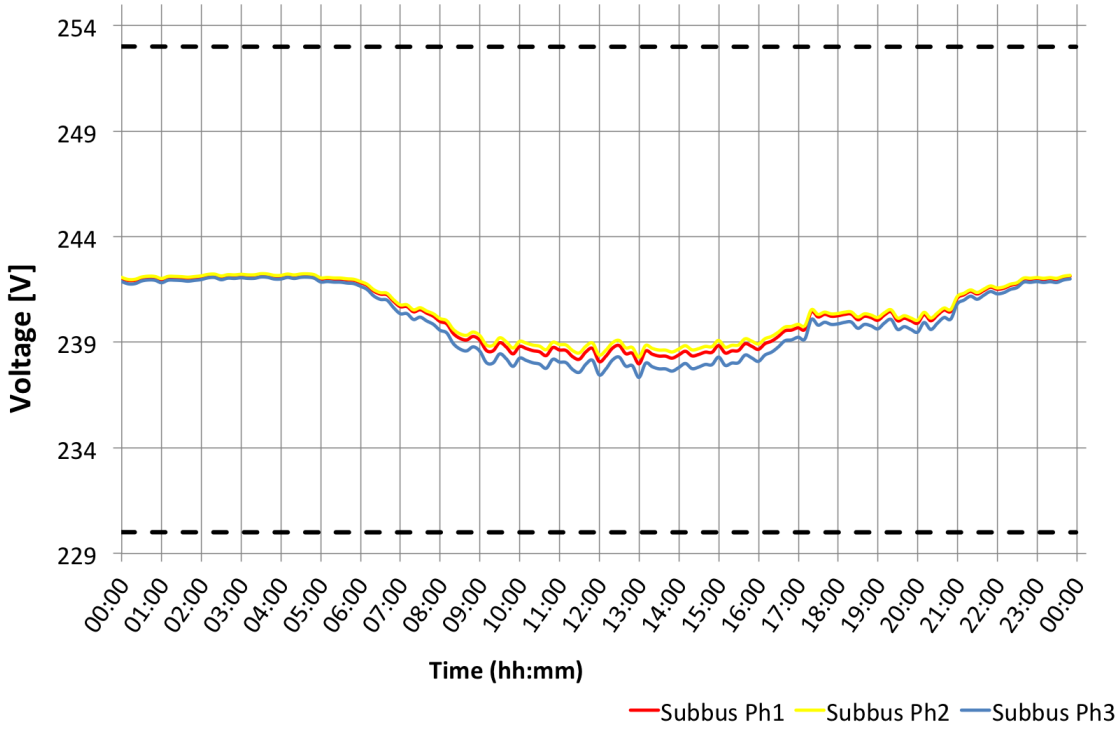

Figure 5.11: voltage variation due to fixed capacitor at the main sub-station

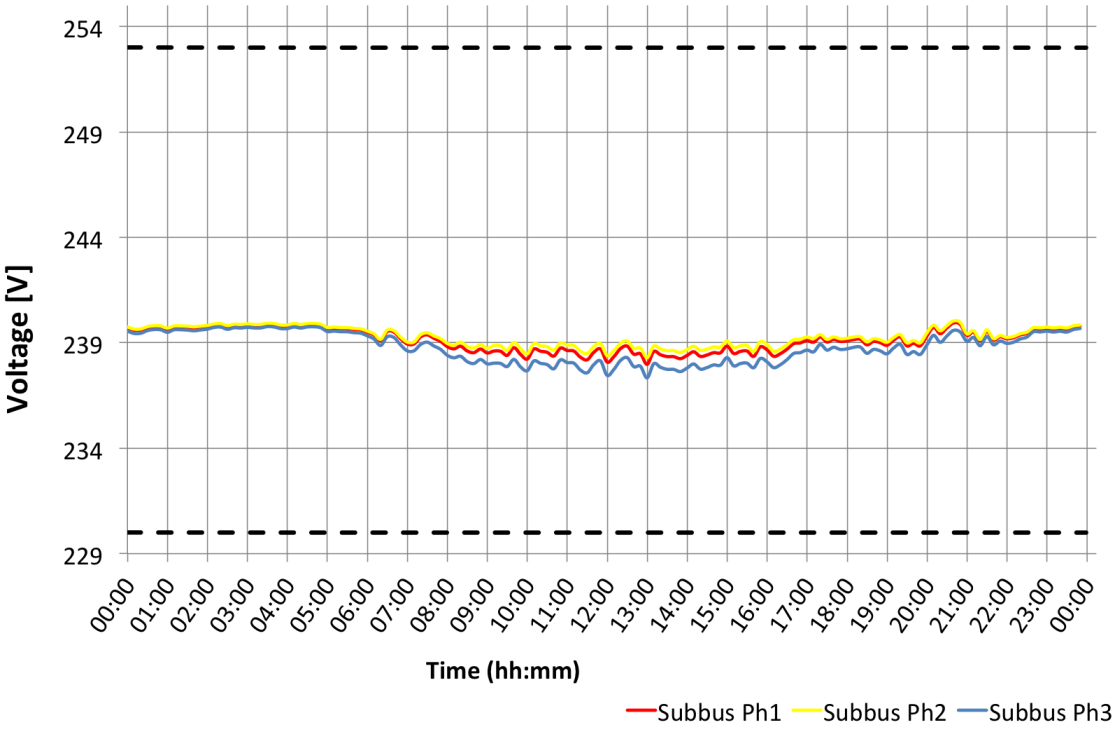

Figure 5.12: Voltage regulation case 1) Central automatic capacitor bank with 6 steps

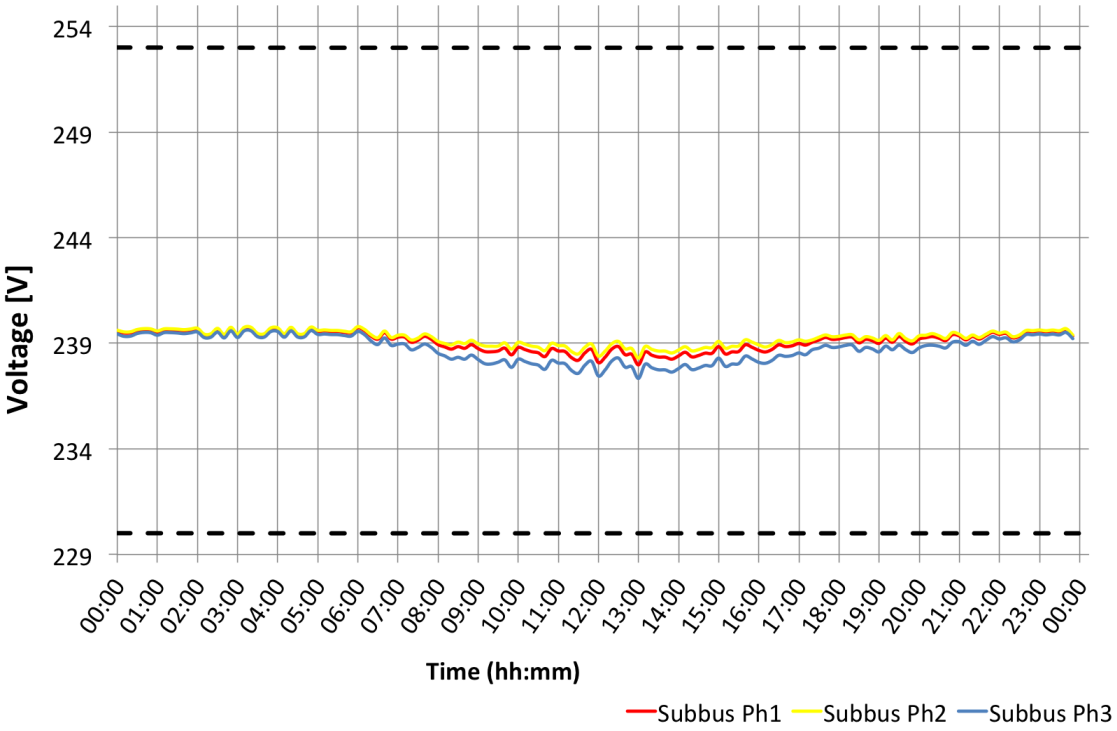

Figure 5.13: Voltage regulation case 2) Central automatic capacitor bank with 10 steps

As one can grasp, the Var control used previously causes an over-compensation in certain intervals during the day, and as a consequence, there is an over voltage on the daily voltage profile at the main sub-station. Referring to available control devices on the marketplace, as seen in section 4.2, a more precious control is identified by defining a bandwidth for the reactive power. In this way there is no risk of overcompensation. The CAP controller has been built in OpenDSS for automatic capacitor banks with six-steps and ten-steps as follows:

- Six-steps case) If the upper limit is greater than 50 kVAr, then switch on a step and if the lower limit is less or equal than zero, then switch off a step.
- Ten-steps case) If the upper limit is greater than 30 kVAr, then switch on a step and if the lower limit is less or equal than zero, then switch off a step.

The connection or disconnection of a step, as shown in figures 5.14 and 5.15, occurs when the reactive power amount exceeds or does not reach the upper limit and the lower limit, respectively, in points A and B. On the contrary, there is no reactive energy regulation when the kVAr are within the bandwidth, for instance, points C. In the simulations, the current transformer CT was positioned as

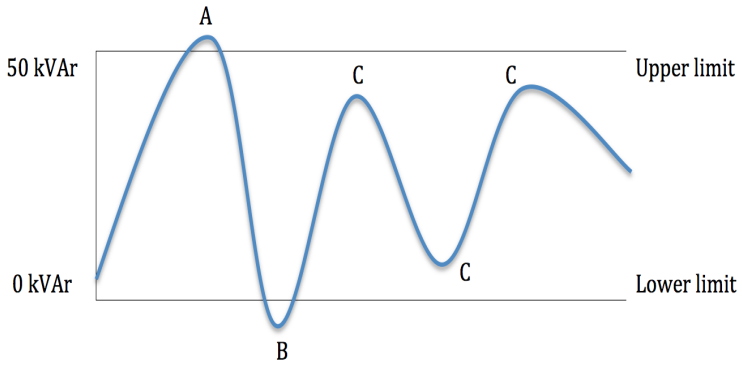

Figure 5.14: Bandwidth for Six-Steps automatic capacitor bank

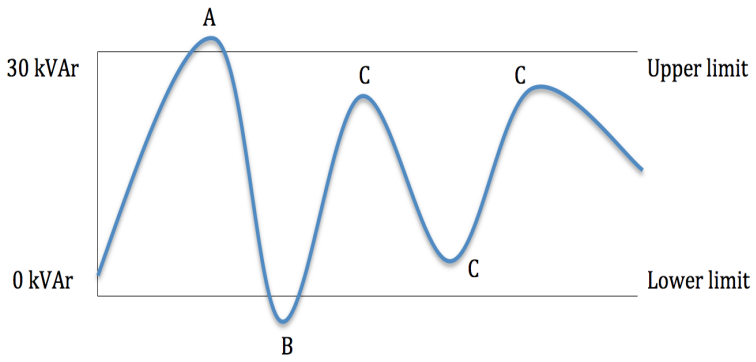

Figure 5.15: Bandwidth for Ten-Steps automatic capacitor bank

discussed in section 4.2 and in figures 5.16 and 5.17 are shown the daily voltage profile at the main sub station, for the controlled reactive power with six-steps and ten-steps, respectively. As a result of voltage regulation with automatic capacitor banks, the voltage fluctuations are reduced to 2.47 and 2.19 (V) in the first and second case on the third phase, respectively compared to the base case. Comparing the latter figures with figures 5.12 and 5.13, it could be noticed the slight over voltage on the daily voltage profile. Furthermore, there is less fluctuation, comparing the two cases performed with ten-steps capacitor bank, using a bandwidth for the control of reactive power.

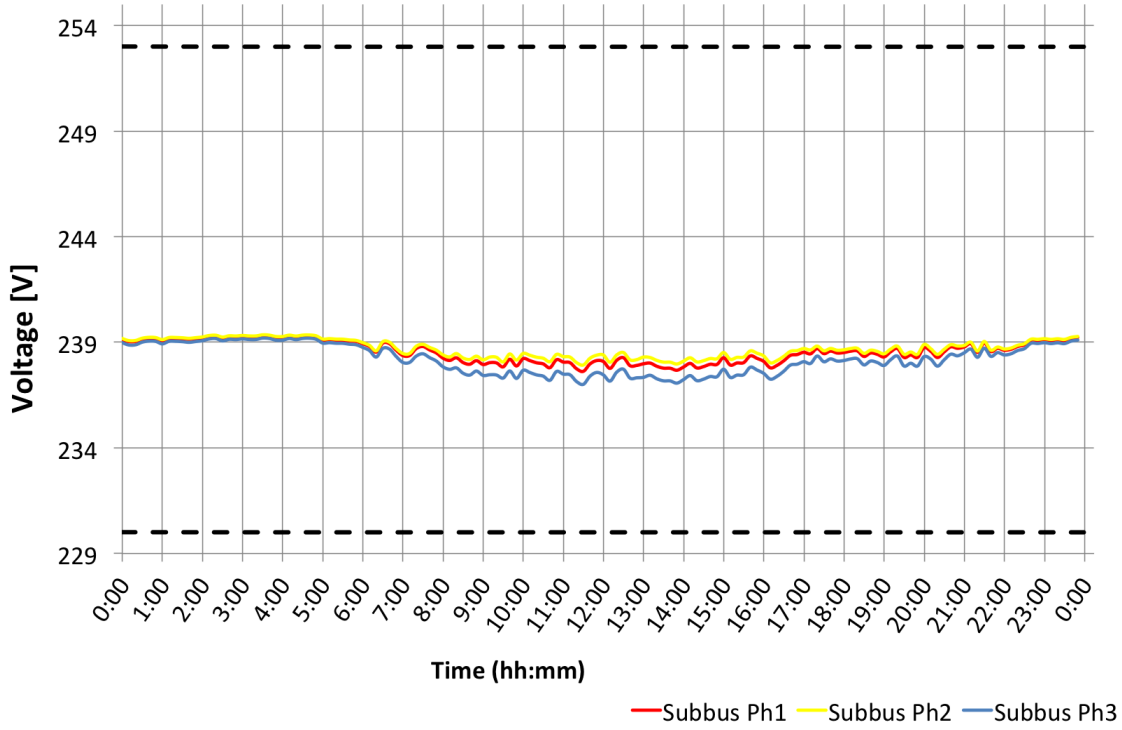

Figure 5.16: Voltage regulation with bandwidth) Central automatic capacitor bank with 6 steps

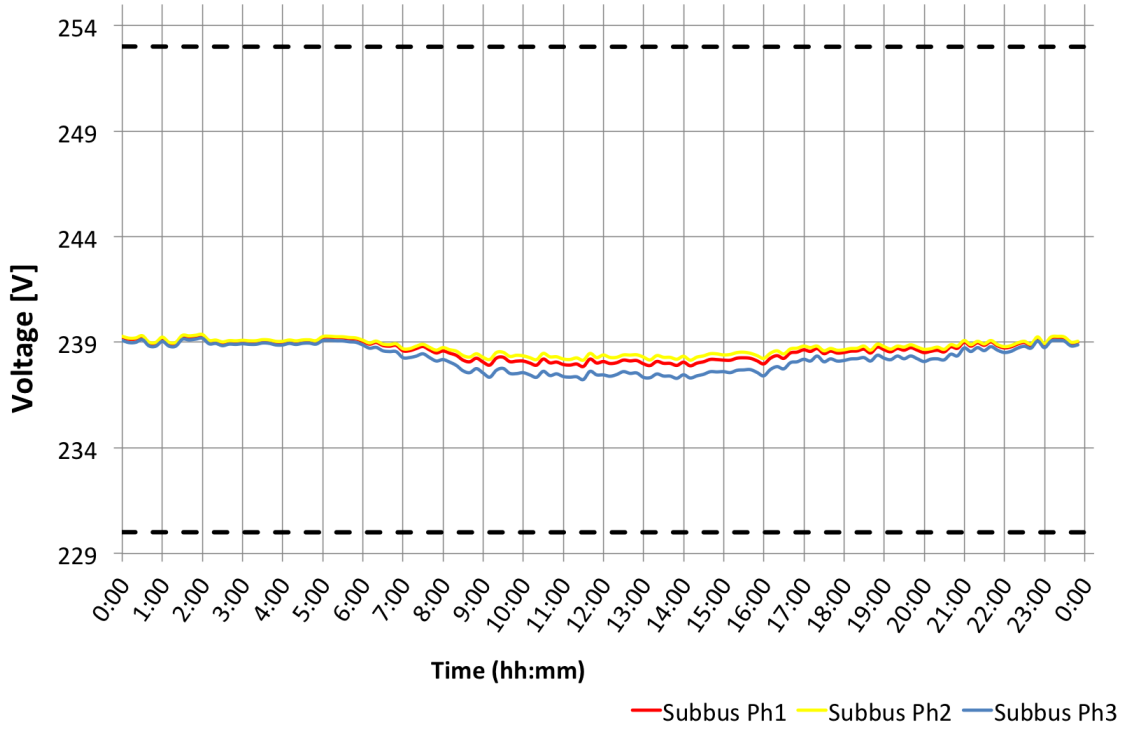

Figure 5.17: Voltage variation for kVAr regulation with bandwidth) Central automatic capacitor bank with 10 steps

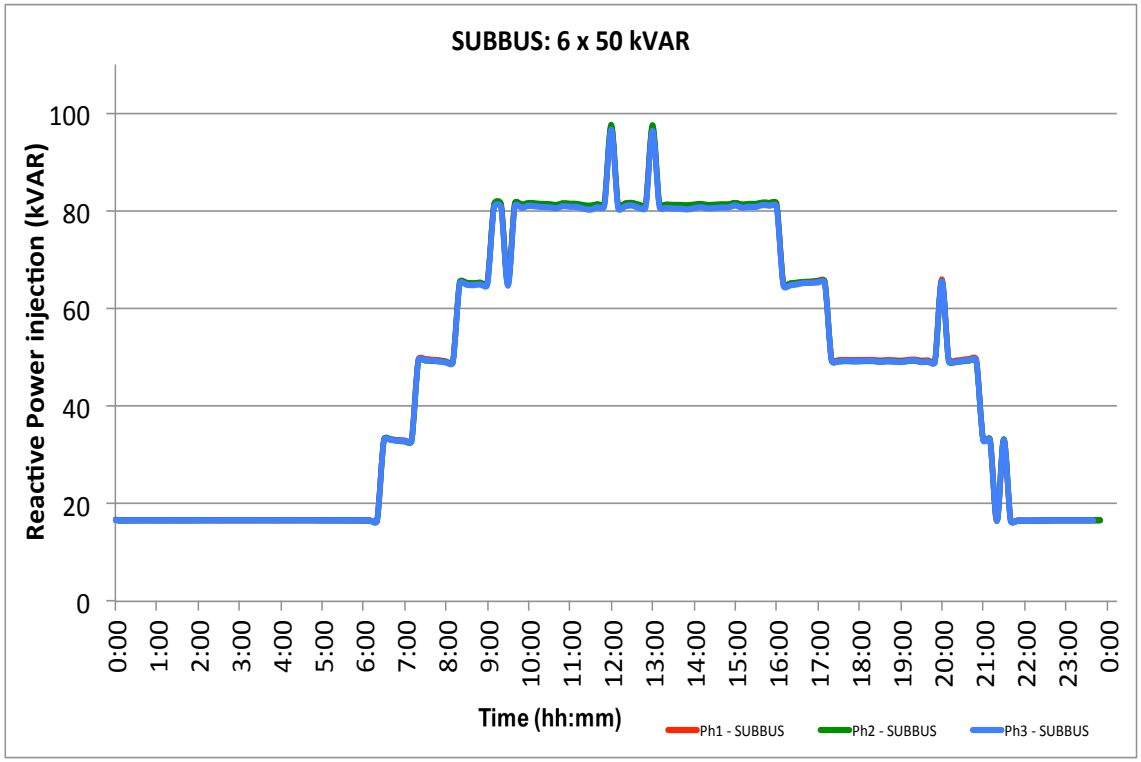

Figure 5.18: Stages ON/OFF sequence of a daily compensation with a Six-Steps automatic capacitor bank

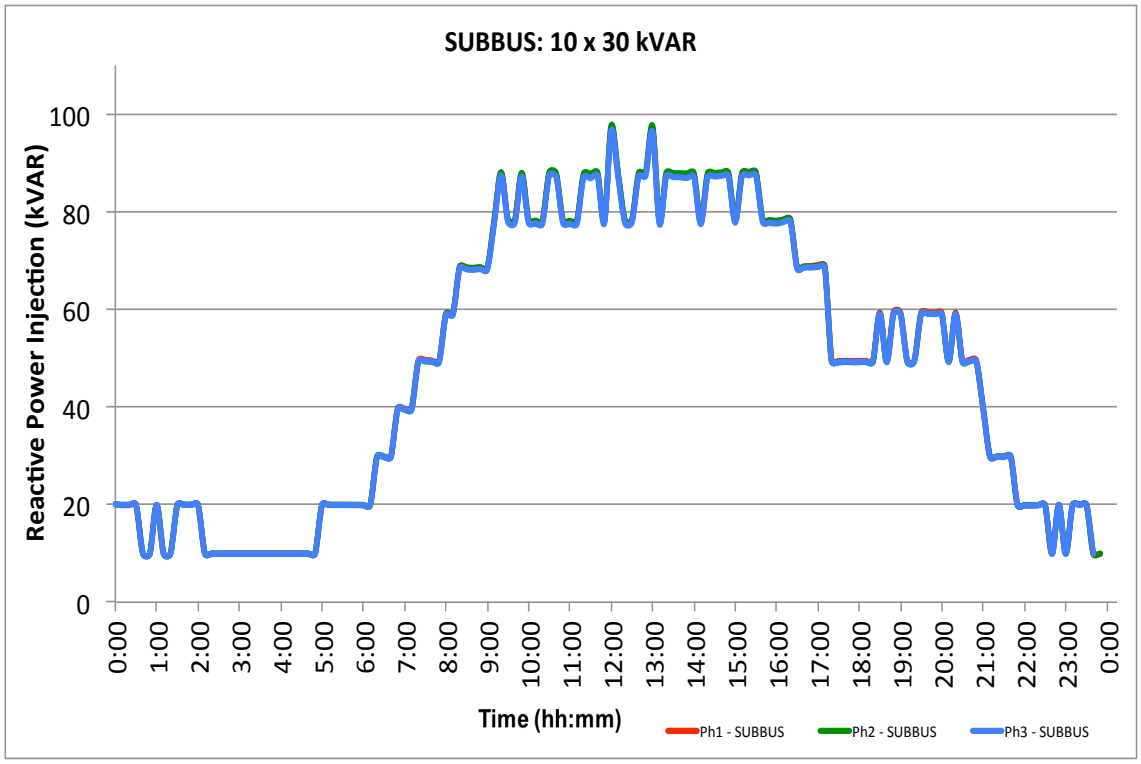

Figure 5.19: Stages ON/OFF sequence of a daily compensation with a Ten-Steps automatic capacitor bank

Chapter 6

Embedded Generation Impacts on LV Network Performance

In this chapter a study on the hosting capacity limits, embedded generation and its effects on Angus street LV network is expounded. The studies have been done with different number of simulations, in order to see the system performance in terms of energy and voltage changes. The network analysis has taken place as follows:

1. Network base case + dispersed connection points of PV over the network
2. case 1) including reactive compensation
3. case 2) assuming the minimum load

Generally, power injected from PV generation is real power as inverters work with a unity PF [50]. Utilising the reactive power capability of smart inverters for voltage control in systems with large penetration of PV generation should be possible with either local and remote control. The latter one is for PV systems of 6 kW or higher. According to the PV installation real power, smart inverters could work as follow:

1. Supplying or absorbing reactive power with 0.98 instantaneous PF for 3 kWp PV systems
2. Supplying or absorbing reactive power with 0.95 instantaneous PF for 6 kWp PV systems
3. Supplying or absorbing reactive power with 0.9 instantaneous PF for PV systems with peek power higher than 6 kWp

In PV generation, supplying / absorbing of reactive energy is conventionally assumed with the purpose of limiting the overvoltage / undervoltage caused by its input of active power. In the above listed simulations has been considered a unity PF. It is interesting to see also the same analysis for different PF utilising the reactive power capability of smart inverters for voltage control. In the following section are reported the current trends of Angus Street, whereas the voltage profiles of the base case were analysed in chapter 3 section 3.3.2. The PQ load curve used in this simulations chapter is the same as the previous one, whereas the photovoltaic load shape used is shown in figure 6.1. Furthermore, it has been considered a DG power peak of 300 kW which was divided equally over the whole network, therefore 60 kWp per feeder at the feeder ends (FDR20, FDR30, FDR50) and among the feeders (FDR10, FDR40). The output power of the PV system is calculated using the typical solar radiation data of the Cardiff area. The DG power peak has been sized up the 30% of the transformer capacity "1000 kVA" considering a dual purpose: firstly to fulfil in terms of cables ampacity and secondly to avoid excessive reversal of power flow.

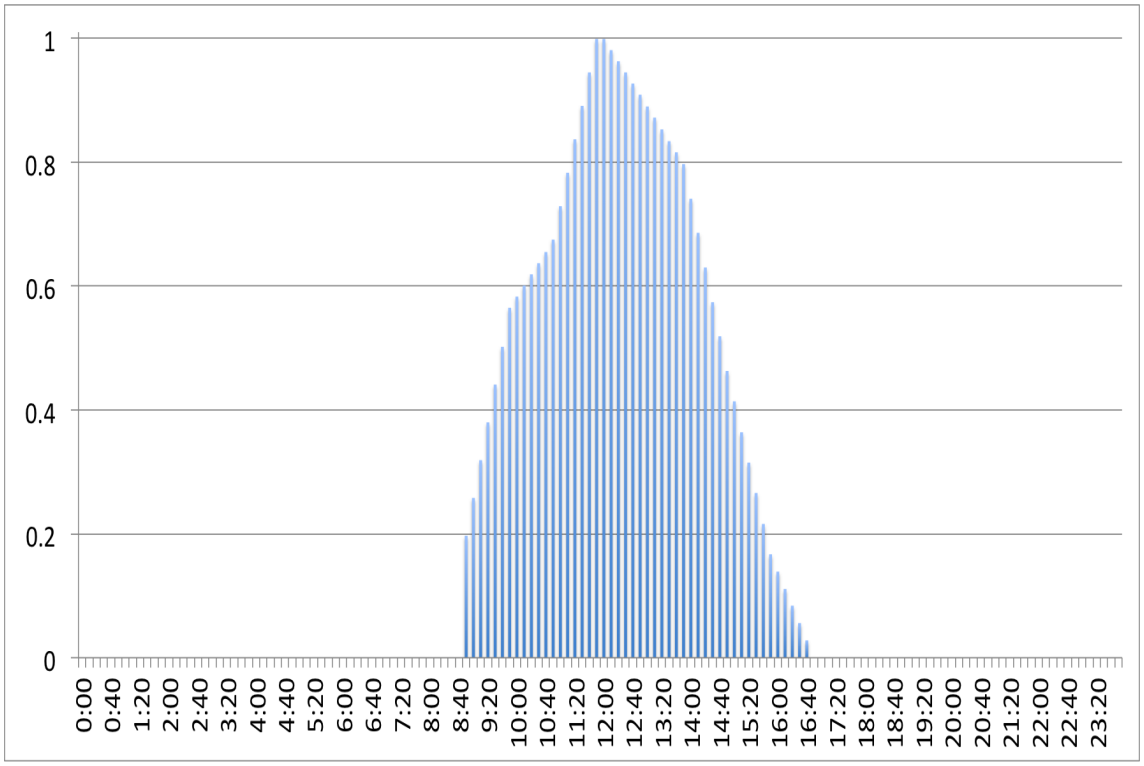

Figure 6.1: Photovoltaic daily load shape

6.1 Result analysis of Angus Street simulations: current limits

In this section current trends of Angus Street are shown in order to understand the impact of DG penetration on the network performance. Figure 6.2 shows the current profiles along Angus Street network under the nominal load case with 0.9 lagging power factor. In this case, simulating a constant PQ load, the phase currents trends are exceeding the cables ampacity only at SUBFDR50-LE103, whereas the first four SUB-FEEDERS are within the cables ampacity. At this stage all of the three phases are violating the cables thermal limits already at the initial supply point. The approximate current gap between ampacity limit and phase is about 130 - 140 A for phase 2 and 3, whereas for phase 1 is just less than 20 A.

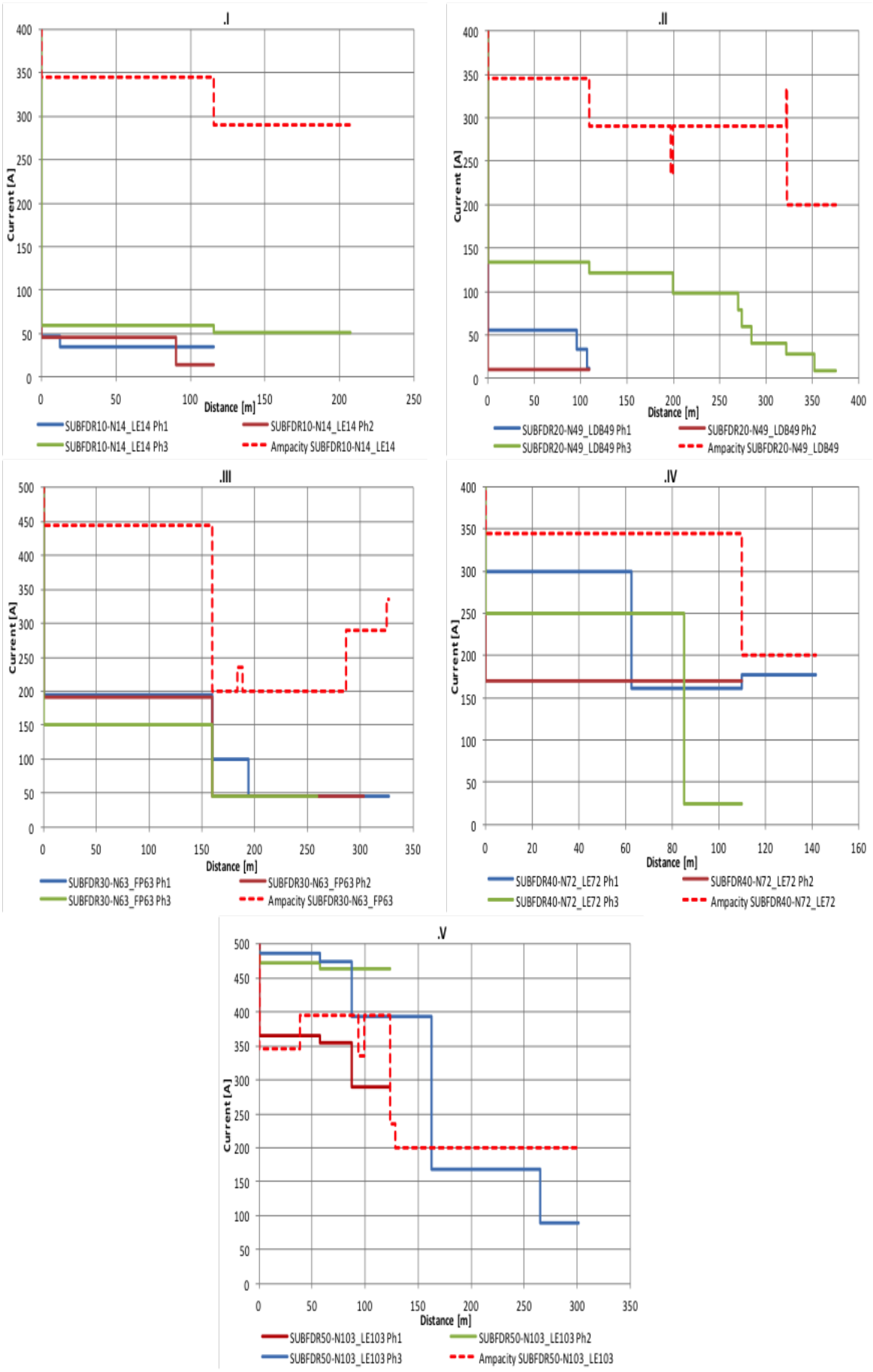

Figure 6.2: Angus street base case current profiles - 5 Sub-Feeders

6.2 Reactive compensation and a unity PF DG units impacts on Angus Street network: current limits

Simulating a unity PF DG units means that only active power is injected into the network. It has been considered the 30% of the MV/LV transformer power as a DG and according to figure 6.1 the real power injected into the system is depicted in figure 6.3.

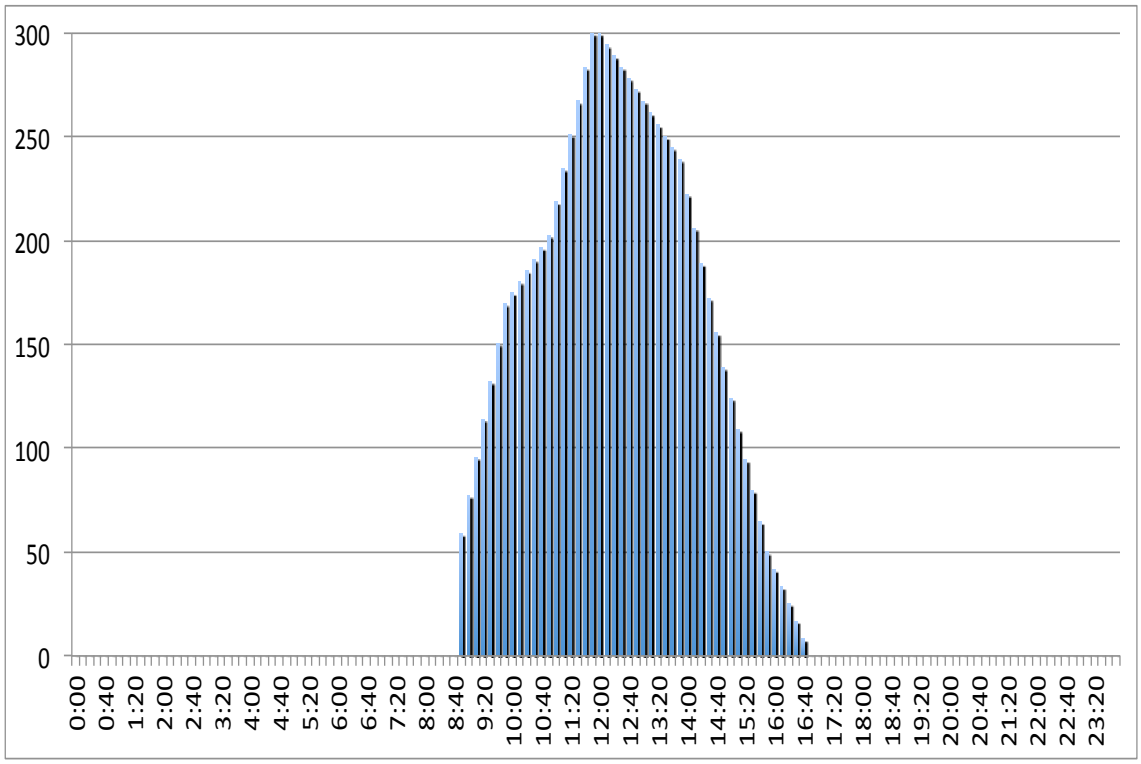

Figure 6.3: Injected active power for a 300 kW unity PF DG units

Considering the 300 kW, divided equally, along the five feeders and the centralised automatic reactive compensation case (50 kVAR by 6 steps), figure 5.16 section 5.3.3, the current trend in this configuration is shown in figure 6.5. As it could be seen, the phase currents trends are exceeding the cables ampacity at SUBFDR20 and SUBFDR50. In the first one the cable ampacity has been violated in the last 100 m, whereas in the second one there is a significant reduction in the third phase current: 487 A before and about 403 A after compensation and DG penetration. As the fifth sub-feeder is the most loaded one, it would be useful to analyse the current trend with the only reactive compensation effect on phase currents reduction, in order to compare the performance enhancement with the latter case. Figure 6.4 shows the current trend along the SUBFDR50 with an automatic centralised compensation (50 kVAR x 6 steps) and no DG. Comparing figures 6.4 and 6.5 (SUBFDR50), it is evident that with a 300 kW injection at the feeder end the power losses decrease and thus the third phase current from 493,45 A to 403 A.

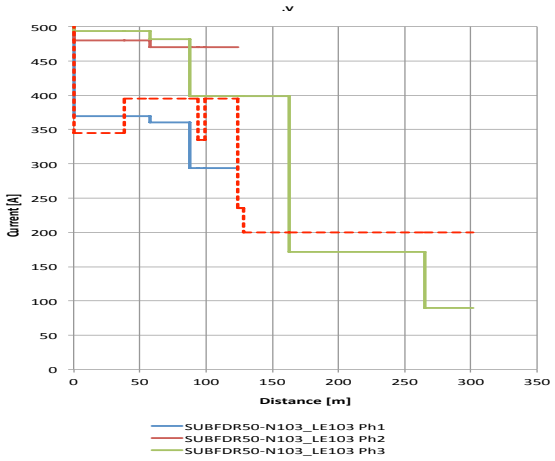

Figure 6.4: Current trends along SUBFDR50 with automatic centralised compensation

6.3 Reactive compensation and a unity PF DG units impacts on Angus Street network: Voltage variation

In the previous chapter the voltage variation and regulation has been studied at the transformer low voltage side. Since the injected active power depends on random changes of solar radiation there is a voltage fluctuation at the DG units points of connection and then in a lower measure among the network. Figure 6.6 shows the voltage trend at the main busbar.

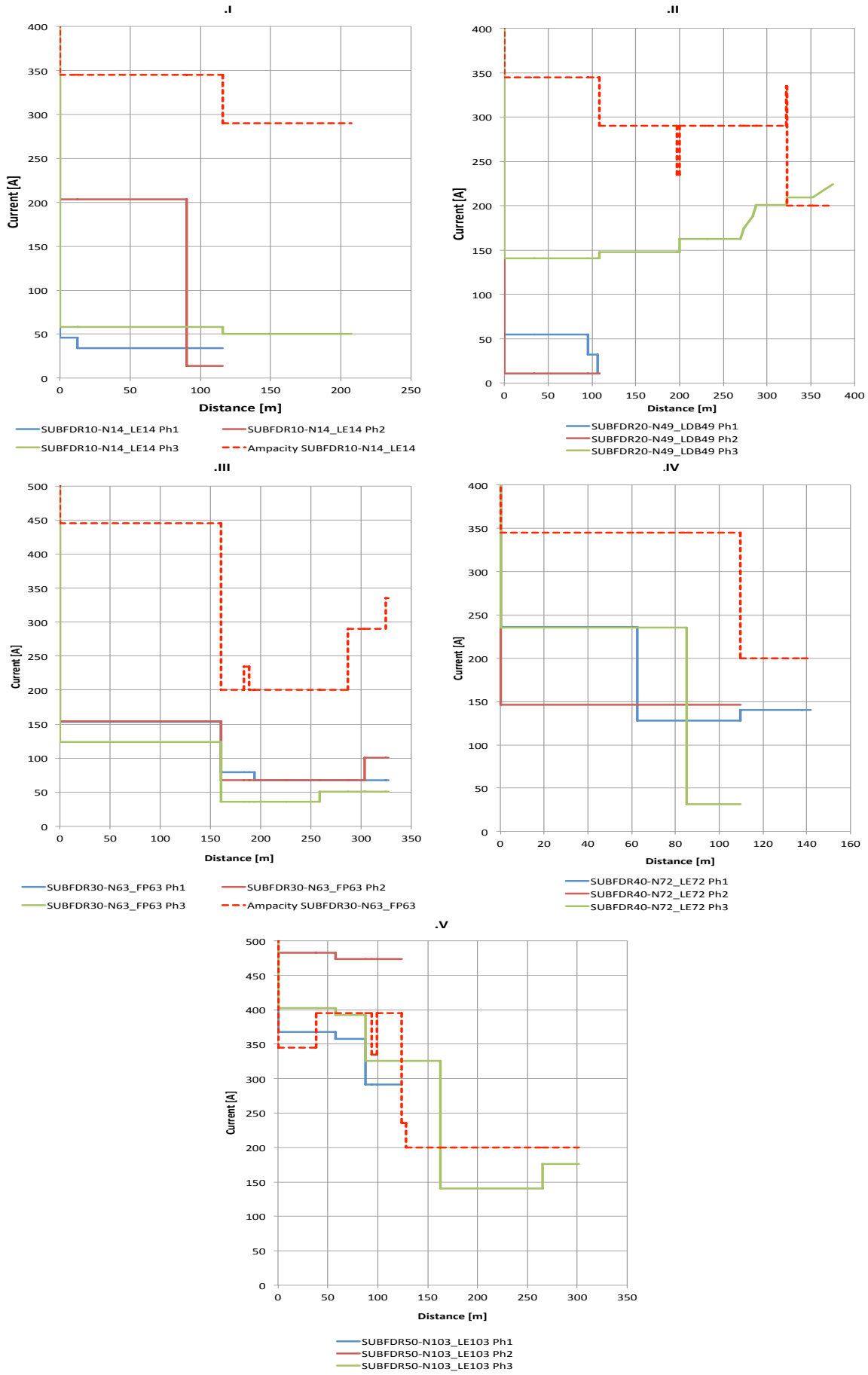

Figure 6.5: Angus street current profiles - including centralised compensation and unity PF DG

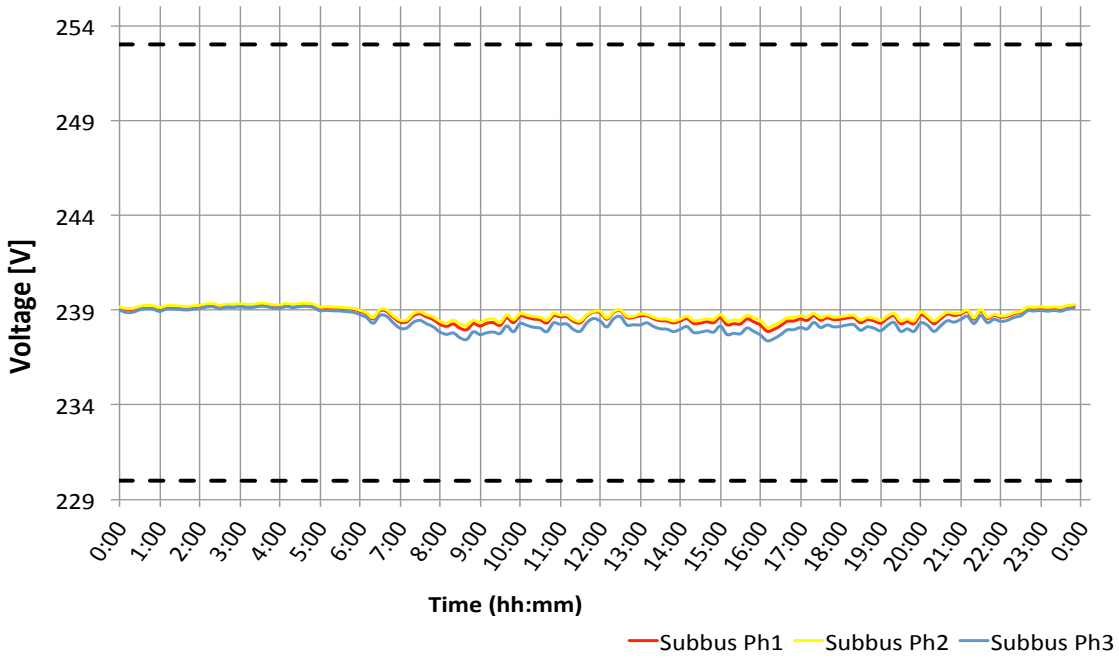

Figure 6.6: Voltage variation due to a unity PF DG penetration and centralised automatic compensation on Angus Street network

6.3.1 Voltage profiles including centralised compensation and 300kW unity PF DG units on Angus Street network

As seen in chapter 3 voltage profiles along each feeder before reactive compensation and after the different strategies of compensation, it is important to verify the same way, specially, in the case of high PV penetration. In figure 6.7 are depicted the voltage profiles which exhibit the voltage unbalance between the three phases due to the DG single phase units connection. Further, there is no violation in voltage profiles on the whole network. However, these voltage values could increase/decrease further according to the load disconnection/connection and due to a higher power generated by the DG units than the load demand on the same feeder, figure 6.8.

6.4 Reverse power flow on Angus Street network

The large amount of PV penetration among the whole network causes a reversal of power flow from downstream to upstream nodes. The studies are carried out, according to the DG units sizes and positions showed in table 6.1. Only on SUBFDR30 the DG single phase units has been distributed on the three phases, while on the other SUBFEEDERS the DG units have only been connected to one phase chosen alternatively. Furthermore, the high amount of active loads has been distributed on the network third phase for a total of 132 kW, whereas a 84 kW have been connected to every other phase. The interaction between the load absorption and the DG injection must be studied as follow:

- case 1) Maximum daily load curve
- case 2) Minimum daily load curve

6.4.1 Case 1) Maximum daily load curve

The three-phase load curves and the active power injected into the network for each SUBFEEDER are shown in figure 6.9. However, the maximum reverse power flow obtained by the simulation analyses

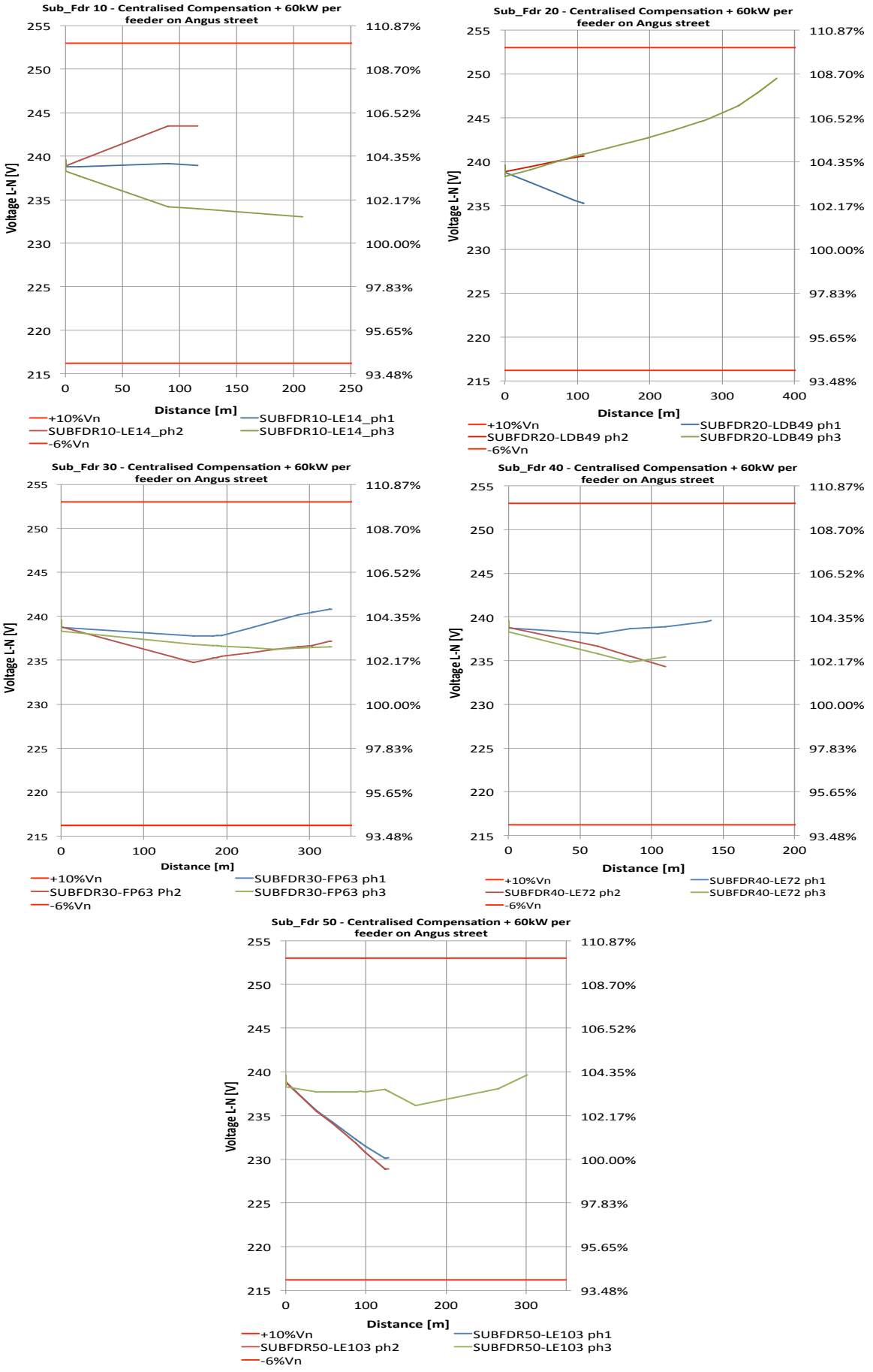

Figure 6.7: Voltage profiles including 300kW unity PF DG units and centralised compensation on Angus Street: Voltage unbalance caused by DG single phase units

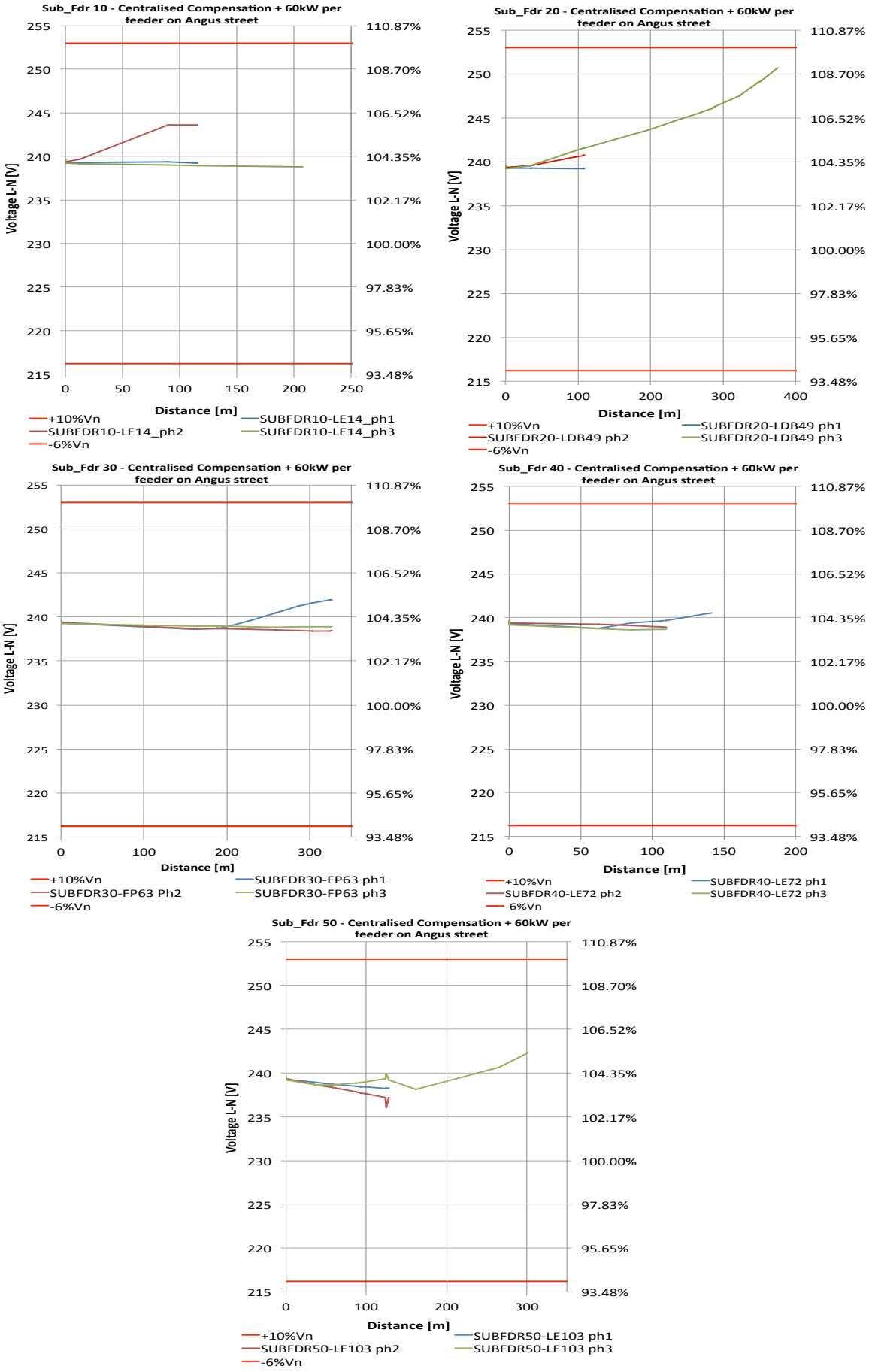

Figure 6.8: Voltage profiles including 300kW unity PF DG units and centralised compensation on Angus Street: Maximum voltage reached along all feeders in a daily PV/load shapes

	kW phase 1	***kW phase 2***	***kW phase 3***
Sub-Feeder 10	/	60	/
Sub-Feeder 20	/	/	60
Sub-Feeder 30	24	24	12
Sub-Feeder 40	60	/	/
Sub-Feeder 50	/	/	60

Table 6.1: Active power sizing for distributed generation - Angus Street network: Total distributed generation amount P = 300 kW

are shown in figure 6.14. As can be seen, there is a large amount of reverse power flow through the first two SUBFEEDERS, on phase 2 and phase 3, respectively, and in a small amount through the forth one. At SUBFDR30, as generators are connected to the three phases, there is no reversal of power flow due to the higher load demand than the injected power on each phase. Finally, on SUBFDR50 there is a significant reduction of active power on the most loaded phase, the third one and no reverse power flow to the main SUBBUS. Despite the reversal of power flow on three SUBFEEDERS in different amounts and on different phases, there is no reverse power flow from the transformer LV side to the MV side, figure 6.14.

6.4.2 Case 2) Minimum daily load curve

In Chapter 1 has been explained how daily load curve shapes vary according to the different type of customers and change with the season of the year. In the previous section the analysis carried out had a maximum daily load curve. In order to see the DG impacts on the system network, and thus on the reversal of power flow, a 0.65 load multiplier is applied to the base kW values of the load to represent variation of the load over some time period. Figure 6.13 shows the power demand at the main SUBBUS after the base kW reduction. However, the base load reduction does not give rise to a reversal of power flow from the transformer LV side to the MV one and the power demand is minimum around mid-day on the third phase.

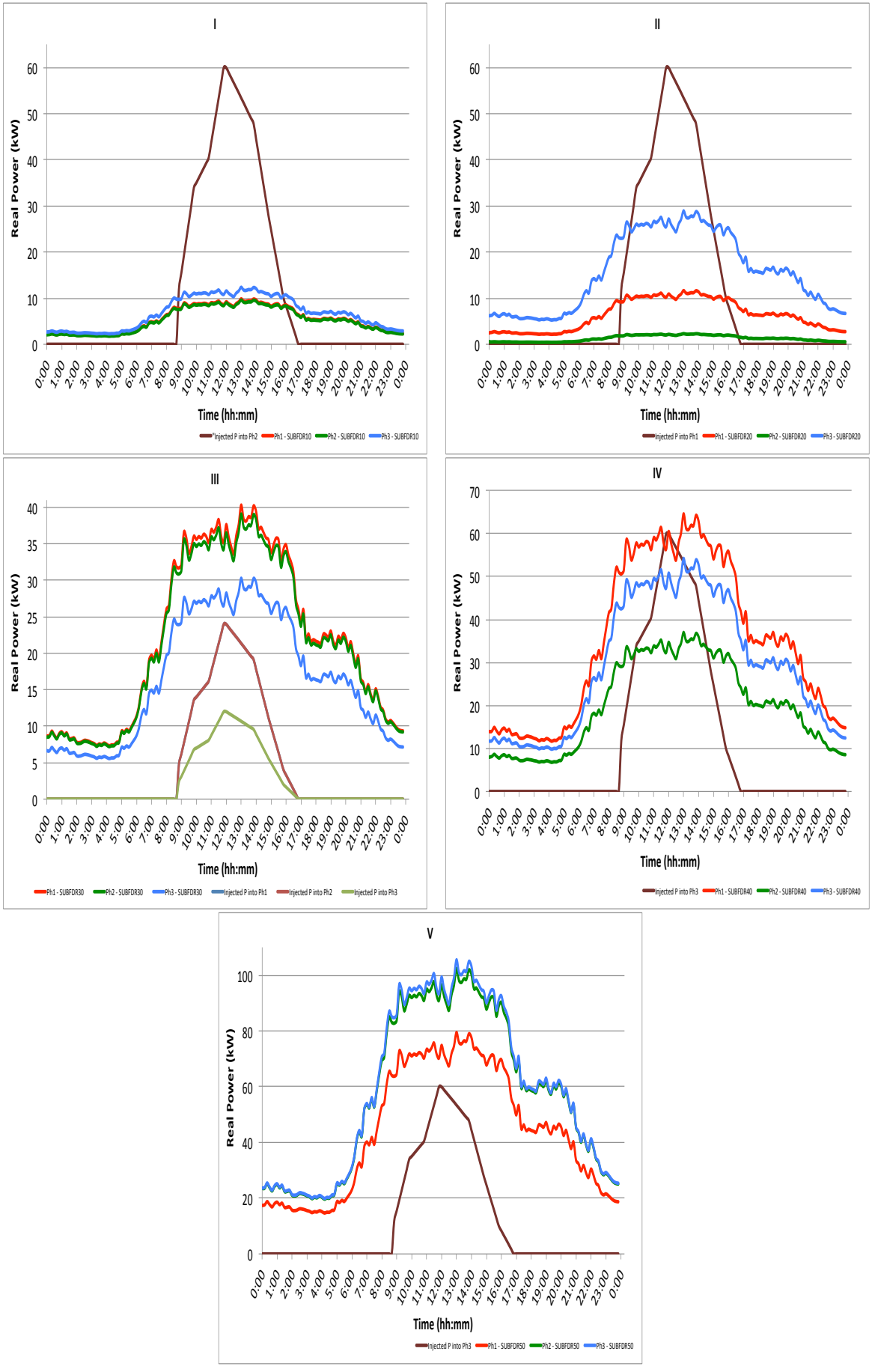

Figure 6.9: Load curve demand and active power curve injection

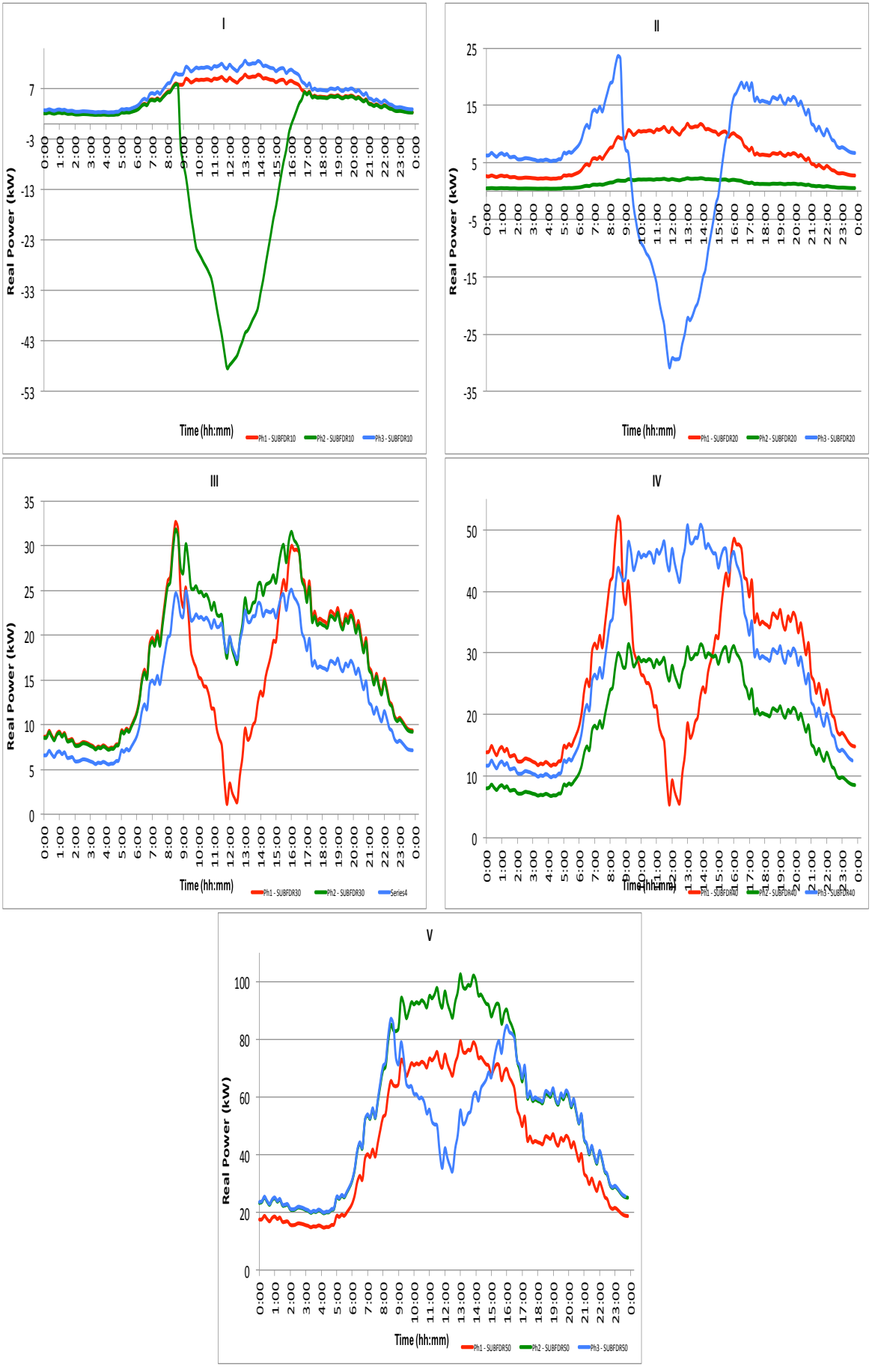

Figure 6.10: Reversal of power flow at each SUBFEEDER

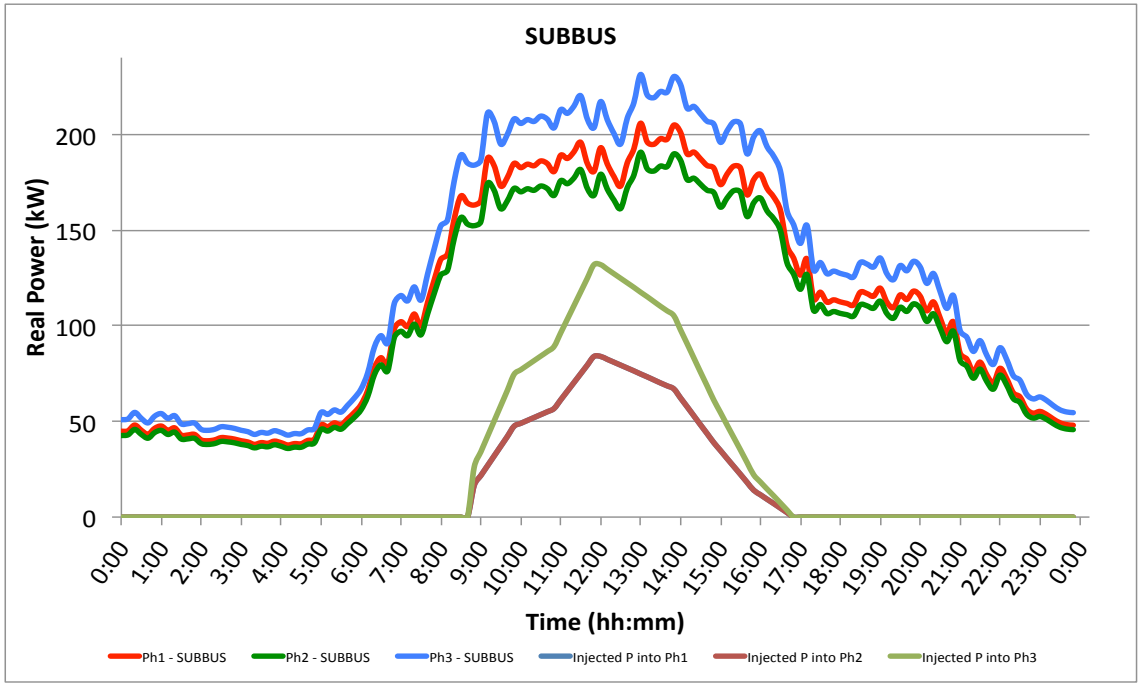

Figure 6.11: Real power demand at the main SUBBUS including an automatic centralised compensation on Angus Street network

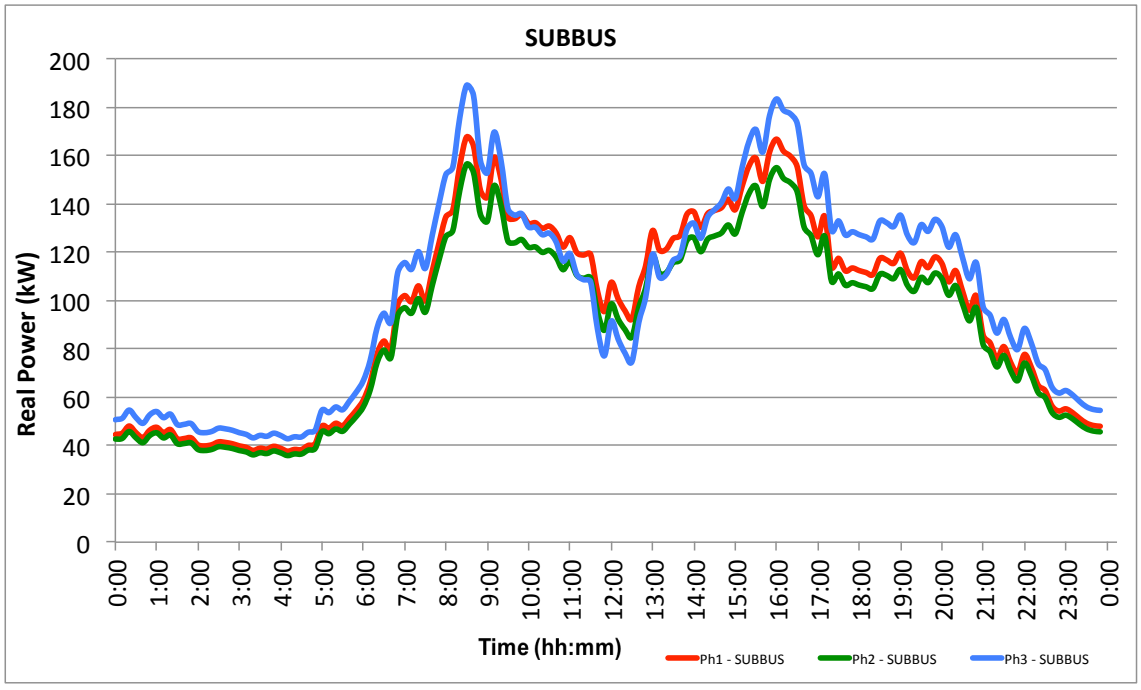

Figure 6.12: Real power demand at the main SUBBUS after the 300kW DG penetration and automatic centralised compensation on Angus Street network

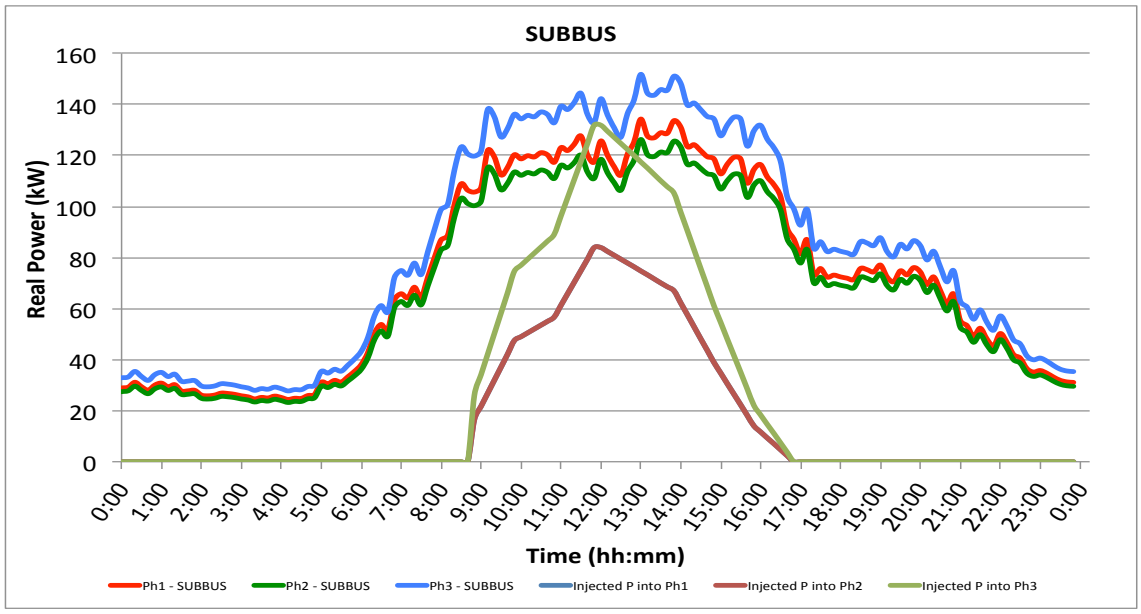

Figure 6.13: Real power demand at the main SUBBUS with base load reduction and including an automatic centralised compensation on Angus Street network

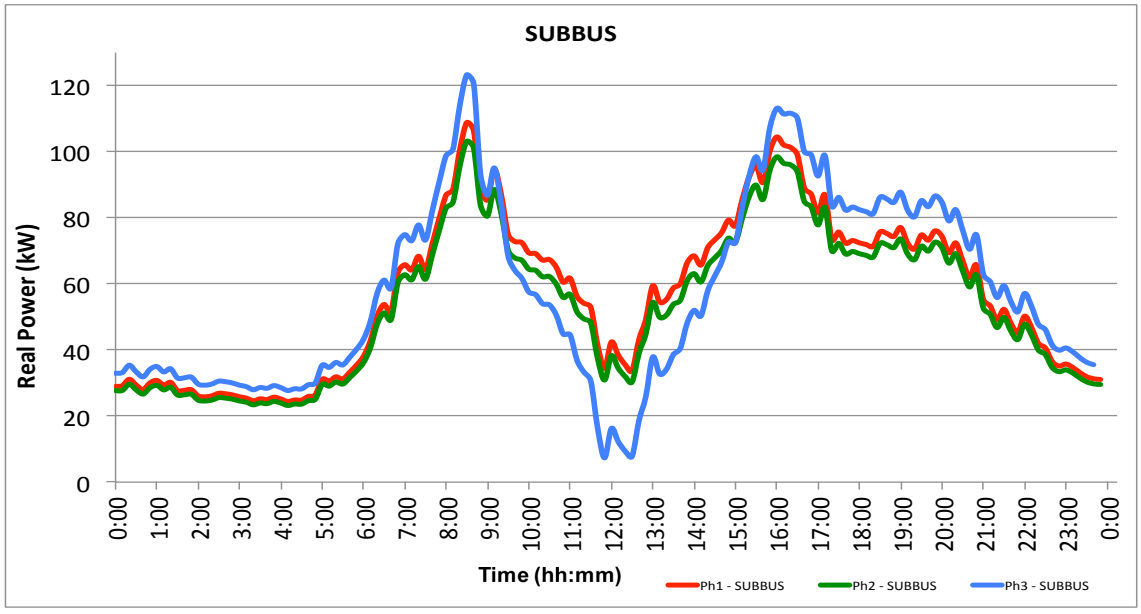

Figure 6.14: Real power demand at the main SUBBUS after the 300kW DG penetration, base load reduction and automatic centralised compensation on Angus Street network

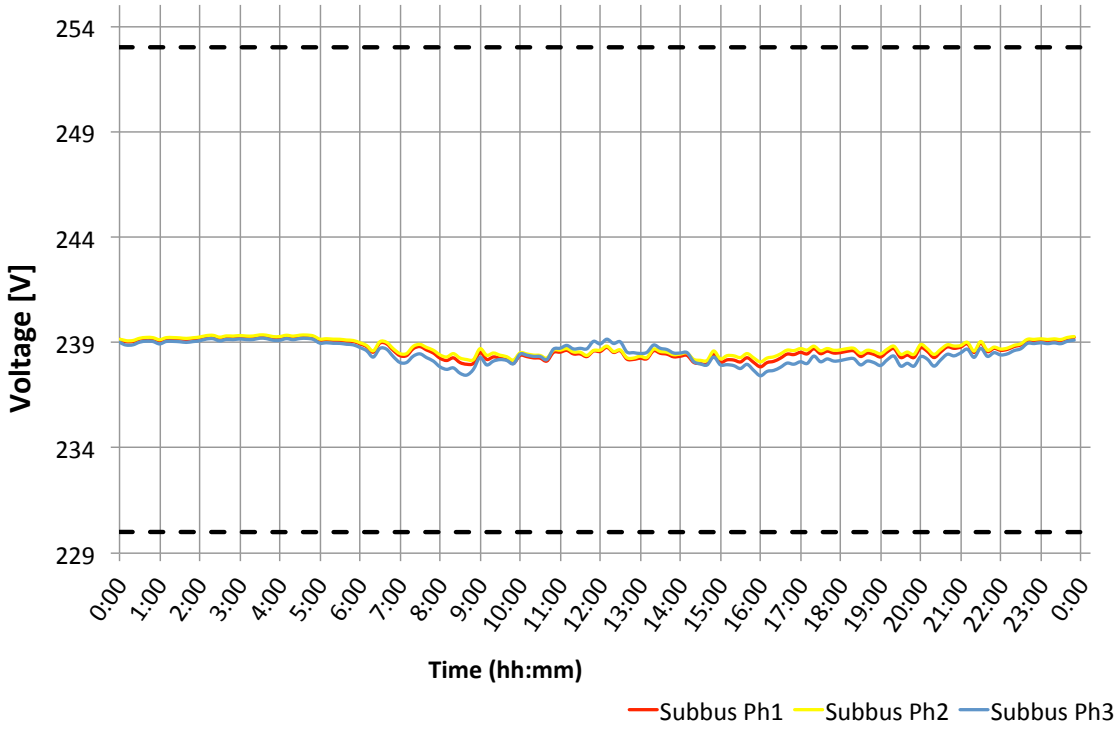

Figure 6.15: Voltage variation at the main SUBBUS with 0.9 (lagging) PF DG units penetration

6.5 Effects of a lagging DG units PF on the voltage profiles and reverse power flow

This study is carried out to understand what impacts have a 0.9 lagging PF of the DG units on voltage profiles and reverse power flow compared to the unity PF case. This case study represent, according to the capability curve section 2.4, an injection of active and reactive power into the network with the same signs. Accordingly, there is a reduction in the injected active power and a further reactive energy compensation due the reactive power injected which causes a higher voltage profiles and some voltage values can easily violate the upper stated limits; it is a side effect of intermittent load and PV variation at the point of connection and over the network caused by other DG connection, and therefore, by reverse power flow from one SUBFEEDER to others, specially in the case of low load demand, like SUBFDR10 and SUBFDR20 as shown in figure 6.10. The latter voltage increase is the same as the overcompensation executed by the capacitors banks seen in chapter 5, where voltages increase linearly with the percentage of compensation, but in this case it depends on the variation of solar radiation. In figure 6.18 are depicted the maximum voltage reached on the daily load curve. As can be seen, SUBFDR20 exhibits a voltage violation on phase 3 at the end of the feeder, whereas the rest of the network is under the upper statutory limits. However, the voltage rise further the upper limit is function of many parameters as described before and the voltage profiles over a shorter period are shown in figure 6.17, among which is highlighted the voltage unbalance between the three phases owing to the single phase units connections. Another aspect which has been investigated in chapter 5 is the voltage variation with the automatic reactive compensation at the main SUBBUS. However, the reactive compensation, during the day, does not result anymore central since the DG units are operating with a lagging power factor. As one can grasp, there is a voltage rise around midday due to the PV penetration peak, particularly, on phase 3, see figure 6.15.

	% kW demand reduction: unity PF	*% kW demand reduction: 0.9 PF*
Phase 1	41	37
Phase 2	42	38
Phase 3	53	49

Table 6.2: Active power demand reduction at the main SUBBUS - Angus Street network

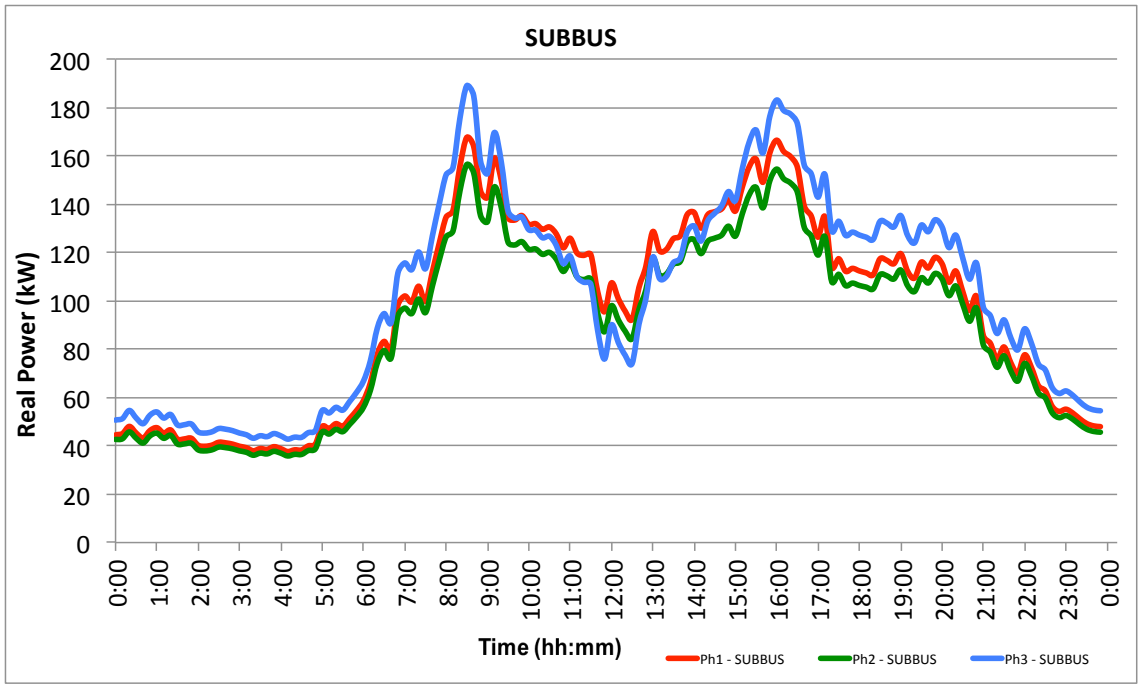

Figure 6.16: Real power demand at the main SUBBUS after the 300kW 0.9 PF lagging DG penetration and automatic centralised compensation on Angus Street network

6.5.1 Reverse power flow reduction

Additionally effects to the injection of reactive power, as said before, is the reduction of reverse of power flow "Active power" compared to unity PF DG units case. Figure 6.16 shows the active power demand at the main SUBBUS with the DG units operating with 0.9 PF lagging, which compared to the simulation results analysis of the unity PF DG case, figure 6.14, the following observations were made:
The kW reduction of the daily load peak of each phase to its minimum demand after the DG penetration in the two cases, unity and a 0.9 (lagging) DG PF, respectively, are summarised in table 6.2, which results in about 9.2, 8 and 7 % reduction of the reverse power flow on phases 1,2 and 3, respectively, for DG units operating with 0.9 PF.

6.5.2 Voltage drops and power losses

In this section, voltage drops along the transformer LV side and along the feeders are reported for the unity and 0.9 lagging DG units power factors and the overall power losses as well. In chapter 3, the voltage drops with the different reactive compensation approaches were shown in table 3.7. However, the voltage drops values decrease significantly with the PV penetration as the power supplied by the transformer is reduced according to the operating DG units PF as shown in figures 6.14 and 6.16 and peak magnitude reduction reported in table 6.2. Furthermore, the unity DG units PF allows the lowest voltage drop along the transformer LV side on phase 1 and while the third phase is more

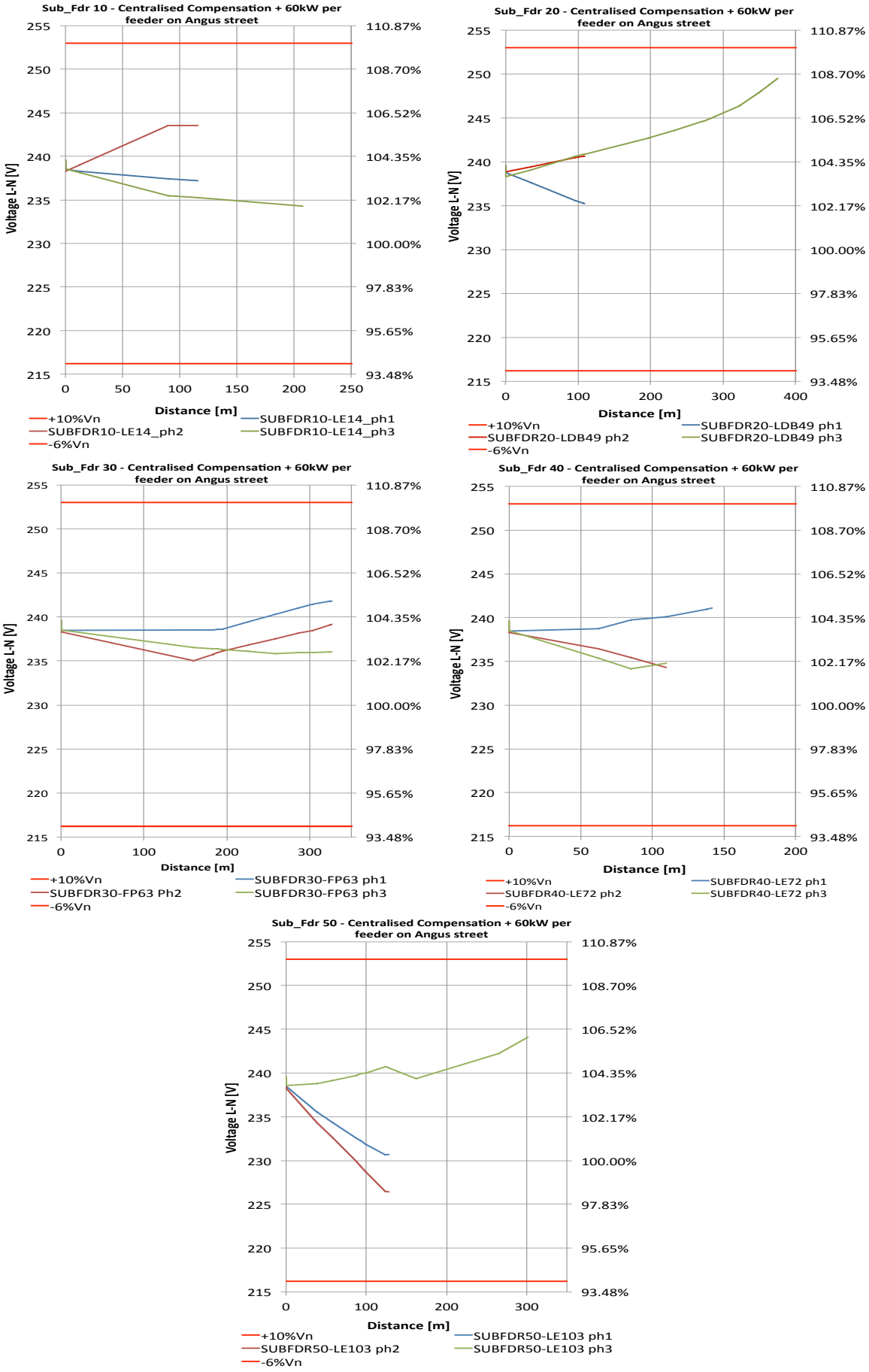

Figure 6.17: Voltage profiles including 300kW 0.9 PF DG units and centralised compensation on Angus Street: Voltage unbalance caused by DG single phase units

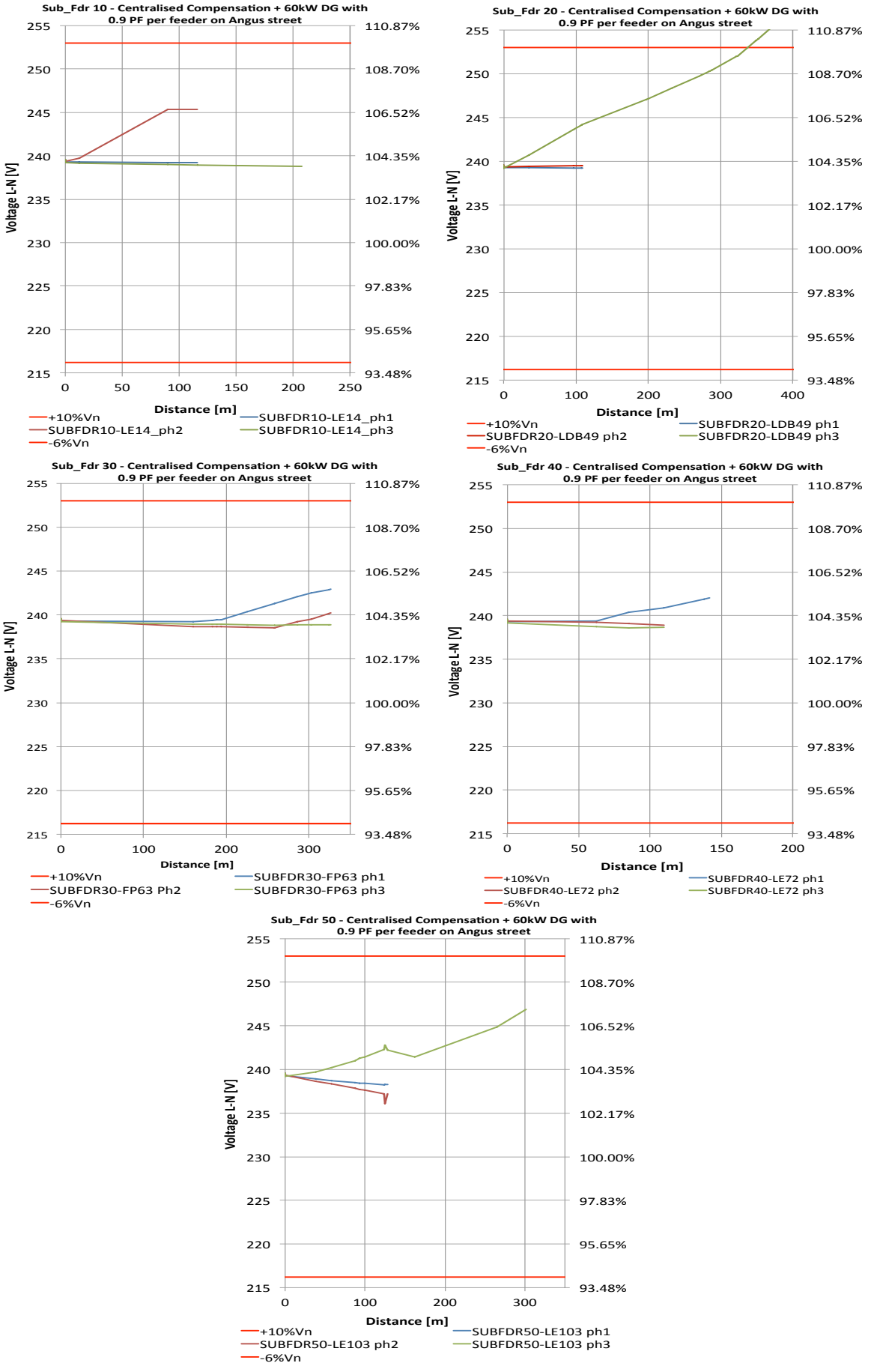

Figure 6.18: Voltage profiles including 300kW 0.9 PF DG units and centralised compensation on Angus Street: Maximum voltage reached along all feeders in a daily PV/load shapes

compensated with the 0.9 PF. Accordingly, the latter voltage drops are negligible compared to the base case ones. Further, the distributed generation close to the feeders load minimises the voltage drops over the feeders importantly comparing the reactive compensation approaches shown in table 3.7 with the network including PV connections in tables: 6.5 and 6.10. The voltage drops values shown in the following tables are included in opposite signs, where the ΔV with negative sign stands for a higher voltage at the user end than the respective sub-feeder. In Chapter 3, the total network power losses and the minimum p.u. voltages were tabulated for the different approaches for reactive compensation realised with no automatic capacitors, as shown in table 6.3, whereas the maximum, minimum p.u. voltages and the allover power losses over the network including the PV connections are shown in table 6.4. However, the maximum voltages is higher than 1 p.u. as expected and the minimum voltage is almost the same. Finally, in terms of power losses, there is a significant reduction, particularly, in reactive power losses which is halved, see table 6.4.

	Max voltage	***Min voltage***	***kW***	***kVAr***
Base case	1	0.904	36	40
Central compensation	1	0.917	35	35
Distributed 1/3 feeder length	1	0.922	34	34
Distributed at lowest voltage	1	0.922	39	37

Table 6.3: Reactive compensation strategies - p.u. voltage and losses

	Max voltage	***Min voltage***	***kW***	***kVAr***
Base case	1	0.904	36	40
Centralised compensation + 1 PF DG units	1.042	0.93	32	21
Centralised compensation + 0.9 PF DG units	1.042	0.92	28	20

Table 6.4: DG connections with centralised reactive compensation - p.u. voltage and losses

	Unity PF: $\Delta V(V)$	***Unity PF:*** $\%\Delta V$	***0.9 lagging PF:*** $\Delta V(V)$	***0.9 lagging PF:*** $\%\Delta V$
Phase 1	0.8	0.3	1.1	0.47
Phase 2	0.77	0.32	1.32	0.55
Phase 3	1.3	0.54	1	0.44

Table 6.5: Transformer LV side voltage drops with unity and 0.9 DG units PFs - Angus Street network

	Unity PF: $\Delta V(V)$	***Unity PF:*** $\%\Delta V$	***0.9 lagging PF:*** $\Delta V(V)$	***0.9 lagging PF:*** $\%\Delta V$
Phase 1	-0.2	-0.072	1.3	0.54
Phase 2	-4.6	-1.9	-5.3	-2.2
Phase 3	5.3	2.2	4.3	1.8

Table 6.6: SUBFDR10 voltage drops with unity and 0.9 DG units PFs - Angus Street network

	Unity PF: $\Delta V(V)$	***Unity PF:*** $\%\Delta V$	***0.9 lagging PF:*** $\Delta V(V)$	***0.9 lagging PF:*** $\%\Delta V$
Phase 1	3.5	1.5	2.3	0.96
Phase 2	-1.8	-0.75	/	/
Phase 3	-6.7	-2.8	11.2	-4.7

Table 6.7: SUBFDR20 voltage drops with unity and 0.9 DG units PFs - Angus Street network

	Unity PF: $\Delta V(V)$	***Unity PF:*** $\%\Delta V$	***0.9 lagging PF:*** $\Delta V(V)$	***0.9 lagging PF:*** $\%\Delta V$
Phase 1	-2	-0.85	-3.32	-1.4
Phase 2	1.6	0.69	-0.88	-0.37
Phase 3	1.8	0.76	2.53	1.06

Table 6.8: SUBFDR30 voltage drops with unity and 0.9 DG units PFs - Angus Street network

	Unity PF: $\Delta V(V)$	***Unity PF:*** $\%\Delta V$	***0.9 lagging PF:*** $\Delta V(V)$	***0.9 lagging PF:*** $\%\Delta V$
Phase 1	-0.8	-0.34	-2.65	-1.11
Phase 2	4.51	1.9	4	1.7
Phase 3	2.8	1.2	3.8	1.6

Table 6.9: SUBFDR40 voltage drops with unity and 0.9 DG units PFs - Angus Street network

	Unity PF: $\Delta V(V)$	***Unity PF:*** $\%\Delta V$	***0.9 lagging PF:*** $\Delta V(V)$	***0.9 lagging PF:*** $\%\Delta V$
Phase 1	8.61	3,61	7.8	3.3
Phase 2	9.95	4.2	11.9	5
Phase 3	-1.31	-0.55	-5.5	-2.3

Table 6.10: SUBFDR50 voltage drops with unity and 0.9 DG units PFs - Angus Street network

Conclusions

Loadflow studies have been carried out on lv WPD network using the OpenDSS software. The results were analysed and presented in the form of voltage and current profiles as a function of route length from the source substation. In this way, the complete network performance was assessed against the statutory voltage limits for the voltage profiles and in terms of plant ampacity in the case of the current profiles. For the assumed base case load conditions which were matched to the maximum recorded power, the voltage drops across the supply transformer and network feeders were not excessive and there were no violations of statutory voltage limits. The power factor was assumed 0.9 to consider the worst case and in the more extensive network study (Angus Street), the greatest overall voltage drop occurred across the longest feeders and in the case of the maximum load (620kW at PF=0.9), the voltage on phase of the longest feeder was close to the statutory limit. The OpenDSS unbalanced simulations of the Angus Street underline the large differences between phase voltages that may be present on such networks. The current profile studies reveal how there are very high thermal margins in many network feeders, while in some cases, the margins are quite narrow and deterioration in power factor can have an impact on thermal loading. The X/R ratios of typical WPD lv network cables and lines lie in the range 0.1 and 0.75 and the ratio is approximately proportional to cable rating (larger cable, lower R, similar X). The corresponding range for typical lv distribution transformers is 1.25 to 4. A study into the effect of reactive compensation applied to LV networks has shown that shunt compensation applied at the main substation may be useful to limit the voltage drop across the transformer and reduce phase current magnitude. Downstream compensation is not effective in reducing transformer voltage drop but may help to reduce network currents and operate within cable ampacity and minimise losses.

A comparison of centralised versus distribution of reactive compensation to the Angus Street case study network has shown that significant voltage improvement can be obtained through the application of centralised compensation and that the practical advantages of this would probably outweigh the further marginal improvements in voltage offered by distributed compensation (some small additional voltage drop reduction along feeder and reduction in current flow and losses in feeder). The advantage of centralised compensation include (i) more likely to be cost effective, as there would be one single unit (ii) more easily physically accommodated due to the likely availability of space at the main substation against the lack of a substation at points along the feeders, (iii) a single point of control and less risk of interaction/hunting compared with distributed compensation, (iv) centralised compensation takes advantage of feeder load diversity and will be more resilient to future network changes compared with a tailored distributed compensation scheme which would require different amounts of compensation on each sub-feeder, (v) the fact that optimisation of a distributed reactive compensation scheme is further limited by constraints on available standard capacitor sizes.

A review of a range of typical manufactured reactive power compensation units indicates that there is good availability and with the required control features for application to a MV/LV substation for downstream voltage improvement.

The simulations carried out to investigate the effect of embedded generation on the Angus Street network have shown that voltage profiles across the network can be improved by achieving a net reduction in power flow. Also as a result, net current flow can be significantly less and there can be a resulting increase in thermal margin. However, when there are very high levels of embedded generation that occur at low loading levels, the thermal limits of parts of the network may be exceeded due to exreessive backfeed and this effect is exacerbated by the presence of 'tapering'. The unbalanced simulations underline the importance of such modelling to take into account the effect of single-phase generation units at lv. In such cases, balanced three-phase studies may be inadequate.

Finally, the application of OpenDSS for the network simulations in this study underlined the importance of being able to account for unbalance in (i) the network (three and single phase cables) (ii) loads and (iii) generation. Without such a model, it would be difficult to carry out studies to predict lv network performance and this would be particularly the case for future smart networks. A graphical user interface is now available for OpenDSS which enables easier construction of network models.

Suggestions for further work

This project has considered only a limited number of substations for both data analysis and network simulations. It is important to establish whether certain characteristics identified with these selected networks are representative of the lv system in general. Further studies could be undertaken to explore this. The OpenDSS software has identified the importance of modelling the unbalance in lv networks for a more realistic representation of network performance. Further work could be carried out using this simulation tool to provide (i) a more comprehensive three phase quantification of embedded generation 'Hosting Capacity' for selected networks, (ii) comparing reactive power compensation control at the main LV substation with other lv voltage control techniques. With more and more inverter-interfaced DG units appearing, there may be a need to carry out harmonic and transient analysis to assess the impact of such devices on low voltage networks.

Appendix A

Angus Street network data

The nodes/buses characteristics and estimated loads magnitude of Angus Street network are shown in the following tables. The network is made up of a single in-feed at SUBBUS and consisting of fifty-three loads.

Transformer Data		P_{sc}	V_{sc}	Rating [KVA]	Ampacity [A]	Rated Voltage	type
TR1		1%	4.75%	1000	1391	11/0.415 kV	Dyn11
Lines Data		R	X	Ampacity [A]		Cable type	
Feeders	Lines	[Ω/Km]	[Ω/Km]				
SUBFDR10	subFDR10-n1_bjt1	0.142	0.0689	345		0.2 4c Cu STA	
	n1_bjt1-n2_sjt2	0.188	0.07	290		0.15 2c Cu STA	
	n2_sjt2-n3_sjt3	0.188	0.07	290		0.15 2c Cu STA	
	n3_sjt3-n4_le4	0.188	0.07	290		0.15 2c Cu STA	
	n1_bjt1-n5_bjt5	0.142	0.0689	345		0.2 4c Cu STA	
	n5_bjt5-n6_sjt6	0.276	0.0733	250		0.1 2c Cu STA	
	n6_sjt6-n7_sjt7	0.276	0.0733	250		0.1 2c Cu STA	
	n7_sjt7-n8_sjt8	0.276	0.0733	250		0.1 2c Cu STA	
	n8_sjt8-n10_bjt10	0.276	0.0733	250		0.1 2c Cu STA	
	n10_bjt10-n11_le11	0.276	0.0733	250		0.1 2c Cu STA	
	n10_bjt10-n12_le12	0.276	0.0733	250		0.1 2c Cu STA	
	n5_bjt5-n13_bjt13	0.142	0.0689	345		0.2 4c Cu STA	
	n13_bjt13-n14_le14	0.188	0.07	290		0.15 2c Cu STA	
	n13_bjt13-n16_bjt16	0.188	0.07	290		0.15 4c Cu STA	
	n16_bjt16-n17_sjt17	0.188	0.07	290		0.15 4c Cu STA	
	n17_sjt17-n18_ldb18	0.188	0.07	290		0.15 4c Cu STA	
	n16_bjt16-n19_bjt19	0.188	0.07	290		0.15 4c Cu STA	
	n19_bjt19-n20_cutout20	0.188	0.07	290		0.15 4c Cu STA	
	n19_bjt19-n21_sjt21	0.188	0.07	290		0.15 4c Cu STA	
	n21_sjt21-n22_le22	0.188	0.07	290		0.15 4c Cu STA	
SUBFDR20	subFDR20-n23_sjt23	0.142	0.0689	345		0.2 4c Cu STA	
	n23_sjt23-n24_bjt24	0.142	0.0689	345		0.2 4c Cu STA	
	n24_bjt24-n25_sjt25	0.276	0.0733	250		0.1 2c Cu STA	
	n25_sjt25-n26_bjt26	0.276	0.0733	250		0.1 2c Cu STA	
	n26_bjt26-n27_le27	0.276	0.0733	250		0.1 2c Cu STA	
	n26_bjt26-n28_ldb28	0.276	0.0733	250		0.1 2c Cu STA	
	n24_bjt24-n29_bjt29	0.276	0.0733	250		0.1 4c Cu STA	
	n29_bjt29-n30_bjt30	0.276	0.0733	250		0.1 2c Cu STA	
	n30_bjt30-n31_le31	0.276	0.0733	250		0.1 2c Cu STA	
	n30_bjt30-n28_ldb28	0.276	0.0733	250		0.1 2c Cu STA	
	n29_bjt29-n33_bjt33	0.142	0.0689	345		0.2 4c Cu STA	
	n33_bjt33-n34_cutout34	0.443	0.0755	203		70 TR XLPE Al 3c	
	n33_bjt33-n36_sjt36	0.188	0.07	290		0.15 2c Cu STA	
	n36_sjt36-n37_sjt37	0.32	0.0735	235		95 Wavcon Al 3c	
	n37_sjt37-n38_sjt38	0.188	0.07	290		0.15 2c Cu STA	
	n38_sjt38-n39_sjt39	0.188	0.07	290		0.15 2c Cu STA	
	n39_sjt39-n40_sjt40	0.188	0.07	290		0.15 2c Cu STA	
	n40_sjt40-n41_sjt41	0.188	0.07	290		0.15 2c Cu STA	
	n41_sjt41-n42_sjt42	0.188	0.07	290		0.15 2c Cu STA	
	n42_sjt42-n43_bjt43	0.188	0.07	290		0.15 4c Cu STA	
	n43_bjt43-n44_fp44	0.164	0.074	335		185 Wavcon Al 3c	
	n43_bjt43-n45_sjt45	0.164	0.074	335		185 Wavcon Al 3c	
	n45_sjt45-n46_sjt46	0.276	0.0733	250		0.1 2c Cu STA	
	n46_sjt46-n47_bjt47	0.276	0.0733	250		0.1 2c Cu STA	
	n47_bjt47-n48_le48	0.276	0.0733	250		0.1 2c Cu STA	
	n47_bjt47-n49_ldb49	0.276	0.0733	250		0.1 2c Cu STA	
SUBFDR30	subFDR30-n51_bjt51	0.092	0.0678	445		0.3 4c Cu STA	
	n51_bjt51-n52_sjt52	0.276	0.0733	250		0.1 4c Cu STA	
	n52_sjt52-n53_sjt53	0.32	0.0735	235		95 Wavcon Al 3c	
	n53_sjt53-n54_bjt54	0.276	0.0733	250		0.1 4c Cu STA	
	n54_bjt54-n55_le55	0.188	0.07	290		0.15 2c Cu STA	
	n54_bjt54-n56_bjt56	0.276	0.0733	250		0.1 4c Cu STA	
	n56_bjt56-n57_le57	0.188	0.07	290		0.15 2c Cu STA	
	n56_bjt56-n58_bjt58	0.276	0.0733	250		0.1 4c Cu STA	
	n58_bjt58-n59_cutout59	0.188	0.07	290		0.15 2c Cu STA	
	n58_bjt58-n60_sjt60	0.276	0.0733	250		0.1 4c Cu STA	
	n60_sjt60-n61_sjt61	0.188	0.07	290		0.15 2c Cu STA	
	n61_sjt61-n62_sjt62	0.188	0.07	290		0.15 4c Cu STA	
	n62_sjt62-n63_fp63	0.164	0.074	335		185 Wavcon Al 3c	
	n51_bjt51-n64_sjt64	0.092	0.0678	445		0.3 4c Cu STA	
	n64_sjt64-n65_fp65	0.113	0.0689	395		0.25 4c Cu STA	
SUBFDR40	subFDR40-n66_bjt66	0.142	0.0689	345		0.2 4c Cu STA	
	n66_bjt66-n67_le67	0.276	0.0733	250		0.1 2c Cu STA	
	n66_bjt66-n68_bjt68	0.142	0.0689	345		0.2 4c Cu STA	
	n68_bjt68-n69_le69	0.276	0.0733	250		0.1 2c Cu STA	
	n68_bjt68-n70_bjt70	0.142	0.0689	345		0.2 4c Cu STA	
	n70_bjt70-n71_sjt71	0.276	0.0733	250		0.1 2c Cu STA	
	n71_sjt71-n72_le72	0.276	0.0733	250		0.1 2c Cu STA	
	n70_bjt70-n73_sjt73	0.142	0.0689	345		0.2 4c Cu STA	
	n73_sjt73-n74_sjt74	0.142	0.0689	345		0.2 4c Cu STA	
	n74_sjt74-n75_sjt75	0.142	0.0689	345		0.2 4c Cu STA	
	n75_sjt75-n65_fp65	0.113	0.0689	395		0.25 4c Cu STA	

Lines Data		R	X	Ampacity [A]	Cable type
Feeders	Lines	[Ω/Km]	[Ω/Km]		
SUBFDR50	subFDR50-n77_sjt77	0.142	0.0689	345	0.2 4c Cu STA
	n77_sjt77-n78_bjt78	0.113	0.0689	395	0.25 4c Cu STA
	n78_bjt78-n79_cutout79	0.32	0.0735	235	95 Wavcon Al 3c
	n78_bjt78-n80_bjt80	0.113	0.0689	395	0.25 4c Cu STA
	n80_bjt80-n81_sjt81	0.113	0.0689	395	0.25 4c Cu STA
	n81_sjt81-n82_sjt82	0.164	0.074	335	185 Wavcon Al 3c
	n82_sjt82-n83_ldb83	0.113	0.0689	395	0.25 4c Cu STA
	n83_ldb83-n85_sjt85	0.113	0.0689	395	0.25 4c Cu STA
	n85_sjt85-n86_ldb86	0.113	0.0689	395	0.25 4c Cu STA
	n83_ldb83-n87_sjt87	0.32	0.0735	235	95 Wavcon Al 3c
	n87_sjt87-n88_sjt88	0.32	0.0735	235	95 Wavcon Al 3c
	n88_sjt88-n90_sjt90	0.276	0.0733	250	0.1 2c Cu STA
	n90_sjt90-n91_sjt91	0.276	0.0733	250	0.1 2c Cu STA
	n91_sjt91-n94_le94	0.276	0.0733	250	0.1 2c Cu STA
	n83_ldb83-n95_sjt95	0.32	0.0735	235	95 Wavcon Al 3c
	n95_sjt95-n96_sjt96	0.32	0.0735	235	95 Wavcon Al 3c
	n96_sjt96-n98_bjt98	0.276	0.0733	250	0.1 2c Cu STA
	n98_bjt98-n99_le99	0.276	0.0733	250	0.1 2c Cu STA
	n98_bjt98-n101_sjt101	0.276	0.0733	250	0.1 2c Cu STA
	n101_sjt101-n103_le103	0.276	0.0733	250	0.1 2c Cu STA
	n80_bjt80-n106_bjt106	0.164	0.074	382	185 TR XLPE Al 3c
	n106_bjt106-n107_le107	0.164	0.074	382	185 TR XLPE Al 3c
	n106_bjt106-n108_cutout108	0.443	0.0755	203	70 TR XLPE Al 3c

Bus Data	Base Loads			Source/Generator Rated Voltage L-N	
	P (Active Power) kW	Cosφ	n-phase	kV	p.u.
mt1	/	/	/	6.3509	1
subbus	/	/	/	239.6	1
subfdr10	/	/	/	239.6	1
n1_bjt1	/	/	/	239.6	1
n1bis_bjt1	/	/	/	239.6	1
n2_sjt2	/	/	/	239.6	1
n3_sjt3	/	/	/	239.6	1
n4_le4	2.5	0.9	1	239.6	1
n5_bjt5	/	/	/	239.6	1
n5bis_bjt5	/	/	/	239.6	1
n6_sjt6	/	/	/	239.6	1
n7_sjt7	/	/	/	239.6	1
n8_sjt8	/	/	/	239.6	1
n10_bjt10	/	/	/	239.6	1
n11_le11	/	/	/	239.6	1
n12_le12	6.5	0.9	1	239.6	1
n13_bjt13	/	/	/	239.6	1
n14_le14	10.5	0.9	1	239.6	1
n16_bjt16	/	/	/	239.6	1
n17_sjt17	/	/	/	239.6	1
n18_ldb18	1.5	0.9	1	239.6	1
n19_bjt19	/	/	/	239.6	1
n20_cutout20	1.5	0.9	1	239.6	1
n20_cutout20	1.5	0.9	1	239.6	1
n20_cutout20	1.7	0.9	1	239.6	1
n21_sjt21	/	/	/	239.6	1
n22_le22	5.8	0.9	1	239.6	1
subfdr20	/	/	/	239.6	1
n23_sjt23	3.8	0.9	1	239.6	1
n24_bjt24	/	/	/	239.6	1
n25_sjt25	/	/	/	239.6	1
n26_bjt26	3.5	0.9	1	239.6	1
n27_le27	/	/	/	239.6	1
n28_ldb28	3.5	0.9	1	239.6	1
n29_bjt29	/	/	/	239.6	1
n30_bjt30	/	/	/	239.6	1
n31_le31	2.3	/	/	239.6	1
n33_bjt33	/	/	/	239.6	1
n34_cutout34	2.3	0.9	1	239.6	1
n34_cutout34	2.3	0.9	1	239.6	1
n34_cutout34	2.5	0.9	1	239.6	1
n36_sjt36	/	/	/	239.6	1
n37_sjt37	5	0.9	1	239.6	1
n38_sjt38	/	/	/	239.6	1

Bus Data	Base Loads			Source/Generator Rated Voltage L-N	
	P (Active Power) kW	Cosφ	n-phase	kV	p.u.
n39_sjt39	4	0.9	1	239.6	1
n40_sjt40	4	0.9	1	239.6	1
n41_sjt41	4	0.9	1	239.6	1
n42_sjt42	/	/	/	239.6	1
n43_bjt43	/	/	/	239.6	1
n44_fp44	2.5	0.9	1	239.6	1
n45_sjt45	/	/	/	239.6	1
n46_sjt46	/	/	/	239.6	1
n47_bjt47	4	0.9	1	239.6	1
n48_le48	/	/	/	239.6	1
n49_ldb49	2	0.9	1	239.6	1
subfdr30	/	/	/	239.6	1
n51_bjt51	/	/	/	239.6	1
n52_sjt52	/	/	/	239.6	1
n53_sjt53	/	/	/	239.6	1
n54_bjt54	/	/	/	239.6	1
n55_le55	11.5	0.9	1	239.6	1
n56_bjt56	/	/	/	239.6	1
n57_le57	/	/	/	239.6	1
n58_bjt58	9.5	0.9	1	239.6	1
n59_cutout59	/	/	/	239.6	1
n60_sjt60	/	/	/	239.6	1
n61_sjt61	9.5	0.9	1	239.6	1
n62_sjt62	/	/	/	239.6	1
n63_fp63	9.2	0.9	1	239.6	1
n64_sjt64	16	0.9	1	239.6	1
n64_sjt64	20.5	0.9	1	239.6	1
n64_sjt64	17.5	0.9	1	239.6	1
n65_fp65	10	0.9	1	239.6	1
subfdr40	/	/	/	239.6	1
n66_bjt66	/	/	/	239.6	1
n67_le67	28.5			239.6	1
n68_bjt68	/	/	/	239.6	1
n69_le69	18.5	0.9	1	239.6	1
n69_le69	18.5	0.9	1	239.6	1
n69_le69	18.5	0.9	1	239.6	1
n70_bjt70	/	/	/	239.6	1
n71_sjt71	/	/	/	239.6	1
n72_le72	36.5	0.9	1	239.6	1
n73_sjt73	/	/	/	239.6	1
n74_sjt74	17.5	0.9	1	239.6	1
n74_sjt74	17.5	0.9	1	239.6	1
n75_sjt75	/	/	/	239.6	1
subfdr50	/	/	/	239.6	1
n77_sjt77	/	/	/	239.6	1
n78_bjt78	/	/	/	239.6	1
n79_cutout79	2	0.9	1	239.6	1
n79_cutout79	2	0.9	1	239.6	1
n79_cutout79	2.5	0.9	1	239.6	1
n80_bjt80	/	/	/	239.6	1
n81_sjt81	/	/	/	239.6	1
n82_sjt82	/	/	/	239.6	1
n83_ldb83	/	/	/	239.6	1
n85_sjt85	/	/	/	239.6	1
n86_ldb86	102	0.9	1	239.6	1
n87_sjt87	/	/	/	239.6	1
n88_sjt88	/	/	/	239.6	1
n90_sjt90	15	0.9	1	239.6	1
n91_sjt91	23	0.9	1	239.6	1
n94_le94	24	0.9	1	239.6	1
n95_sjt95	/	/	/	239.6	1
n96_sjt96	/	/	/	239.6	1
n98_bjt98	24	0.9	1	239.6	1
n99_le99	24	0.9	1	239.6	1
n101_sjt101	18	0.9	1	239.6	1
n103_le103	20	0.9	1	239.6	1
n106_bjt106	/	/	/	239.6	1
n107_le107	10	0.9	1	239.6	1
n108_cutout108	7	0.9	1	239.6	1
n108_cutout108	7	0.9	1	239.6	1
n108_cutout108	7	0.9	1	239.6	1

Appendix B

Power Losses single versus three-phase

In a three-phase circuit, active and reactive losses (when the maximum current has been determined) can be calculated as follows:

$$P_l = 3I^2 R_l \tag{B.1}$$

$$P_l = \left(\frac{P}{V}\right)^2 R_l + \left(\frac{Q}{V}\right)^2 R_l \tag{B.2}$$

$$Q_l = 3I^2 X_l \tag{B.3}$$

$$Q_l = \left(\frac{P}{V}\right)^2 X_l + \left(\frac{Q}{V}\right)^2 X_l \tag{B.4}$$

where Rl and Xl refer to the circuit series resistance and reactance. For a 3-phase symmetrical load the load P is dived between three phases and the current on each is I/3:

$$P_{l3ph} = (\frac{I}{3})^2 (3R) = \frac{I^2 R}{3} = \frac{1}{6} P_{l1ph} \tag{B.5}$$

Thus, when the same real power is being delivered, the losses in a single-phase line are six times the losses in a balanced three-phase line. For the four-conductor three phase line operating at a single phase this would result in two wires in parallel being used for both phase and neutral and the losses are reduced to three times the losses:

$$P'_{l1ph} = \left(\frac{R}{2}\right) 2I^2 = I^2 R \tag{B.6}$$

$$P_{l3ph} = \frac{I}{3}^2 (3R) = \frac{I^2 R}{3} = \frac{1}{3} P'_{l1ph} \tag{B.7}$$

Appendix C

Transformer Voltage Drop

The simplified equivalent circuit of a transformer, suitable for the analysis of short-circuit and loading conditions, consists of a resistance, representing the ohmic winding losses or copper losses, and a reactance, representing the leakage inductance. As already known, the voltage on the secondary side of the transformer is reduced while loading the transformer.
The voltage drop ΔU can be estimated with sufficient accuracy from equation:

$$\Delta U = U_r cos\phi + U_x \sin\phi \tag{C.1}$$

For a partial loading of the transformer, the voltage drop ΔU is proportional to the rated load:

$$\Delta U = (U_r cos\phi + U_x \sin\phi).\frac{I}{I_r} \tag{C.2}$$

The relative reactive voltage drop u_X is called the leakage voltage:

$$u_X = \sqrt{u_k^2 - u_R^2} \tag{C.3}$$

The relative ohmic voltage drop u_R is determined from

$$u_R = \frac{P_{kr}}{S_r}.100\% \tag{C.4}$$

Where,
u_k = impedance voltage
u_R = ohmic part of impedance voltage
u_X = leakage voltage (reactive part of impedance voltage)
P_{kr} = rated short-circuit losses
S_r = rated apparent power
U_1 = transformer voltage at high-voltage side (input voltage)
U_2 = transformer voltage at low-voltage side (full-load voltage or output voltage)
ΔU = voltage drop
I_r = rated current
$cos\phi_1$ = fundamental frequency power factor
Table C.1 outlines some tentative values of u_R, $u_X$and P_{kr} of transformers according to DIN 42500. Note that, in relation to table C.1, the recommended impedance voltage of low-voltage transformers in distribution systems is $u_k = 4\%$ in order to limit the permissible voltage drop. Low voltage transformers in industrial systems have a more preferable impedance voltage of $u_k = 6\%$ in order to limit short-circuit currents.

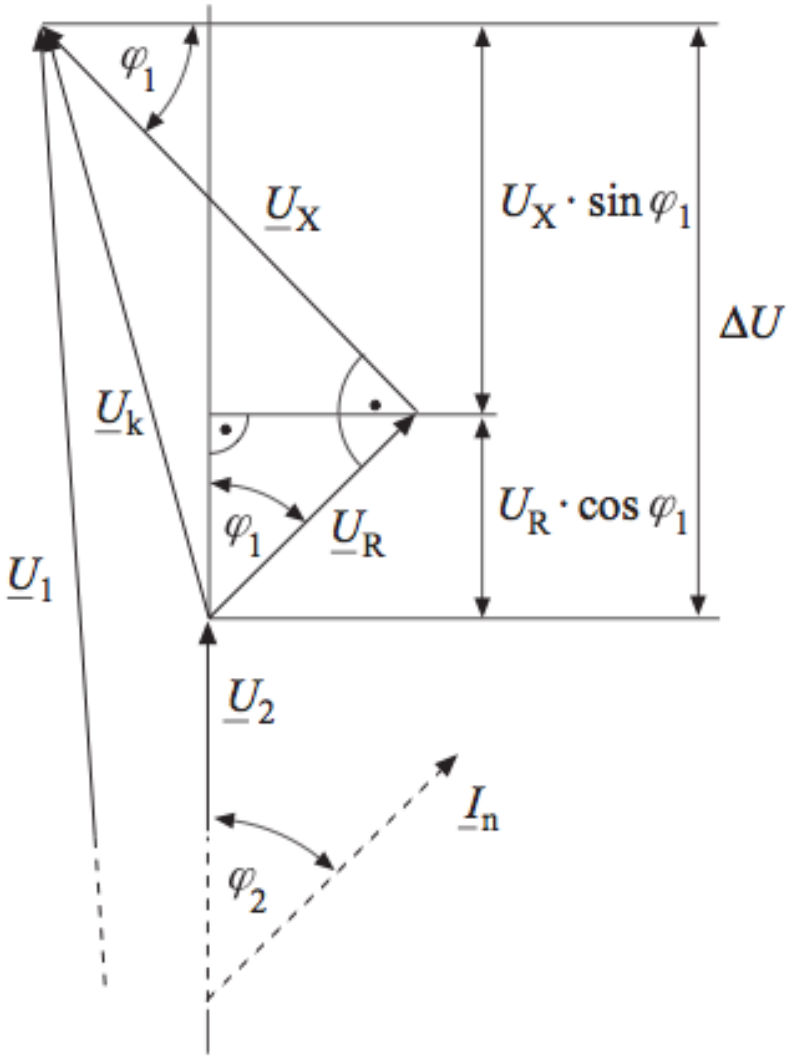

Figure C.1: Transformer voltage drop and Kapp's triangle

S_r (kVA)	100	160	250	400	630
u_R (%)	1.75	1.43	1.30	1.15	1.03
u_X (%)	3.60	3.72	3.78	3.83	3.86
P_{kr} (kW)	1.75	2.35	3.25	4.60	6.50

Table C.1: Tentative values of u_R, $u_X$and P_{kr}

Appendix D

Line Voltage Drop

During normal load-flow conditions the angle between the receiving end and the sending end voltages is only a few degrees. For most practical cases the approximation of angles equality is acceptable and a scalar relationship can be written as:

$$V_s = V_r + IR\cos\phi + IX\sin\phi \tag{D.1}$$

For three-phase systems the voltage drop is calculated from:

$$V_d \approx \sqrt{3}(I_p R + I_q X) \tag{D.2}$$

The R/X ratio for LV lines and cables is usually high. Thus reactive loads do not often cause voltage drop problems, but that high ratio considerably affects the power losses [5]:

$$\frac{R_l}{X_l} = \frac{P_l}{Q_l} \tag{D.3}$$

Appendix E

DSSim-PC: OpenDSS Interface

The DSSim-PC system is a graphic Distribution network Simulator for PC and Real Time (RT) systems. This software is based in the EPRI's OpenDSS software to solve the electrical system and includes almost all the functionalities [49]. Unlike OpenDSS, performing a network with the graphical interface software DSSim is not such complicated as there is no long scripts to write and run, particularly, when it has to do with large networks. See figure E.1.

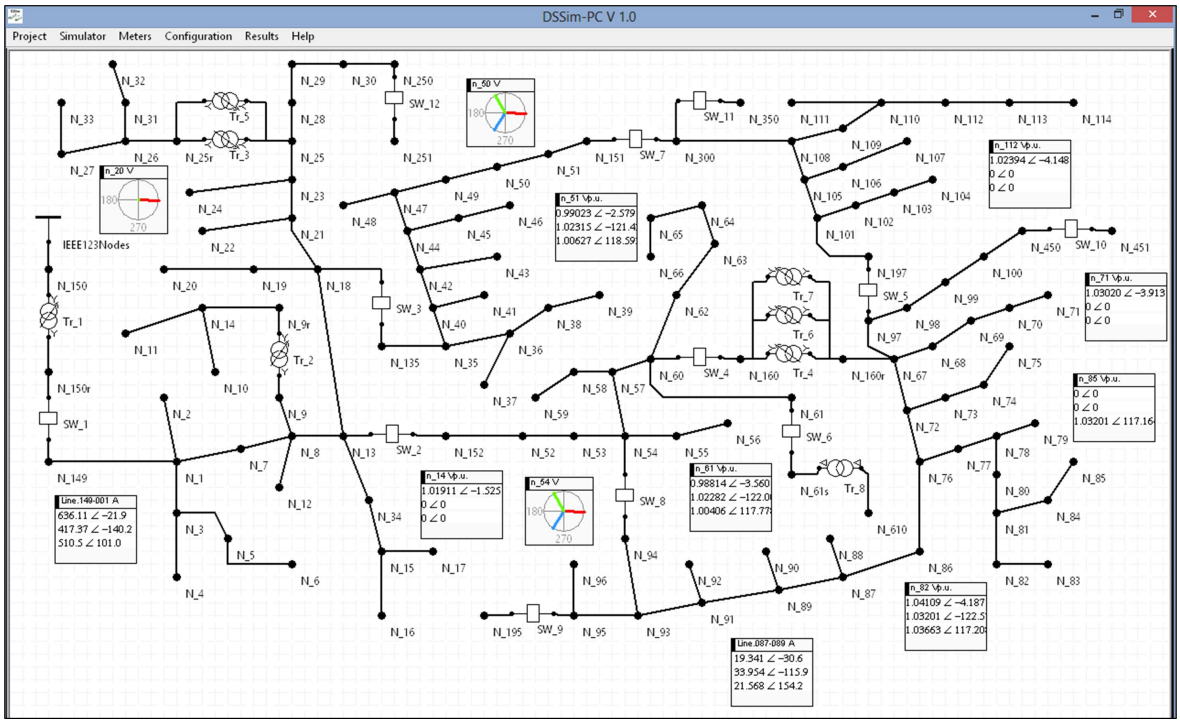

Figure E.1: Large networks performed with the graphical interface DSSim

In this way, the powerful EPRI's open source for distribution systems analysis becomes much more useful and easier for industrial use and DNOs. In fact, in order to simulate a network it needs to build a new circuit using the constructor module where it is located in the Project Menu as shown in figure E.2.

Once the constructor is enabled, in order to build a network it needs firstly to define a new system as shown in figure E.3, then begin to insert the equipment and its connection from "components" on the tool bar.

Finally, in order to simulate the circuit, the constructor must be disabled and then it will be possible to carry out a simulation. One important advantage of this graphical interface is that nodes

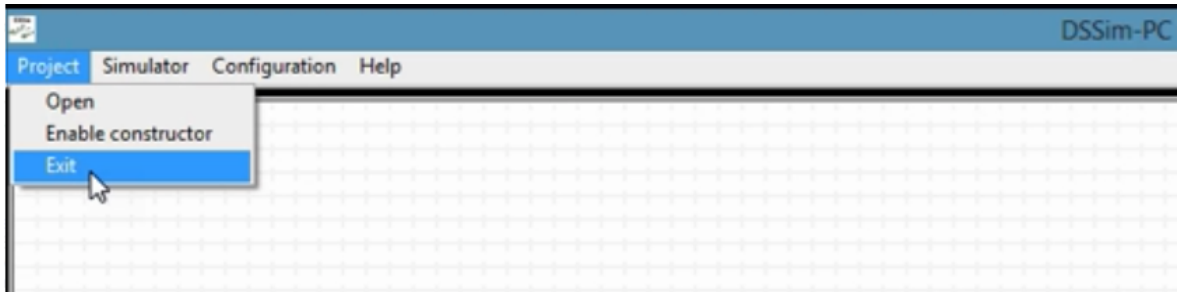

Figure E.2: Building a new circuit with the graphical interface DSSim

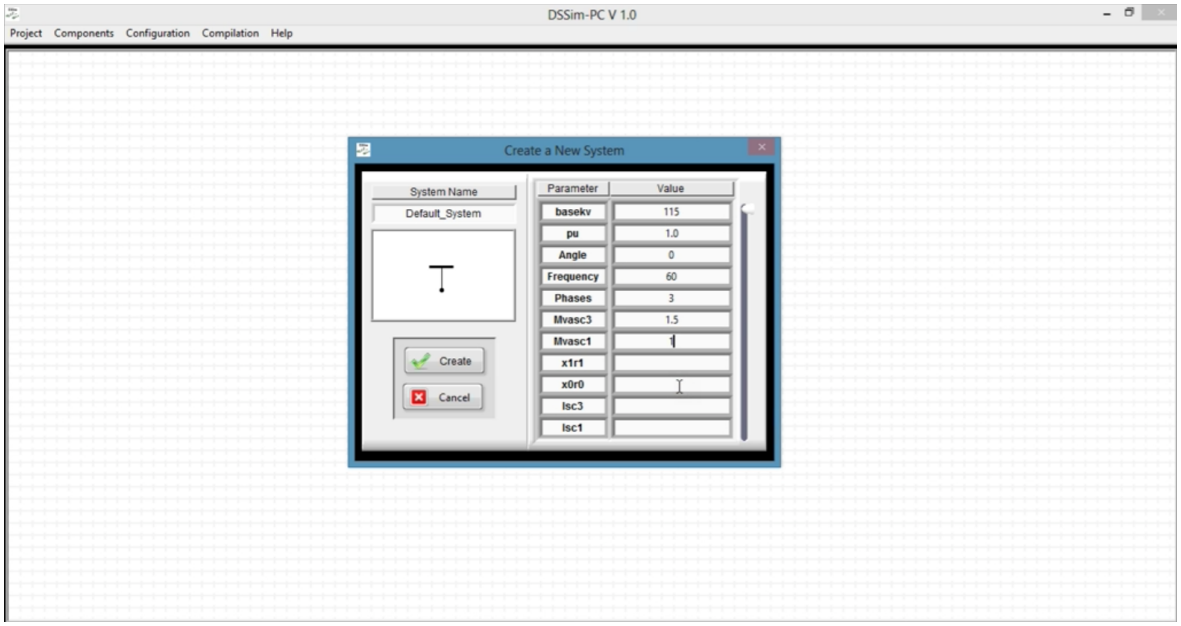

Figure E.3: Defining a new system with the graphical interface DSSim

could be controlled with meters as shown in figure E.1, particularly, in dynamic conditions it is possible to control in real time all network parameters.

Appendix F

Schneider-Electric: Power Factor correction quotation

Email

Building Systems and Solutions
Power Quality Correction Group

From: **Steven Adams**
Tel: 01952 220551
Fax: 01952 292238
E-mail: steven.adams@schneider-electric.com

date: 4th February 2014
our ref.: T77269A
your ref.:

Page: 1/3

***To*:** **Remon Afty**
Email: remon.afty@hotmail.com

Subject: **T77269A – Cardiff University**

Hello Remon,

Thank you for your enquiry and interest in our products.

Further to your request for Power Factor Correction, please find the attached quotation for your consideration. This quotation has been completed as per the 630kW peak with a power factor of 0.9.

630kW	@0.9PF	700kVA	305.1kVAr
630kW	@0.96PF	656.3kVA	183.8kVAr

Based on the calculations above, the installation of **125kVAr of power factor correction** would bring the power factor up to 0.96 (above the threshold for reactive charges on electricity bills). Installing this amount of power factor correction will also result in a released capacity of 43.8kVA which will equate to 63.1A available for additional loading (based on 400V supply).

Should this quotation result in an order, please forward your order to the Stafford Park 5 address as detailed below or to the fax number shown above. Please note that if faxing your order through, it would be beneficial to also email myself shortly after to confirm receipt.

Payment Terms	**:**	Nett Cash 30 days from date of invoice.
Carriage	**:**	Paid to kerbside - UK mainland site.
Validity	**:**	30 Days from the above date.

Product and Services are supplied strictly in accordance with our UK and Ireland Conditions of Sale for the Supply of Goods and Related Works, which apply in all instances unless alterations and/or deviations have been agreed in writing prior to order acceptance. Our Terms and Conditions can be viewed/down-loaded by going to www.schneider-electric.co.uk, www.schneider-electric.ie, www.getplc.com, or by ringing 0870 608 8 608 for a hard copy.

If you have any questions, or if you would like someone from this office to assist you in deliberations, please don't hesitate to call our Area Contact or this office.

Yours faithfully,
Steven Adams
Power Quality Correction Group

Quotation
Since the network pollution level in relation to harmonics is not known, please read the below clause for assistance making a decision on whether ‘standard’ or ‘detuned’ equipment is required.

Many modern electrical installations contain significant amounts of non-linear type loads e.g. Computers and IT equipment, High Frequency Lighting, Variable Speed Drives, and these types of load generate harmonic current distortion on the distribution system. Although capacitors themselves do not generate harmonics, they will potentially interact with those harmonics present on the system. This being the case, it is essential that the potential harmonic distortion level of the system is taken into account when specifying the capacitor installation. For applications that require power factor correction in harmonic rich environments, ensure that a 'Detuned' or filtered capacitor bank is applied in place of 'Standard' automatic capacitor banks. It is incumbent upon the purchaser to ensure that the application is suitable for 'Standard' power factor correction equipment if specified. 'Detuned' equipment should be considered where between 10 and 15% of the load consists of non-linear elements. Schneider Electric recommends 'Detuned' equipment when 15% or more of the load is non-linear.

Option 1 – 125kVAr Standard Power Factor Correction

Quantity	:	1 off
Description	:	125kVAr Standard, Automatic VarSet Power Factor Correction cubicle at 400V, 50Hz with incoming integral circuit breaker and with a power per step of 25kVAr.
Network Pollution Level	:	Lowly Polluted (Standard)
Connection	:	Bottom Entry
Colour	:	RAL9003 (White)
Internal Protection	:	Circuit Breaker Protection w/Rotary Handle (35kA) Safety: IPxxB
Ingress Protection	:	Environment: IP31
Unit Dimensions	:	1200mm H x 800mm W x 300mm D (Wall Mounted)
Delivery	:	Currently 6-8 working weeks from receipt of your full and final written instructions, subject to suitable credit clearance.

tem	Equipment	No.	Catalogue Number	Unit Cost	Total Nett Cost (Ex. Vat)
1	**125kVAr Standard VarSet**	1 off	**VLVAW2N03509AA**	£2,706.00	£2,706.00
2	**Split Core MR CT**	1 off	-	£63.00	£63.00
3	**Carriage**	1 off			Included
				Total Cost	£2,769.00

Notes
All Automatic Power Factor Correction equipment requires signalling from a current transformer fitted to the red (L1) phase of the supply that required correcting. This is normally the incoming mains to the building and the fitting of this CT is be done by yourselves upon installation.

Merlin Gerin
Square D
Telemecanique

Schneider Limited

Merlin Gerin Low Voltage Equipment
Stafford Park 5, Telford
Shropshire TF3 3BL
Tel. 01952 290029 Fax. 01952 209548
Web: http://www.schneider.co.uk

Registered to ISO 9001
ASTA cert. No. 11564

Registered to ISO 14001
ASTA cert. No. 13037

Registered in England
1407228

Registered Office:
Stafford Park 5
Telford TF3 3BL

All equipment quoted is suitable for use on a 400V, 3 Phase, 50 Hz supply

Option 2 – 125kVAr Detuned Power Factor Correction

Quantity	:	1 off
Description	:	125kVAr Detuned, Automatic VarSet Power Factor Correction cubicle at 400V, 50Hz with incoming integral circuit breaker and with a power per step of 25kVAr.
Network Pollution Level	:	Polluted (Detuned) Tuning Factor: 3.8 (190Hz)
Connection	:	Bottom Entry
Colour	:	RAL9003 (White)
Internal Protection	:	Circuit Breaker Protection w/Rotary Handle (35kA) Safety: IPxxB
Ingress Protection	:	Environment: IP31
Unit Dimensions	:	1300mm H x 1600mm W x 300mm D (Floor Standing)
Delivery	:	Currently 6-8 working weeks from receipt of your full and final written instructions, subject to suitable credit clearance.

tem	Equipment	No.	Catalogue Number	Unit Cost	Total Nett Cost (Ex. Vat)
1	**125kVAr Detuned VarSet**	1 off	**VLVAF4P03509AA**	£3,687.00	£3,687.00
2	**Split Core MR CT**	1 off	-	£63.00	£63.00
3	**Carriage**	1 off			Included
				Total Cost	£3,750.00

Notes

All Automatic Power Factor Correction equipment requires signalling from a current transformer fitted to the red (L1) phase of the supply that required correcting. This is normally the incoming mains to the building and the fitting of this CT is be done by yourselves upon installation.

Bibliography

[1] N. Jenkins, R. Allan, P. Crossley, D. Kirschenand G. Strbac, Embedded Generation, The Institution of Electrical Engineers, London,2000.

[2] Lakervi, E. and Holmes, E.J., Electricity distribution network design, IEE Power series 21, 1995, London, UK, 325 p.

[3] A. Paolucci, Lezioni di trasmissione dell'energia Elettrica. Padua, Italy, 1976.

[4] Panagis N. Vovos, Centralized and Distributed Voltage Control: Impact on Distributed Generation Penetration.

[5] E. Clarke, Circuit analysis of A-C power systems, Wiley 1943

[6] EPRI, Smart Distribution System Research in EPRI's Smart Grid Demonstration Initiative, 2011, IEEE.

[7] EPRI, Active distribution management, CIGRE Canada 2009 symposium.

[8] Nick Jenkins, Ron Allan, Peter Crossley, David Kirschen, Goran Strbac Embedded Generation Power 2000.

[9] Nick Jenkins, Electricity distribution network Design, 2nd Edition.

[10] H. L. Willis. Spatial Electric Load Forecasting. Marcel Dekker, 1996.

[11] An Overview of Electricity Demand Forecasting Techniques, Vol.3, No.3, 2013-National Conference on Emerging Trends in Electrical, Instrumentation and Communication Engineering.

[12] C.W. Gellings, Demand forecasting for electric utilities, PE (1991) The Fairmont Press, Inc.

[13] Short-term load forecasting using lifting scheme and ARIMA models.

[14] Kathleen A. Cullen, Forecasting Electricity Demand using Regression and Monte Carlo Simulation Under Conditions of Insufficient Data, 1999.

[15] John Grainger, Jr.,William Stevenson Power System Analysis 1994.

[16] Non-parametric short-term load forecasting, Electrical Power and Energy Systems 29, 2007.

[17] Bignucolo Fabio, Il controllo delle reti attive di distribuzione, Tesi dottorato, Padova.

[18] H. Lee Willis, Power Distribution Planning Reference Book, 2nd Edition Power Engineering, 2004.

[19] Load Flow Analysis Framework for Active Distribution Networks Based on Smart Meter Reading System, scientific research, Engineering, 2013, 5, 1-8.

[20] H. K. Alfares and M. Nazeeruddin, "Electric Load Forecasting: Literature Survey and Classification of Methods," International Journal of Systems Science, Vol. 33, No. 1, 2002, pp. 23-34.

[21] H. Wang and N. Schulz, "A Load Modeling Algorithm for Distribution System State Estimation," IEEE/PES Transmission and Distribution Conference and Exposi- tion Volume 1, Atlanta, 28 October-2 November 2001, pp. 102-105.

[22] R.Cicoria - G.L.Fracassi - G. Gambelli -M. Mazmni - W.Palenzona - E. Ricci:"Load flow calculations on distribution networks by using a statistical approach".

[23] Garthw. Miln: "Response of the ordinary least squares estimator (OLS) to deterministic and stochastic noise".

[24] Zhaoyang Dong, Pei Zhang, Jian Ma, Junhua Zhao, Mohsin Ali, Ke Meng, Xia Yin Emerging Techniques in Power System Analysis 2010.

[25] T. J. Miller, "Reactive power Control in Electric Systems," John Willey and Sons, 1982.

[26] L. , R. Otto, T. Putman, "Principles and Applications of Static, Thyristor-Controlled Shunt Compensators," IEEE Trans. on PAS, vol. PAS-97, no 5, pp. 1935-1945, Oct. 1980.

[27] Gelen, A. Yalcinoz, T.:"The behavior of Thyristor Switched Capacitor (TSC) installed in an infinite bus system" IEEE

[28] Carlos, Juan "Binary controlled static VAR compensator, Based on Electronically Switched Capacitors", http://web.ing.puc.cl/ power/paperspdf/dixon/33a.pdf

[29] S. Torseng, "Shunt-connected reactors and capacitors controlled by thyristors," IEE Proc. Part C, vol. 128, no. 6, pp. 366-373, Nov. 1981.

[30] www.schneider-electric.com.au/documents/electrical-distribution/en/local/electrical-installation-guide/EIG-L-power-factor-harmonic.pdf

[31] ABB: "http://www.abb.co.uk/product/us/9aac124853.aspx"

[32] Schneider-electric:
"http://www.schneider-electric.co.uk/sites/uk/en/products-services/
electrical-distribution/products-offer/power-factor-correction/
power-factor-correction"

[33] Eaton Capacitors:
"http://www.eaton.uk.com/EatonUK/ProductsSolutions/Electrical/ProductsServices/
PowerDistributionMonitoring/PowerFactorCorrectionCapacitors/index.htm"

[34] Gentec Capacitors: "http://www.gentec.ca/eng/capacitors.asp"

[35] http://www.engineeringtoolbox.com/ip-ingress-protection.html

[36] Schneider-electric:
"www.schneider-electric.com.au/documents/electrical-distribution/en/local/electrical-installation-guide/EIG-L-power-factor-harmonic.pdf"

[37] ABB: http://www02.abb.com/global/huabb/huabb008.nsf/0/bfab9ce091a25dc0c1257a2c0043d7ea

[38] R. Sastry Vedam, Mulukutla S. Sarma: Power Quality, CRC Press 2009.

[39] International Energy Agency, "I E A S T A T I S T I C S: CO2 EMISSIONS FROM FUEL COMBUSTION H I G H L I G H T S,"International Energy Agency, Paris, 2011 Edition.

[40] C. Schwaegerl , M.H.J. Bollen: "VOLTAGE CONTROL IN DISTRIBUTION SYSTEMS AS A LIMITATION OF THE HOSTING CAPACITY FOR DISTRIBUTED ENERGY RESOURCES", CIRED, Turin, 6-9 June 2005.

[41] Tom'as Yebra Vega: "Distributed Generation and Hosting Capacity Need for stochastic analysis" University of Manitoba Power System group.

[42] Etherden, N. and Bollen, M.H.J.. " Increasing the hosting capacity of distribution networks by curtailment of renewable energy resources", PowerTech, 2011 IEEE Trondheim, 2011.

[43] N. Dalla Rizza: "Performance limits of UK low voltage networks and potential for reactive power compensation", Cardiff University, 2013.

[44] Western Power Distribution, "Standard technique: SD5A/1: Design of Low Voltage Domestic Connections", UK, 20 April 2012.

[45] Thomas M. Blooming, Daniel J. Carnovale, P.E: "CAPACITOR APPLICATION ISSUES", IEEE 2008.

[46] "IEEE Standards Interpretations for IEEE Std 18-2002," http://standards.ieee.org/reading/ieee/interp/18- 2002.html, © Institute of Electrical and Electronics Engineers, Inc. 2005.

[47] http://icar.it/chisiamo.php?lingua=2

[48] W. Hofmann, J. Schlabbach: "Reactive Power Compensation - A Practical Guide", 2012 John Wiley and Sons, Ltd.

[49] D. Montenegro. (2013, 01, 07). DSSim-PC, Electrical Distribution Network simulator for PC. Available: http://sourceforge.net/projects/dssimpc/?source=navbar

[50] F. Dughiero, A. Rigoni: "Approfondimenti tecnici di incentivazione, fiscali, connessione e autorizzazione per impianti FV", Corso di tecnologie fotovoltaiche, 2012

[51] D. Q. Hung, N. Mithulananthan, and R. C. Bansal, "Analytical expressions for DG allocation in primary distribution networks," IEEE Trans. Energy Convers., vol. 25, no. 3, pp. 814-820, Sep. 2010.